INSTITUTE OF THERMOMECHANICS
Academy of Sciences of the Czech Republic, v. v. i.

Colloquium

FLUID DYNAMICS 2007

Proceedings

Edited by
Pavel JONÁŠ and Václav URUBA

Prague, 24. – 26. 10. 2007

Institute of Thermomechanics AS CR, v. v. i., Dolejškova 5, CZ-18200 Prague 8

The editors did their best to ensure the printing quality of the Proceedings. However, some manuscripts were already damaged upon receipt, or the authors did not comply with instructions when preparing their camera-ready manuscripts. Therefore, the editors cannot accept responsibility for the final appearance of these manuscripts.

Účelový náklad ÚT AV ČR, v. v. i. pro účastníky konference
DYNAMIKA TEKUTIN 2007,
vydáno v počtu 76 výtisků

Adresa vydavatele: Ústav termomechaniky AV ČR, v. v. i.
Dolejškova 5
182 00 Praha 8
Česká republika

ISBN 978-80-87012-07-09

SOUČASNÉ MĚŘENÍ RYCHLOSTI A TEPLOTY ŽHAVENOU SONDOU SE DVĚMA ČIDLY

Simultaneous measurement of velocity and temperature with two-sensor hot-wire probe

Pavel Antoš
Ústav termomechaniky AV ČR, v.v.i., Praha

Úvod

Současně lze měřit rychlost a teplotu pomocí termoanemometrické sondy se dvěma čidly, která jsou žhavena na různé teploty. Čidlo sondy je citlivé současně na rychlost a teplotu proudu. Pro měření rychlosti by měl být rozdíl teploty čidla a teploty proudu co největší. Tehdy má čidlo velkou citlivost na rychlost. Citlivost čidla na teplotu je naopak největší při minimálním žhavení.
Pro žhavení sond se běžně používají dva způsoby: žhavení na konstantní teplotu čidla (CTA) a žhavení konstantním proudem (CCA). Z teoretického rozboru modelu CTA obvodu (*Antoš 2007*) vyplývá, že z důvodu dynamického nastavení je skutečné žhavení odchýleno od nastavené hodnoty. Tuto odchylku nelze zanedbat právě v oblasti nízkého žhavení, které je vhodné pro měření teploty. Pro určení skutečné hodnoty žhavení by bylo nutno provést specielní kalibrační proceduru. Z tohoto důvodu je lépe pro žhavení teploměrných čidel použít metodu konstantního proudu CCA.

Rekonstrukce signálu

Drátková sonda je tvořena jedním rychlostním a jedním teploměrným čidlem. Zaměřme se nyní na frekvenční vlastnosti teploměrného drátku. Z rovnice tepelné rovnováhy drátku a ochlazovacího zákona lze odvodit teoretický vztah pro časovou konstantu drátku τ v režimu CCA:

$$\tau = d_w^2 \rho_w c_w \frac{1}{4Nu\lambda_g} = m_w c_w \frac{R_w - R_a}{\alpha_0 R_0 R_a I^2}, \qquad (1)$$

kde d_w je průměr drátku, ρ_w je hustota drátku, m_w je hmotnost drátku, c_w je tepelná kapacita drátku, R_w je střední odpor žhaveného drátku, R_a je odpor nežhaveného drátku při střední teplotě tekutiny, R_0 je odpor drátku při referenční teplotě, ke které je vztažen teplotní součinitel odporu drátku α_0 (teplotní součinitel odporu druhého řádu se neuvažuje) a konečně I je střední hodnota proudu protékajícího drátkem.
Z časového průběhu měřené teploty T_M lze teoreticky rekonstruovat skutečnou teplotu tekutiny T:

$$T(t) = T_M(t) + \tau \frac{\mathrm{d}T_M(t)}{\mathrm{d}t}. \qquad (2)$$

Typický průběh přenosové funkce drátkové sondy ukazuje následující graf pro dvě různé štíhlosti drátku.

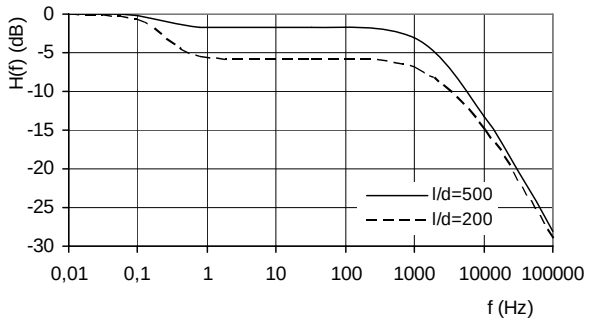

Graf 1. Přenosová funkce drátku $H(f)$

Jak je z grafu patrné, přenosovou funkci drátku $H(f)$ lze považovat v jisté oblasti za konstantní. Je ohraničena hodnotami frekvencí, které odpovídají časové konstantě elektrod sondy (držáků drátku) τ_0 a časové konstantě drátku τ. Velikost přenosové funkce v této oblasti H_0 lze určit (*Freymuth 1979*):

$$H_0 = 1 - \frac{1}{\Lambda}\sqrt{Nu\lambda_g/\lambda_w} \quad ; \quad 1/2\pi\tau_0 \ll f \ll 1/2\pi\tau\,, \tag{3}$$

kde Λ je štíhlost drátku, λ_g je tepelná vodivost tekutiny, λ_w je tepelná vodivost drátku. Zásadní vliv na přenosovou funkci má geometrie sondy; čím je větší štíhlost drátku, tím k menšímu zkreslení signálu dochází. Pro fluktuace skutečné teploty lze psát:

$$\Delta T = H_0^{-1}\,\Delta T_M \tag{4}$$

Prakticky lze měřenou teplotu numericky korigovat s použitím diskrétní Fourierovy transformace. Rekonstruovaná teplota tekutiny T bude dána součinem FFT s inverzní přenosovou funkcí.

Závěr

Současné měření rychlosti a teploty lze realizovat pomocí termoanemotrické sondy se dvěma čidly. Teploměrný drátek je žhaven konstantním proudem a při měření turbulentních charakteristik jeho frekvenční vlastnosti vyžadují rekonstrukci signálu. Numericky lze měřenou teplotu korigovat pomocí diskrétní Fourierovy transformace.

Literatura

Antoš, P. (2007): *Correct interpretation of the CTA measuremnts at low overheats*. Engineering Mechanics 2007. Praha. Institute of Thermomechanics AS CR, v.v.i.: 7-8. ISBN 978-80-87012-06-2.

Elsner, J. W., Drobniak, S. (1995): *Metrologia turbulencji przeplywów*. Maszyny Przeplywowe Tom 18. Wydawnictwo Polskiej Akademii Nauk. Wroclaw. ISBN 83-04-04289-4.

Freymuth, P. (1979): *Engineering estimates of heat conduction loss in constant temperature thermal sensors*. TSI Quaterly 5: 3-9.

Poděkování

Poděkování projektu PP 07-01089 (ÚT AV ČR).

REGULAČNÍ VENTILY S PROFILOVANÝM PŘECHODEM A ROVNÝM DNEM KUŽELKY

Control Valve with Shaped Cone and Flat Bottom

Lukáš Bednář, Ladislav Tajč
ŠKODA POWER a. s., Plzeň

Abstrakt

Popisuje se aerodynamický tunel na testování ventilů. Uvádějí se výsledky měření silového namáhání tří variant ventilů. Uvažuje se ventil s volně zavěšenou neodlehčenou částečně tvarovanou kuželkou s přechodem do rovného dna, ventil s perforovanou kuželkou a ventil se sítem. Srovnává se namáhání vřetena v tahu a maximální rozkmit ohybového momentu.

Úvod

Při konstruování parních turbin se používá celá řada návrhů kuželek ventilů. Tvarová rozmanitost je dána požadavkem na spolehlivost při všech provozních režimech turbíny a tím daných proudových poměrech ve ventilech. V některých případech je potřebné použít odlehčené ventily, aby se snížila síla nutná k odtržení kuželky od sedla. Na kuželku působí zejména aerodynamické síly. Aerodynamickým silám se přisuzuje největší vliv na nestabilitu proudu a rozkmitání kuželky. Mezi nejčastější poruchy patří vytloukání sedel ventilu a praskání vřeten. V procesu vývoje a hledání optimálního provedení kuželky se upustilo od kulového zakončení dna kuželky a přešlo se k variantám s tvarovanou kuželkou a kuželkou s rovným dnem a podpíchnutím.

Podle tvaru kuželky můžeme uvažovat proudění nerozšířenou dýzou s náhlým rozšířením průřezu (u kuželky s rovným dnem a podpíchnutím) a proudění konvergentně-divergentní (Lavalovou) dýzou. V důsledku odtržení proudu je u podpíchnuté kuželky větší tlak na dno kuželky, než jaký vzniká při stejných proudových poměrech u profilované kuželky. Přítlačná aerodynamická síla je u profilované kuželky větší.

U podpíchnuté kuželky se proud odtrhne na koncové hraně kuželky a přimkne se k stěně difuzoru. V prostoru difuzoru nastává volná expanze s místními maximálními rychlostmi. U tvarované kuželky se naopak proud odtrhne od stěny difuzoru a přimkne se k stěně kuželky. Místo odtržení není v tomto případě pevně stanovené. Z výpočtového rozboru, který byl proveden na ZČU Plzeň je zřejmé, že u podpíchnuté kuželky se vyskytuje místní Machovo číslo $M > 1$ již pro tlakové poměry $p_2/p_0 < 0{,}65$. Nadzvukové proudění je zdrojem rozruchu a rázových vln. Pokud se tlakové pulsace přenášejí přímo na vřeteno, může dojít k jeho destrukci nebo nekontrolovanému kmitání ventilu. Předností podpíchnuté kuželky je větší provozní spolehlivost při spouštění turbiny. Tvarovaná kuželka však má menší ztráty při jmenovitých provozech. Byla snaha využít předností tvarových řešení kuželky.

Experimentální zařízení a modely kuželek ventilů

Ve ŠKODA POWER a. s. existuje aerodynamický tunel, který umožňuje pracovat v rozmezí tlakových poměrů $\varepsilon = 0{,}3 \div 1$ při zdvihu kuželky $\bar{h} = 0 \div 0{,}3$.

Pro experimentální účely se vyrobila neodlehčená částečně profilovaná kuželka s přechodem na rovné dno, obr. 1 a kuželka s odlehčením. Centrální výtokový otvor je nahrazen perforovanou stěnou, obr. 2. Podle podkladů MEI je centrální otvor zdrojem větších rozruchů než sada malých výtokových dýz.

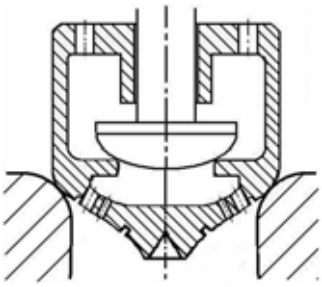

Obr. 1: Tvarovaná kuželka MEI s perforovanou stěnou

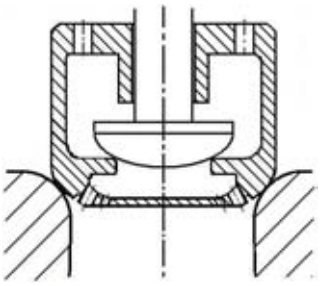

Obr. 2: Kuželka s profilovaným přechodem a rovným dnem

Silové působení na vřeteno ventilu

Silové namáhání vřetena bude odvislé od rozložení tlaku na povrchu kuželky. Výsledná síla bude závislá na přilnutí nebo odtržení proudu od stěny kuželky i na výskytu skokových změn tlaku v rázových vlnách. Zkoušelo se provedení kuželky bez perforace a s perforací. Síla v tahu na vřeteno ventilu s kuželkou bez perforace je vynesena na obr. 3. Při růstu tlakového poměru dochází k skokové změně osové síly.

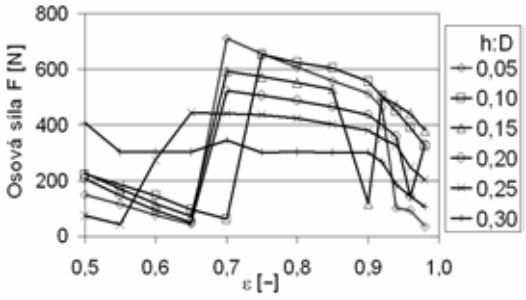

Obr. 3: Osová síla na vřeteno s kuželkou bez odlehčení

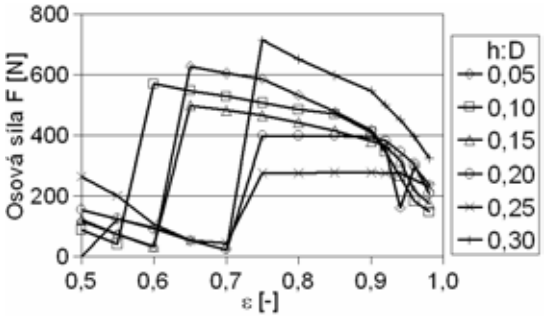

Obr. 4: Osová síla na vřeteno u odlehčené kuželky

Vliv odlehčovacích otvorů na osovou sílu kuželky je ukázán na obr. 4. Výtok media přes odlehčovací otvory způsobuje větší rozptyl tlakových poměrů, při kterých dochází ke změně charakteru proudění ventilem a ke skokové změně osové síly.

Závěry

- Perforace kuželky obecně napomáhá k tlumení tlakových pulsací.
- U částečně profilované kuželky lze vypozorovat skokové změny v silovém působení na vřeteno při změně tlakového poměru i při změně zdvihu kuželky.
- Síto ve vstupní části ventilu má vliv na proudové poměry pod kuželkou ventilu.

Poděkování

Autoři příspěvku děkují MPO České republiky za finanční podporu grantu TANDEM.

THE CAPILLARY FLOW OF A YIELD-STRESS FLUID

Volfango Bertola
University of Edinburgh, United Kingdom

The wicking of a Newtonian liquid in a capillary tube is described by the well-known Washburn equation [1]. In the absence of gravity effects (horizontal tube), the motion is entirely determined by a force balance between capillarity and the frictional force on the wall, which becomes increasingly larger as the liquid advances:

$$\tau_w \pi d x = \pi d \sigma \qquad (1)$$

This force balance does not depend on the fluid rheology, so that it is true also for non-Newtonian fluids. Here, we want to investigate the behaviour of yield-stress fluids, i.e. those fluids which respond like elastic solids for applied stresses lower than a certain threshold value τ_0 (the yield stress), and flow only when the yield stress is overcome.

When a yield stress fluid flows in a horizontal tube under the action of the capillary force only, according to Eq. (1) there is a critical distance from the tube inlet for which the wall shear stress equals the yield value:

$$\bar{x} = \sigma / \tau_0 \qquad (2)$$

Since the shear stress is maximum at the wall, this means that $\tau < \tau_0$ everywhere inside the capillary tube, so that the fluid cannot flow anymore [2].

This work brings experimental evidence that the theory outlined above cannot describe the behaviour of a model yield-stress fluid (a commercial gel). In particular, the maximum penetration length of the fluid in the capillary is one order of magnitude larger than the prediction of Eq. (2), and is strongly dependent on the tube diameter.

Experiments were carried out using borosilicate glass tubes 125 mm long and with diameters ranging from 0.46 to 1.5 mm; the position of the advancing fluid was measured by means of a CCD camera placed above the tubes (a typical image is shown in Fig. 1).

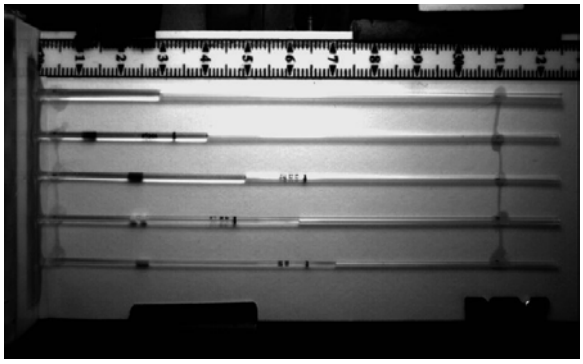

Figure 1. Experimental arrangement.

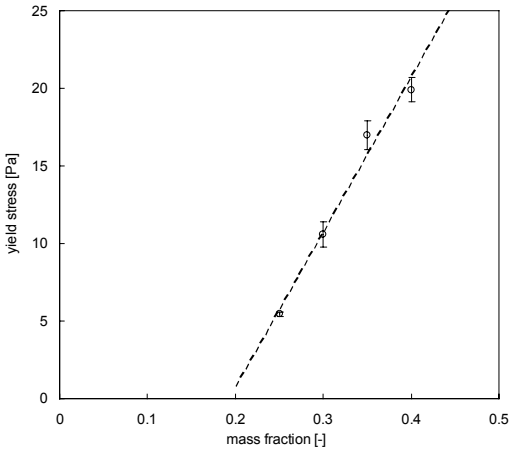

Figure 2. Yield stress vs. mass fraction of gel in the solution

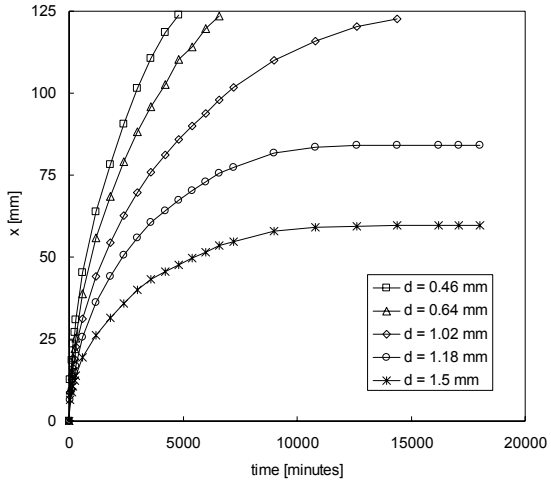

Figure 3. Fluid penetration vs diameter in different tubes ($\tau_0 = 10.7$ Pa).

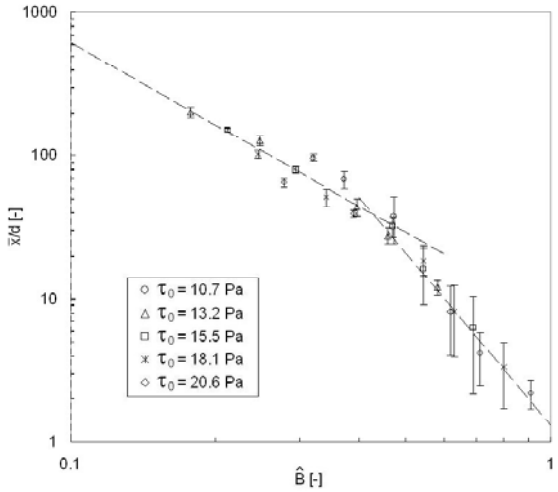

Figure 4. Dimensionless maximum penetration length as a function of the Bingham-capillary number.

The surface tension of solutions (measured by a De Nouy tensiometer) was 34 mN/m, while the yield stress (measured by a rotational rheometer with plane-plane geometry) could be varied from about 5 to 20 Pa by diluting the gel in water at different concentrations, as shown in Fig. 2. Such values yield maximum penetration distances of a few mm.

A typical result obtained for a given yield stress is reported in Fig. 3, which shows that the fluid does not stop at the distance predicted by Eq. (2) and that the maximum penetration length is strongly dependent on the tube diameter.

Because Eq. (1) is always true, the simplest explanation for such experimental results is that the fluid does not remain homogeneous under shear flow in the vicinity of the wall, causing a substantial reduction of the effective yield stress. In particular, when a fluid consists of a particle suspension (including colloids), which is the case of most yield-stress fluids, this phenomenon is caused by a depletion of particles near the wall and is known as "apparent wall slip" [3].

In the present system, wall slip seems to be related to the competition between the yield stress and the capillary pressure, which can be expressed by the dimensionless number $\hat{B} = \tau_0 d/\sigma$ (the product of the Bingham and the Capillary numbers). If one plot the dimensionless maximum penetration length of the fluid in the capillary with respect to this parameter, all data collapse on a single curve, as shown in Fig. 4. The best-fit of experimental data leads to a scaling law of the form:

$$\bar{x}/d \sim \hat{B}^n \qquad (3)$$

where $n = -2$ for $\hat{B} < 0.5$ and $n = -4$ for $\hat{B} > 0.5$.

References

[1] E.W. Washburn, Phys. Rev. 273-283 (1921).
[2] A.H. Skelland, Non-Newtonian Flow and Heat Transfer, Wiley, New York, 1967.
[3] H.A. Barnes, J. Non-Newtonian Fluid Mech. 56, 221–251 (1995). Z.D> Jastrzebski, Ind. Eng. Chem. Fundam. 6, 445–453 (1967).

EXPERIMENTAL INVESTIGATION OF LAMINAR AND TURBULENT DRAG IN CLASSICAL AND QUANTUM OSCILLATORY BOUNDARY LAYER FLOW

M. Blažková[b], D. Schmoranzer[a], L. Skrbek[a]
Joint Low Temperature Laboratory, [a]Institute of Physics ASCR, v. v. i., Prague
and [b]Faculty of Mathematics and Physics, Charles University, Prague

Introduction

Various types of oscillating structures have been important for probing the hydrodynamic properties of quantum fluids since the discovery of superfluidity. The famous Andronikashvili experiment, the basis for the two fluid model, was a measurement of the torsional oscillations of a pile of closely spaced discs and provided the first direct determination of the densities of the normal (ρ_n) and superfluid (ρ_s) fractions in He II. It was soon realized that the ideal picture – according to which the normal fluid is dragged along with the discs because of its finite viscosity while the inviscid superfluid remains stationary and does not participate in the flow – can only hold at sufficiently low oscillation amplitudes. Both the classical viscous boundary layer flows and the quantum flows due to oscillating objects display transitions from laminar to turbulent drag regime. It is interesting to compare classical and quantum cases.

Experimental results and discussion

Experimentally, it is best to use a tool capable of probing both classical and quantum flow that can be changed at will *in situ*. Such a tool indeed exists – the quartz tuning fork. The flow due to its oscillatory motion and transition to turbulent drag regime in classical fluids (cryogenic helium gas and normal liquid helium) has been investigated by our group [1] and some aspects of it were reported at this workshop last year [2]. Based on measurements of the velocity versus the driving force, it has been found that in viscous flow the critical velocity for the crossover from laminar to turbulent drag in the limit $U/\omega \ll \ell \gg \delta$ scales as $U_{\rm cr} \propto \sqrt{\nu\omega}$ over at least two decades of kinematic viscosity ν. Here U is the peak velocity of the fork, ℓ its characteristic size, and ω denotes the angular frequency of the fork. The validity of this scaling was recently tested further by performing measurements with forks of various sizes and oscillating at different frequencies. The scaling can be explained qualitatively by equating the linear and the turbulent drag forces at $U_{\rm cr}$, using the approach described in Ref. [1].

The experiments and analysis has been recently extended from the classical viscous He I to He II (a preliminary report is Ref. [2]). The left panel of Fig. 1 shows no appreciable qualitative change in the character of the dependence of the velocity versus the driving force when crossing T_λ. On decreasing the temperature of He II along the saturated vapor pressure curve further, however, the crossover from laminar to turbulent flow becomes gradually sharper and the character of the curve above the critical velocity changes. This change is seen more clearly in the right panel of Fig. 1, where the drag coefficient $C_{\rm d}$ is plotted for three different temperatures. $C_{\rm d}$ is defined from the equation $F = \frac{1}{}$

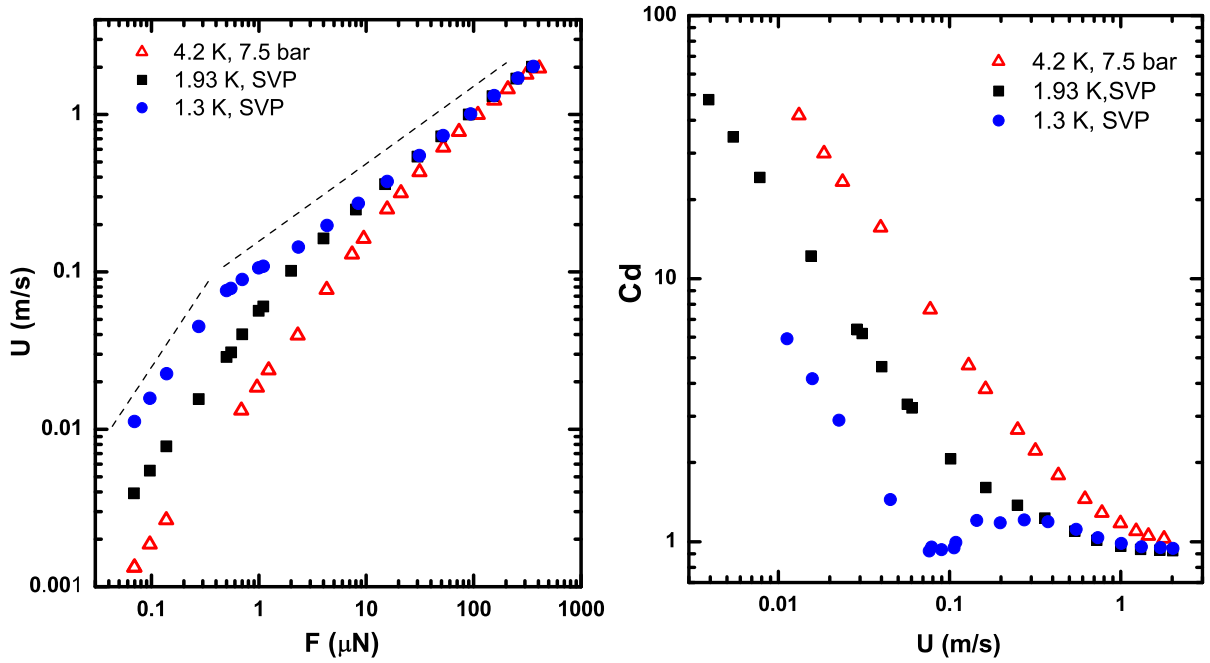

Figure 1: *(Left)* Transition from laminar to turbulent drag regime in ^{4}He, measured with a tuning fork in normal liquid He I and superfluid He II at three temperatures. At low drive level (in the laminar regime) the measured velocity is a linear function of the applied drive; around its critical value the crossover to the turbulent regime occurs, characterized by a driving force proportional to the square of the velocity. The dashed lines indicate the slopes $U \propto F$ and $U \propto \sqrt{F}$. *(Right)* A plot of the drag coefficient $C_{\rm d}$ versus the velocity of the fork shows that in a classical fluid (He I) there is a gradual change towards a constant value well above the transition to turbulence; while in He II there is a sharp transition at a critical velocity $U_{\rm cr}^{\rm S}$ of the superfluid.

classical viscous He I, in the vicinity of $U_{\rm cr}$, the measured dependence $C_{\rm d}(U)$ gradually levels off and $C_{\rm d}$ acquires an approximately constant value of order unity. In He II well below T_λ $C_{\rm d}(U)$ behaves differently. It displays the laminar part, where the drag is due to the viscous normal fluid only, and then, beyond a sharp minimum, $C_{\rm d}(U)$ increases again and displays a broad maximum above which it gradually becomes constant as in the classical case.

This behavior of the drag coefficient $C_{\rm d}(U)$ can be understood in the framework of the two-fluid model. The superfluid fraction produces the sharp minimum where the turbulent drag sets in, which is identified as its critical velocity $U_{\rm cr}^{\rm S}$. It was found, at least approximately, frequency independent, in contrast with the behaviour of classical fluid where the critical velocity was found $\propto \sqrt{}$

CAVITATION IN LIQUID HELIUM DUE TO A VIBRATING QUARTZ FORK

M. Blažková[b], T.V. Chagovets[b], M. Rotter[a], D. Schmoranzer[a], L. Skrbek[a]
Joint Low Temperature Laboratory, [a]Institute of Physics ASCR, v. v. i., Prague
and [b]Faculty of Mathematics and Physics, Charles University, Prague

Introduction

The quartz tuning fork proves to be a robust, cheap and widely available tool for generating and probing oscillatory boundary layer flows, especially at cryogenic conditions [1, 2]. Its peak velocity in helium fluids can be easily varied and detected over seven orders of magnitude, up to very high values of order m/s. An experimental setup containing a quartz tuning fork inside a pressure cell in a glass helium cryostat enables us to experimentally observe additional effects in liquid He, which we ascribe to cavitation (as these are absent in gaseous He), taking place in the vicinity of the fork.

Liquid helium can be prepared extremely clean and wets almost ideally any solid surface – it provides an ideal model system to study cavitation. Numerous studies have been performed over the last fifty years – see [3] for a comprehensive review of the early experiments on nucleation of bubbles in liquid helium, and [4, 5] for more recent results. As many experimental results remain poorly understood, it is of considerable interest to revisit this field using a new tool.

Experimental results and discussion

Our detection protocol is based on sweeping the fixed driving voltage applied to the quartz tuning fork, of the form $U = U_0 \, cos \, \omega t$, across the resonance frequency. At low driving voltages, the response signal from the fork is represented by the absorption and dispersion curves of Lorentzian form [1, 2]. On increasing the driving voltage the response ceases to be Lorentzian, the absorption resonant curve widens and the maximum response shifts towards lower frequency. As explained in detail in our previous publication [2], this behavior is observed in both liquid and gaseous helium and is caused by the transition from laminar to turbulent drag regime. These features occur in both liquid and gaseous helium.

In liquid He I and He II an additional pronounced feature occurs. On further increase of the drive, at high enough amplitude, the observed signal breaks down when the frequency is swept towards resonance. This breakdown event serves as a definition of the critical cavitation velocity v_{cav}. When repeating the sweeps, this character of the signal persists but the response is generally not exactly reproducible. When v_{cav} is plotted versus temperature, a striking feature is observed, see Fig. 1. It is a very steep increase in v_{cav} right below the λ-point - here v_{cav} rises by factor 3-5 within about 20 mK. This step-like feature is detailed in the inset of Fig. 1. We have measured this feature with various forks; it displays a reasonable degree of reproducibility for the data series from different runs as well as for the data obtained with different forks.

While performing the cavitation experiments in an open helium bath of a glass cryostat, in He II (where no bubbles are present in the bulk, thanks to its extremely high thermal conductivity) we have indeed visually observed a bubble occurring between the prongs of the vibrating fork. Having available the pressure cell [2], we have performed the measurements showing the dependence of v_{cav} versus an externally applied overpressure at 4.2 K (see Fig. 1, right).

As the "breakdown" effects described above never occurred in gaseous helium, we naturally

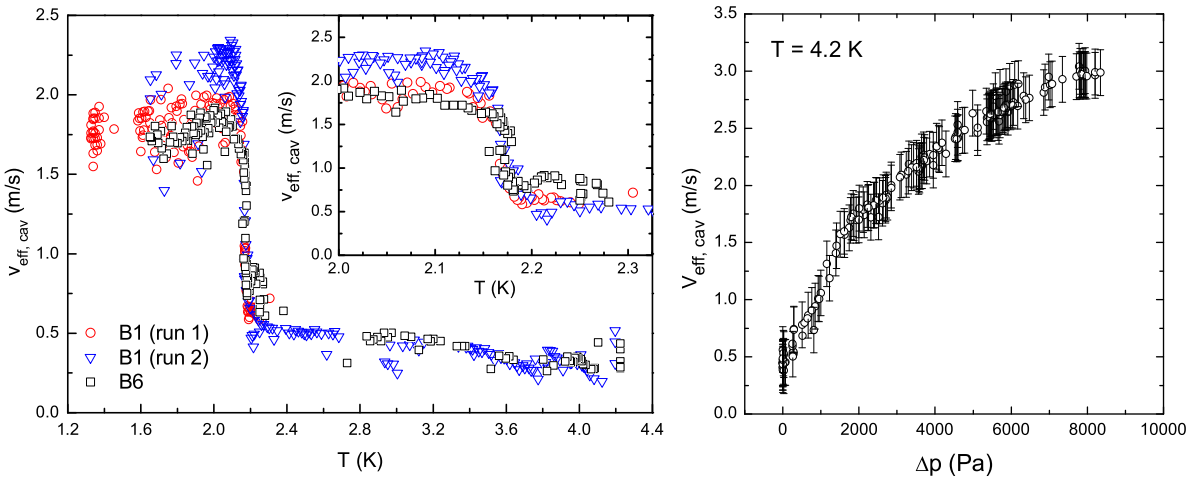

Figure 1: The observed critical cavitation velocity plotted versus the temperature at SVP. The inset magnifies the data in the vicinity of the λ-transition (left). The observed critical cavitation velocity plotted versus the applied overpressure in the cell at 4.2 K (right).

assume that they arise as a consequence of cavitation/boiling processes in liquid He I and He II. The most simple, perhaps naive, explanation would be that due to the Bernoulli equation the local pressure in the flow due to a vibrating quartz fork decreases. The overpressure data at 4.2 K can indeed be fitted by the expected $v_{\rm cav} \propto \sqrt{\Delta p}$ dependence, however, they lead to a pressure drop comparable with the hydrodynamic static pressure head in the cryostat, far too low for what would be required for homogeneous cavitation. Moreover, this simple approach does not explain the almost step-like change in $v_{\rm cav}$ close to T_λ. We believe that in He I thermal effects are influencing the observed velocity, since the vicinity of the fork is locally overheated and cavitation occurs at a temperature which is significantly (about 1 K) higher than that at which the surrounding helium bath is kept. This strongly suggests that combined boiling/cavitation rather than pure cavitation occurs. The steep increase of the cavitation velocity by factor 3-4 observed just below the superfluid transition can be understood as a consequence of the high convective heat transfer efficiency in superfluid He II. Our data do not allow us to unequivocally conclude whether the observed cavitation is heterogeneous or homogeneous in nature; however, homogeneous cavitation [5] would require superflow velocity enhancement past sharp corners by a factor of about 30. We are currently performing more accurate analysis along these thoughts, taking into account the measured values of force and velocity of the fork.

This research is supported by research plans MS 0021620834, AVOZ 10100520, by GAČR under 202/05/0218 and GAUK 7953/2007.

Bibliography

[1] R. Blaauwgeers et al., *J. Low Temp. Phys.*, **146**, 537 (2007).
[2] M. Blažková et al., *Phys. Rev. E***75**, 025302 (2007); *J. Low Temp. Phys.* **148**, 305 (2007).
[3] H.J. Maris, S. Balibar, M.S. Petersen, *J. Low Temp. Phys.* **93**, 1069 (1993).
[4] F. Caupin, S. Balibar, H.J. Maris, *Physica B* **329-333**, 356 (2003).
[5] S. Balibar, *J. Low Temp. Phys.* **129**, 363 (2002).

NUMERICAL SIMULATION OF FREE SURFACE FLOW IN A CHANNEL WITH RIBBED BOTTOM

T. Bodnár and K. Kozel
Department of technical mathematics, Faculty of mechanical engineering,
Czech Technical University in Prague

Introduction

Numerical simulation of free-surface flows is one of the most complicated tasks of CFD. Up to now several methods have been developed for this kind of simulations. The method we have used in our study is based on one of the possible implementations of interface capturing methods. The case solved here is the flow in a 2D channel with ribbed bottom (see Fig. 1), which is partially filled by the water. Because of the action of the inertia and gravity forces, the water-air interface is deformed in proximity of ribs. The shape of the free-surface is relatively simple in this case, however its correct resolution at high Reynolds number in a fully turbulent flow is a very complicated task.

Mathematical Model

The approach used in our model is based on the assumptions for variable-density incompressible flow. It means the flow is treated as if the domain is filled by only one fluid, which density is variable. The discontinuity in density profile arises at the free-surface. This method can be seen as an elementary implementation of VOF method introduced in [3].

For the turbulence modeling we have chosen the SST $k-\omega$ turbulence model see e.g. [4]. The model modification adopted here is exactly the one of [2].

Numerical Solution

Numerical solution of the above presented mathematical model is based on finite-volume cell-centered semi-discretization on structured mesh. The time-integration of the resulting system of ordinary differential equations is carried out using explicit Runge-Kutta multistage scheme. Because of the use of the central-differencing in spatial discretization, suitable stabilization technique is used to avoid non-physical oscillations in the solution.

Numerical simulations

Numerical tests were performed for segment of a 2D channel with two ribs of square crossection. Channel is partially filled by water, while the remaining volume is occupied by air. The geometrical configuration can be seen in the Figure 1. The fully developed velocity profile with

maximum speed $0.25, 0.5, 1.0$ and $2.0\ m/s$ was assumed for both fluids on the inlet. The length scale **h** was set to $1cm$.

In order to avoid complicated multiblock mesh structure, a cartesian grid was used and velocity was set to zero "inside" of the obstacle. This simplifies significantly the computation in the case of multiple obstacles. The mesh structure detail can be seen in the Figure 2.

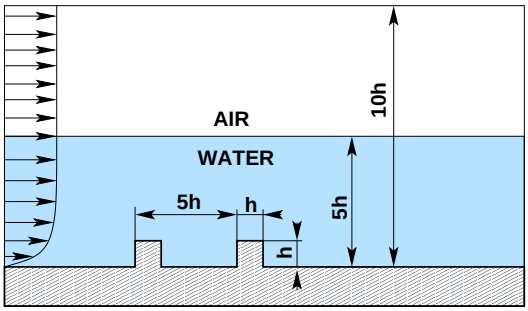

Figure 1: Computational geometry

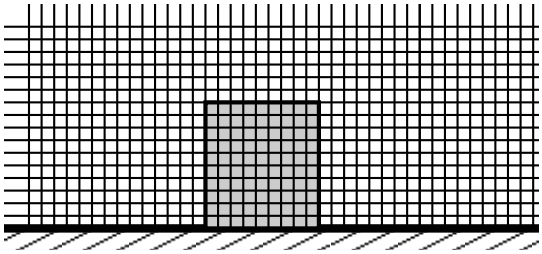

Figure 2: Cartesian grid structure

Conclusions, remarks

The numerical results presented in this contribution were chosen to show the resolution of the flow in the proximity of the ribs and the ability of the model to capture the free surface for selected range of inlet velocities.

From the presented tests of the whole numerical model directly follows that the method used here is applicable for this class of problems. Multiple ribs configurations will be extensively studied in detail.

Acknowledgment

The financial support for the present project was partly provided by the *Czech Grant Agency* under the *Grant No.103/06/0461* and by the Research Plan *MSM 6840770010* of the *Ministry of Education of Czech Republic*.

References

[1] BODNÁR, T. & PŘÍHODA, J.: Numerical simulation of turbulent free-surface flow in curved channel. *Journal of Flow, Turbulence and Combustion*, vol. 76, no. 4: (2006) pp. 429–442.

[2] HELSTEN, A.: Some improvements in Menter's $k-\omega$ SST turbulence model. Tech. rep., American Institute of Aeronautics and Astronautics (1998). AIAA-98-2554.

[3] HIRT, C. W. & NICHOLLS, B.: Volume of fluid (VOF) method for dynamics of free boundaries. *Journal of Computational Physics*, vol. 39: (1981) pp. 201–221.

[4] MENTER, F. R.: Two-Equation Eddy-Viscosity Turbulence Models for Engineering Applications. *AIAA Journal*, vol. 32, no. 8.

IMPLEMENTATION OF AN ALGEBRAIC BYPASS TRANSITION MODEL INTO TWO-EQUATION TURBULENCE MODEL FOR A FINITE VOLUME METHOD SOLVER

Jiří Dobeš[1)], Jaroslav Fořt[1)], Jaromír Příhoda[2)]
[1]) Department of Technical Mathematics, Faculty of Mechanical Engineering, Czech Technical University in Prague, Karlovo náměstí 13, 12135 Praha 2, Czech Republic
[2)] Institute of Thermomechanics AS CR, v.v.i., Dolejškova 5, 182 00 Praha 8, Czech Republic

1 Introduction

The mathematical model of turbulent flow, based on the finite volume method and two-equation turbulence model, was extended by an algebraic model of the bypass transition taking into account the effect of free-stream turbulence and pressure gradient on the laminar/turbulent transition. The intermittent feature of flow in the transition region is described by the algebraic relation for the intermittency parameter and empirical relations for the onset and length of the transition region.

2 Numerical model

We solve a system of averaged Navier-Stokes equations in two spatial dimensions

$$\frac{\partial \mathbf{w}}{\partial t}+\frac{\partial \mathbf{f}}{\partial x}+\frac{\partial \mathbf{g}}{\partial y}=\frac{\partial \mathbf{r}}{\partial x}+\frac{\partial \mathbf{s}}{\partial y} \tag{1}$$

with **w** vector of conserved variables, **f** and **g** are inviscid flux vectors, **r** and **s** are viscous flux vectors. The system of governing equation was closed by the turbulence model with the turbulent viscosity. The k-ω SST model proposed by Menter [1] was considered. Appropriate initial and boundary conditions are prescribed.

The finite volume method of the cell centered type with the modification of the approximative Roe's Riemann solver, the linear least square reconstruction and the Barth's limiter was developed. The viscous fluxes are discretized in the central manner on a mesh dual to the cell faces. Time integration is performed with linearized Euler backward formula and local time stepping is used. The system of equations is solved with GMRES method and ILU(0) preconditioning. The method works on general unstructured meshes.

3 Transition model

Transition models is based on the algebraic equation for the intermittency coefficient

$$\gamma = 1-\exp\left[-\hat{n}\sigma\left(Re_x - Re_{xt}\right)^2\right] \tag{2}$$

proposed by Narasimha [2]. The position of the transition onset is described by the Reynolds number Re_{xt} determined by means of the momentum Reynolds number $Re_{\vartheta t}$ = f (Tu, λ_t) where Tu (%) is the free-stream turbulence level and λ_t is the pressure gradient parameter. Both parameters are considered at the location of the transition onset. Příhoda et al. [3] proposed the relation

$$Re_{\vartheta t} = Re_{\vartheta to}\left[1+0.25\exp(-Tu)\frac{1-\exp(-40\lambda_t)}{1+0.4\exp(-40\lambda_t)}\right] \tag{3}$$

The length of the transition region is given by parameters describing the spot generation rate $\hat{n}$ and spot propagation parameter σ. The simplest correlation uses the empirical parameter

$$N = \hat{n}\sigma Re_{\vartheta t}^3 \tag{4}$$

proposed by Narasimha [2]. The effect of free stream turbulence and pressure gradient on the parameter N is correlated by empirical relation N = f(Tu, λ_t) according to Solomon, Walker, Gostelow [4]. To avoid the calculation of the momentum Reynolds number $Re_{\vartheta t}$ in cases with complicated geometry and unstructured meshes, the vorticity Reynolds number Re_v is used. According to Menter et al. [5], the correlation for the Blasius boundary layer in the form $Re_\vartheta = Re_{vmax}/2.193$ is used.

4 Numerical results

Two types of test cases were considered: a) flat-plate transitional 2D boundary layers flows with different free-stream turbulence level – ERCOFTAC test cases; b) transonic flow through the SE1050 turbine blade cascade. For example, the distribution of the skin friction coefficient for ERCOFTAC test cases is given in Fig.1.

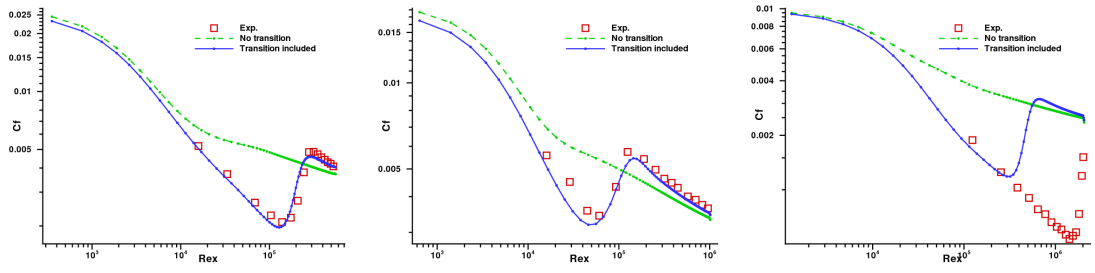

Figure 1: Distribution of skin friction coefficient for ERCOFTAC test cases
(left to right cases T3A, T3B, T3Aminus)

The computations for test cases T3A and T3B give a good agreement with experimental data. For test case T3Aminus with Tu ≈ 1%, the predicted transition onset starts sooner in comparison with experimental data. It can be caused by many factors that are not taken into account. This effect is much more obvious for relatively low turbulence levels.

5 Conclusions

The proposed algebraic bypass transition model was implemented into the unstructured finite volume method solver. The calculation procedure was validated for transitional flat-plate boundary layers with different free-stream turbulence level and for transonic flow through the SE1050 blade cascade. The transition in internal flows is influenced by many various factors and so the prediction of the bypass transition is the most problematic part of the whole calculation. Further progress can be achieved by the application of the transition model based on a transport equation for the intermittency coefficient.

Acknowledgement

The research was supported by the research project No.A200760614 funded by the Grant Agency of AS CR as well as by the project No.101/07/1508 funded by the Czech Science Foundation and by the Research Plan No.AV0Z20760514.

References

[1] Menter F.R. (1994): Two-equation eddy-viscosity turbulence models for engineering applications, AIAA J., 32, 1598-1605

[2] Narasimha R. (1985): The laminar-turbulent transition zone in the boundary layer, Progress in Aerospace Science, 22, 29-80

[3] Příhoda J., Hlava T., Kozel K. (1997): Testing of the transition length using a two-layer turbulence model, Proc. Conf. Engineering Mechanics´97, Svratka, Vol. 4, 157-162 (in Czech)

[4] Solomon W.J., Walker G.J., Gostelow J.P. (1996): The laminar-turbulent transition zone in the boundary layer, Trans. ASME, J. Turbomachinery, 118, 744-751

[5] Menter F., Esch T., Kubacki S. (2002): Transition modelling based on local variables, Proc. 5th Int. Symposium on Engineering Turbulence Modelling and Experiments (Eds. Rodi W., Fueyo N.), Elsevier Science Ltd., 555-564

NUMERICKÉ ŘEŠENÍ STACIONÁRNÍHO A NESTACIONÁRNÍHO TRANSSONICKÉHO PROUDĚNÍ VE VNĚJŠÍ AERODYNAMICE

Numerical solution of steady and unsteady transonic flow in outer aerodynamics

Jiří Dobeš[1], Jaroslav Fořt[1], Petr Furmánek[2], Jiří Fürst[2], Milan Kladrubský[2], Karel Kozel[1]
[1]České vysoké učení technické, Fakulta strojní, Ústav technické matematiky, Praha
[2]Výzkumný a zkušební letecký ústav, a.s., Aerodynamika vysokých rychlostí, Praha

Úvod

Příspěvek obsahuje výsledky výpočtu stacionárního turbulentního proudění (model $k-\omega$) kolem profilu RAE 2822, nestacionárního nevazkého proudění kolem kmitajícího profilu NACA0012 a srovnání stacionárního nevazkého proudění kolem křídla Onera M6 počítaného čtyřmi různými metodami s experimentem.

Matematické modely

Pro řešení dvourozměrného stlačitelného stacionárního turbulentního proudění bylo použito WLSQR schematu (modifikace WENO schematu). Numerické toky jsou počítány pomocí AUSMPW+ metody. Jako model turbulence je použit Kokův TNT model $k-\omega$.

Pro řešení nevazkého oscilujícího profilu pro stlačitelně proudění bylo použito implicitní WLSQR schéma a nestacionarita řešení, daná změnou polohy profilu, byla řešena užitím ALE (Arbitrary Lagrangian–Eulerian) metody.

V případě simulace transsonického obtékání křídla byly zvoleny čtyři rozdílné metody a zároveň tři různé typy výpočetních sítí a to sice strukturované sítě typu H a C a nestrukturovaná síť tvořená čtyřstěny.

Schéma 1. Pro výpočet bylo užito 3D MacCormackova schematu (cell–centered) ve formě prediktor – korektor s přidanou Jamesonovou umělou vazkostí třetího řádu (C i H síť).

Schéma 2. Bylo použito jednokrokové explicitní schéma typu Laxe–Wendroffa v cell–vertex formulaci s umělou vazkostí Jamesonova typu.

Schéma 3. Úloha byla řešena metodou konečných objemů v cell–centered formulaci. Na každé straně konečného objemu se řeší Riemannův problém. Toto řešení je aproximováno užitím Roeho Riemannova řešiče. Pro zvýšení přesnosti metody v prostoru byla použita lineární rekonstrukce pomocí metody nejmenších čtverců. Pro diskretizaci v čase byla implementována linearizovaná zpětná Eulerova metoda. Výsledný systém lineárních rovnic je pak řešen pomocí GMRES metody s ILU předpodmíněním.

Dosažené výsledky

Použití metody pro turbulentní proudění je předvedeno na případu obtékání profilu RAE 2822 při $M_\infty = 0.734,\ \alpha = 2.54°,\ Re = 6.5 \cdot 10^6$. Byla použita síť 164×96, z toho na profilu bylo 124 buněk, vzdálenost středu první buňky od profilu byla přibližně $5 \cdot 10^{-6}$, což odpovídá přibližně $y^+ \approx 1$.

Pro výpočet oscilujícího profilu byl použit profil NACA 0012. Machovo číslo je rovno 0.755, rozkmit úhlu náběhu byl $\pm 2.5°$. Výsledky výpočtů jsou porovnány s experimentem v průbězích $c_m(\alpha)$, $c_n(\alpha)$ a rozložení c_p po tětivě při různých úhlech náběhu.

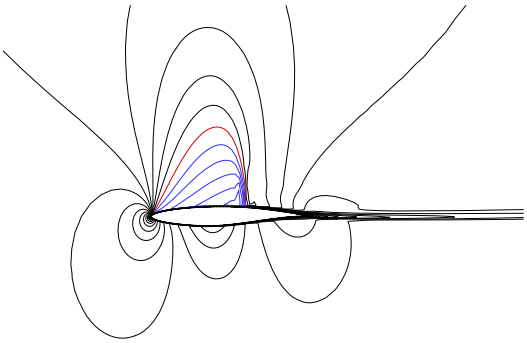

Turbulentní výpočet RAE 2822

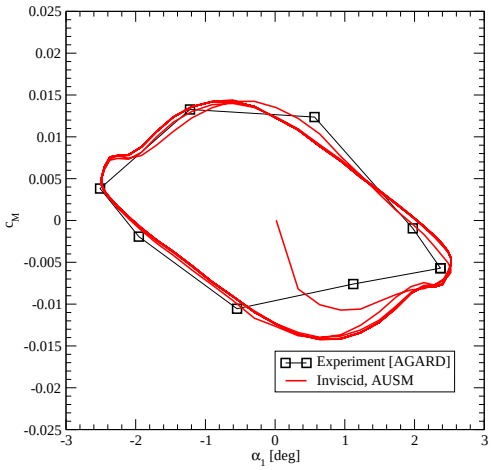

Oscilující profil NACA 0012

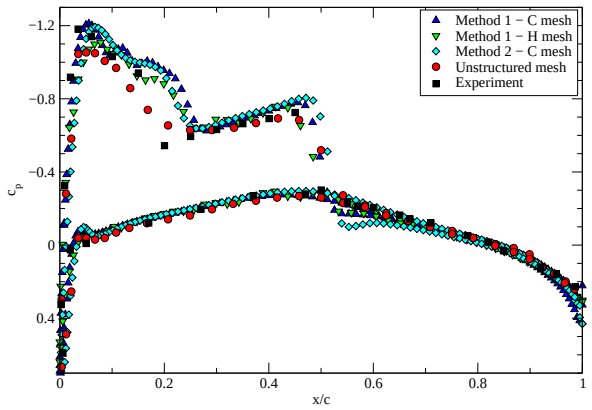

řez 65%

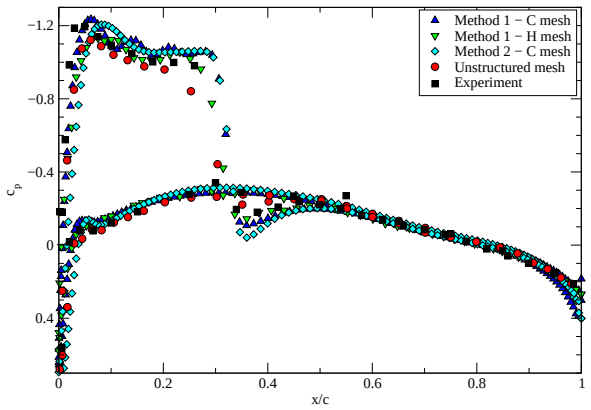

řez 90%

Křídlo Onera M6

Pro výpočet nevazkého obtékání křídla Onera M6 byl ve všech případech použit režim se vstupním Machovým číslem rovným 0,8395 a úhlem náběhu $3,06°$, který je dobře experimentálně zdokumentován. Ve schématu 1 byla použita H i C–O síť, ve schématu 2 C–O síť a ve schématu 3 byla použita s nestrukturovaná síť, přičemž jednotlivými objemy byly čtyřstěny. Vypočtené rozložení c_p v různých řezech křídla je porovnáno s měřením.

Poděkování: Práce byla realizována za finanční podpory z prostředků státního rozpočtu prostřednictvím projektu Ministerstva školství, mládeže a tělovýchovy MSM 684077001 a MSM 0001066902 a GAČR 201/05/04.

Literatura

1. Dobeš J., Fořt J., Furmánek P., Fürst J., Kladrubský M., Kozel K., Louda P.: Numerické řešení transsonického obtékání profilu a křídla II, VZLU V-1850/05, Praha, 2005
2. Dobeš J., Fořt J., Furmánek P., Fürst J., Kladrubský M., Kozel K.: Numerické řešení transsonického obtékání profilu a křídla III, VZLU R-4008, Praha, 2006

STUDY OF OPTIMIZATION OF LOBED NOZZLE FOR MIXING

Václav Dvořák
Technical University of Liberec, Department of Power Engineering Equipment, Liberec

Introduction

It is well known that mixing process in ejectors is effected by the shape of the trailing edge of primary nozzle [1]. The article deals with a simple optimization algorithm used for design of lobed nozzle. Influences of number and size of lobes are studied with the help of numerical simulation. It was found out that the objective function is not unimodal and one of the local optimum is represented by the circular nozzle.

Methods

First cycle of Rosenbrock method was used as an optimization procedure. Only one parameter was changed in each optimization step. The cross-section shape of the nozzle is given by relation with optimization parameters H and n

$$r = R + H/2 \cdot \cos(n\varphi), \qquad (1)$$

where $[\varphi, r]$ are polar coordinates of the mixing chamber, H represents the high of lobes and n number of lobes. R is middle radius of generating curve, which is calculated from the last optimization parameter, the equivalent diameter of the nozzle d_e.

Results and discussions

Changes of three optimization parameters during optimization are seen in fig. 1a. First run of the optimization between steps 0 and 15 began with $n = 8$ and $H = 4$ mm and led to the nozzle with negligible lobes of the high 1 mm. Second optimization between steps 16 and 22 began with less but bigger lobes, $n = 4$, $H = 8$. In this case the optimum was found for $n = 3$, $H = 10$, while the equivalent diameter is $d_e = 18.76$ mm.

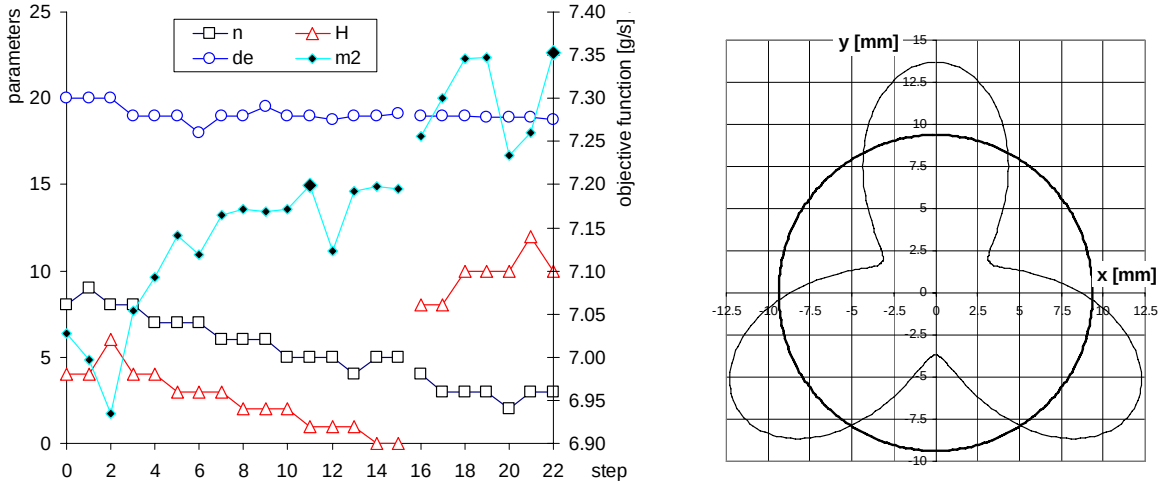

Fig. 1: a – process of optimization parameters and objective function during optimization; b – resulting shapes of the primary nozzle.

Resulting shapes of nozzles are in fig. 1b. Curves of kinetic energy given by radial and tangential velocity components are curried in fig. 2. The lobed nozzle has nonzero tangential velocity component, two peaks are evident on corresponding kinetic energy. The first maximum matches the place, where the free shear layer rising from tops of lobes encounter the boundary layer on the mixing chamber wall. The second maximum similarly matches the collision of boundary layer with free shear layer rising from the bottom of the lobes. Area between maximums can be called transition region of mixing.

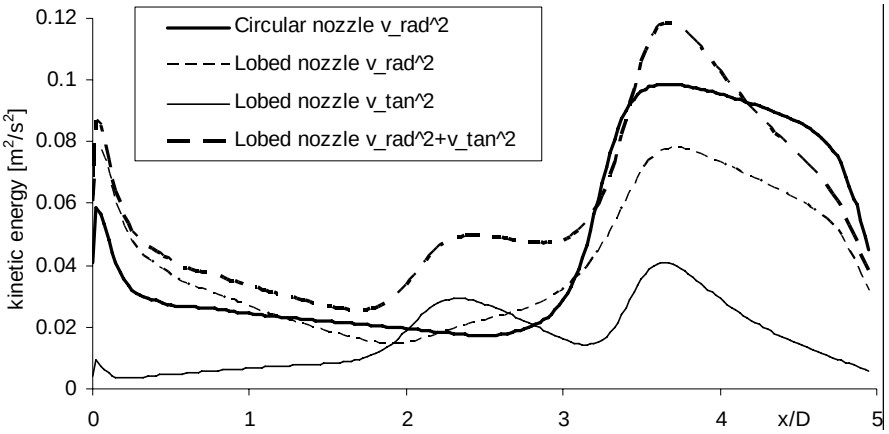

Fig. 2: Averaged kinetic energy given by radial and tangential velocity components during the mixing.

The growth of the free shear layer is higher for lobed nozzle because of larger bound between primary and secondary stream. Lobed nozzle has higher turbulent kinetic energy in the initial region of mixing and this energy grows more uniformly, than it is for circular nozzle, which has higher turbulent kinetic energy in the main region of mixing. The maximum of turbulent kinetic energy is in point of $x/D = 4.2$ for lobed nozzle, but $x/D = 5$ for circular nozzle. So we can consider that the mixing process is faster with the lobed nozzle.

Conclusion

A simple optimization of lobed nozzle for the ejector was made. It was shown that the mixing is faster when using lobed nozzle. A transition region of mixing was interpreted for using lobed nozzle. This region represents successive encounter of the free shear layer with the boundary layer. The real three-dimensional shape of the nozzle will be solved in next optimization.

Acknowledgments

This project was realized with financial support from the state resources by the Czech Science Foundation, grant no. 101/05/P298 "Optimization and control of mixing processes" and with financial support from MSM 4674788501.

References

[1] Ginevsky A.S., Vlasov Y. V., Karavosov, R. K.: Acoustic Control of Turbulent Jets, Springer-Verlag Berlin Heidelberg 2004, Germany.

[2] Dvorak, V.: Shape Optimization and Computational Analysis of Axisymmetric Ejector, 8th International Symposium on Experimental and Computational Aerothermodynamics of Internal Flows, July 2-5, 2007 - Ecole Centrale de Lyon, France, 2007.

[3] Hu H., Saga T., Kobayashi T., Taniguchi N.: A study on a lobed jet mixing flow by using stereoscopic particle image velocimetry technique, Journal Physics of Fluids, Volume 13, number 11, November 2001.

MICROSCALE AIRFLOW MODELLING USING THE IMMERSED BOUNDARY METHOD AND IMPLICIT LES.

Vladimír Fuka, Josef Brechler
Department of Meteorology and Environment Protection, Faculty of Mathematics and Physics, Charles University, Prague

Abstract
This contribution describes preliminary results dealing with computation of the turbulent flow around a square cylinder by 2D implicit large eddy simulation. The solid wall boundary conditions were described by the immersed boundary method.

1. INTRODUCTION

We choose this example as a part of the validation of the CFD model we are developing for flows in geometrically complex (urban, for example) areas. In this study we present the first results of the turbulence parametrization when so-called ILES method (see Drikakis, 2003 or Grinstein et al., 2007, for example) has been used. We used a square cylinder as a prototype of bluff body instead of a real 3D building. The reason for the 2D approach consists in the reduction in the amount of time needed for one model run. Obtained results were compared with other 2D and 3D simulations and also with the laboratory experiment.

2. NUMERICAL METHODS

The fractional step method (Brown et al., 2001) has been used for time discretisation of incompressible Navier-Stokes equations and for the spatial discretization we have used the finite volume method. The advective fluxes are formularized via the central high-resolution scheme of Kurganov and Tadmor, 2000). The turbulence was treated in the context of ILES (implicit large eddy simulation (Drikakis, 2003 or Grinstein et al., 2007). It was possible to use this approach thanks to using the Kurganov-Tadmor method that is, in fact, the high resolution non-linear one. The complex geometry on Cartesian grid can be implemented via the immersed boundary method (Kim et al., 2001).

3. RESULTS

Due to the computational resources and the present state of our model we performed the calculation in 2D. Although the turbulence is inherently the 3D phenomenon according to Bouris and Bergeles (1999) the 2D computation can capture most of important features of the quasi-two dimensional flow. In addition, in 2D one can use the grid with better resolution. Reynolds number for this experiment was equal to 5000 instead of more often used value about 22 000, because we use no wall model at this time.

Resulted flow-field of this experiment clearly shows the vortex shedding behind the bypassed obstacle. Strouhal number of this vortex shedding was 0.12, which is slightly less than 0.13–0.14 reported by Bouris and Bergeles, 1999. When the averaged horizontal velocity profile of this experiment at the centreline is compared with other

results, both numerical and laboratory, it can be seen that the recirculation length was 0.6, which is less than experimental value, but it is consistent with 2D calculations of Bouris and Bergeles, 1999.

4. CONCLUDING REMARKS

This experiment clearly shows some advances of the non-linear schemes when they are used for formulation of the advective terms. The properties of them enable us to use relatively simple approach for modelling the turbulent regime without utilizing the explicit subgrid model. For the future it can be seen from the results that when we want to model the higher Reynolds number flows that the application of some wall model will be necessary.

ACKNOWLEDGEMENTS

This research has been supported by the Grant Agency of the Czech Academy of Sciences, grant no. T400300414 and by the Grant Agency of the Czech Republic, grant no. 205/06/0727. This work is also supported by the Czech Ministry of Education, Youth and Sports via research plan no. MSM0021620860.

REFERENCES

Bouris B. and G. Bergeles, 1999, 2D LES of vortex shedding from a square cylinder, Journal of Wind Engineering and Industrial Aerodynamics 80, 31.

Brown D. L., R. Cortez and M. L. Minion, 2001, Accurate Projection Methods for the Incompressible Navier-Stokes Equations, J. Comput. Phys. 168, 464.

Drikakis D., 2003, Advances in Turbulent Flow Computations Using High-resolution methods, Progress in Aerospace Sciences 39, 405.

Grinstein, F. E., Margolin, L. G,.Rider, W. J., 2007. Implicit Large Eddy Simulation. Computing Turbulent Fluid Dynamics. Cambridge University Press: Cambridge.

Kim J., D. Kim and H. Choi, 2001, An Immersed-Boundary Finite-Volume Method for Simulations of Flow in Complex Geometries, J. Comput. Phys. 171, 132.

Kurganov A. and E. Tadmor, 2000, New High-Resolution Central Schemes for Nonlinear Conservation Laws and Convection-Diffusion Equations, J. Comput. Phys. 160, 241.

NUMERICAL SOLUTION OF STEADY AND UNSTEADY FLOW OVER A PROFILE IN A CHANNEL

Ing. Petr Furmánek[1], Ing. Jaromír Horáček DrSc[2], Prof. RNDr. Karel Kozel DrSc.[1]
1) Department of Technical Mathematics, Faculty of Mechanical Engineering, CTU in Prague.
2) Institute of Thermomechanics, Czech Academy of Science, Prague.

Abstract

The work deals with steady and unsteady solution of subsonic flow over a profile DCA 18% in a channel. For the computation the predictor-corrector MacCormack scheme with modified TVD Causon's artificial dissipation is used. Firstly, the steady state solution compared to the experimental results is presented. Than a simple unsteady model based on pressure change at the outlet area of the computational domain and finaly an unsteady model obtained with the use of ALE method (moving mesh) are presented.

Mathematical Model The behaviour of flow in both cases (steady and unsteady) is described by the system of compressible Euler equations in conservation form:

$$W_t + F_x + G_y = 0. \tag{1}$$

where the vector of conservative variables W and inviscid fluxes F, G are

$$W = \big\|\rho, \rho u, \rho v, e\big\|^T,\ F = \big\|\rho u, \rho u^2 + p, \rho uv, (e+p)u\big\|^T,\ G = \big\|\rho v, \rho uv, \rho v^2 + p, (e+p)v\big\|^T.$$

To solve this system following relation (equation of state for ideal gas) is added $p = (\kappa - 1)\Big[e - \frac{1}{2}\rho(u^2 + v^2)\Big]$, $\kappa = \frac{c_p}{c_v}$. We consider ρ - density, (u, v) - velocity vector, p - pressure and e - total energy per unit volume. Boundary conditions in the inlet area are given by three prescribed values, fourth one is extrapolated, whereas in the outlet area the conditions are given by prescribed pressure.

Nonstationary effects Two models of nonstationary flow have been implemented:

1. The first one was caused by pressure change in the outlet area of computational domain given by the condition $p_{outlet} = p_\infty(1 + 0.2sin(ft))$, where $f\,[s^{-1}]$ is frequency and $t\,[s]$ is time.
2. Considering the second model, prescribed oscillations of the profile fixed in the point of an elastic exis were given by the formula $\varphi = \varphi_0\, sin(2\pi ft)$, where $\varphi\,[rad]$ is the angle of rotation of the profile from equilibrium position and $\varphi_0\,[rad]$ is amplitude of oscillations. To treat the vibrating profile, the ALE method is used (the mesh is deformed with respect to profile rotation).

Numerical Scheme The system (1) was numericaly solved by finite volume method with the use of predictor-corrector MacCormack scheme (cell-centered form) with Jameson's and modified Causon's TVD artificial dissipation. Computational area was discretized by structured H-type mesh containing 156×112 cells (i.e. 17472). Development of nonstationary flow in the case of ALE computation was observed on behaviour of lift coefficient given as $c_n = \frac{\oint P dx}{\frac{1}{2}u_{ref}^2 \rho_{ref}}$.

Numerical Results At first, we present numerical results for stationary flow compared with experimental results of the Institute of Thermomechanics CAS followed by the results of mentioned nonstationary models.

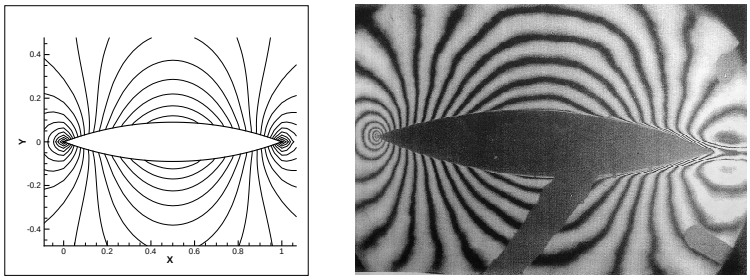

(a) Numerical result. (b) Experimental result.

Figure 1: DCA 18%, $M_\infty = 0.526$, $\alpha = 0^\circ$, isolines of Mach number, stationary computation.

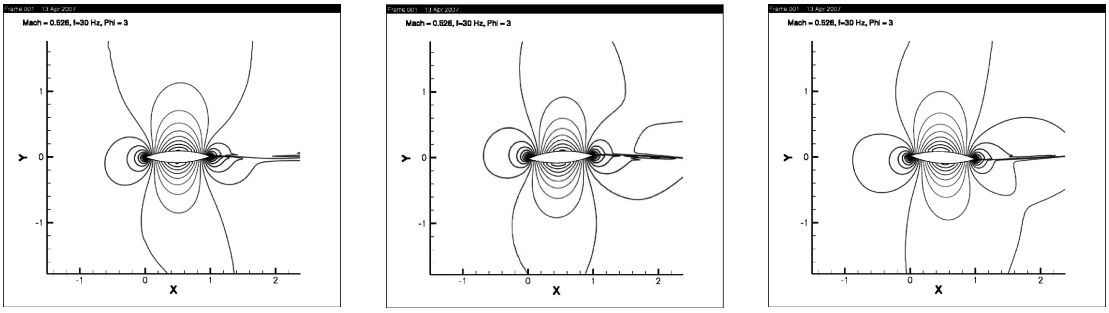

(a) $t = \frac{1}{2}\pi$. (b) $t = \frac{1}{2}\pi$. (c) $t = \frac{3}{2}\pi$.

Figure 2: DCA 18%, $M_\infty = 0.526$, Mach number isolines, unsteady computation, prescribed oscillations, ALE.

Conclusion The numerical method solving steady and unsteady inviscid compressible flow around a profile with one degree of freedom in a channel has been developed and preliminary results (showing all the flow characteristic as expected) have been presented. Future steps intended are implementing a model able to handle one or two number of freedom and also flow induced aeroelastic effects.

Acknowledgement *This work was partly supported by Research Plan MSM 6840770010 and grant GA AV CR c. IAA200760613.*

References

[1] Dvořák, R., Kozel, K.: Matematické modelování v aerodynamice, ČVUT, Praha 1996

[2] Feistauer, M.: Mathematical methods in fluid dynamics, Longman Scientific & Technical, New York, 1993.

[1]

NUMERICAL SIMULATION OF VISCOUS FLOW IN CHANNELS WITH MOVING WALLS

Martin Hadrava[1)], Miloslav Feistauer[1)] and Petr Sváček[3)]
[1)] **Charles University Prague, Faculty of Mathematics and Physics,** [2)] **Czech Technical University Prague, Faculty of Mechanical Engineering**

Introduction

The subject of this paper is the numerical simulation of viscous incompressible flow in two-dimensional channels with moving walls. The Navier-Stokes equations and the continuity equation are written in the ALE (Arbitrary Lagrangian-Eulerian) form and discretized in space by conforming finite elements satisfying the Babuška-Brezzi condition and in time by the second order backward difference formula (BDF). The applicability of the developed method is proved by the solution of a test problem of flow in a channel with a wall moving in a prescribed way.

Formulation of the problem

We consider the flow in a bounded 2D domain Ω_t depending on time t with boundary $\partial\Omega_t = \Gamma_D \cup \Gamma_O \cup \Gamma_{W_t}$, where Γ_D represents inlet or parts of impermeable fixed walls, Γ_O is outlet and Γ_{W_t} represents moving impermeable walls.

The dependence of the domain on time is taken into account with the aid of a regular ALE mapping $\mathcal{A}_t : \overline{\Omega}_0 \to \overline{\Omega}_t$, i.e. $\boldsymbol{X} \mapsto \boldsymbol{x} = \boldsymbol{x}(\boldsymbol{X}, t)$. Further, we define the ALE velocity: $\tilde{\boldsymbol{w}}(\boldsymbol{X}, t) = \frac{\partial}{\partial t}\boldsymbol{x}(\boldsymbol{X}, t) = \frac{\partial}{\partial t}\mathcal{A}_t(\boldsymbol{X})$, $\boldsymbol{w}(\boldsymbol{x}, t) = \tilde{\boldsymbol{w}}(\mathcal{A}_t^{-1}(\boldsymbol{x}), t),\ t \in [0, T],\ \boldsymbol{x} \in \overline{\Omega}_t$ and the ALE derivative of a function $f = f(\boldsymbol{x}, t)$: $\frac{D^A}{Dt} f(\boldsymbol{x}, t) = \frac{\partial \tilde{f}}{\partial t}(\boldsymbol{X}, t)|_{X = \mathcal{A}_t^{-1}(x)}$, where $\tilde{f}(\boldsymbol{X}, t) = f(\mathcal{A}_t(\boldsymbol{X}), t),\ \boldsymbol{X} \in \Omega_0$.

The Navier-Stokes system attains the following ALE form:

$$\mathrm{div}\boldsymbol{u} = 0, \quad \frac{D^A}{Dt}\boldsymbol{u} + ((\boldsymbol{u} - \boldsymbol{w}) \cdot \nabla)\,\boldsymbol{u} + \nabla p - \nu\Delta\boldsymbol{u} = 0. \tag{1}$$

Here $\boldsymbol{u}$ is the fluid velocity, p is the pressure and ν is the kinematic viscosity. System (1) is equipped with the following initial and boundary conditions:

$$\boldsymbol{u}(\boldsymbol{x}, 0) = \boldsymbol{u}_0(\boldsymbol{x}),\ \boldsymbol{x} \in \Omega_0, \qquad \boldsymbol{u}|_{\Gamma_D \times (0,T)} = \boldsymbol{u}_D, \tag{2}$$

$$\boldsymbol{u}|_{\Gamma_{W_t} \times (0,T)} = \boldsymbol{w}|_{\Gamma_{W_t}, \times (0,T)}, \quad -p\boldsymbol{n} + \nu\frac{\partial \boldsymbol{u}}{\partial \boldsymbol{n}} = -p_{ref}\boldsymbol{n} \quad \text{on } \Gamma_O \times (0, T), \tag{3}$$

where p_{ref} is a given reference pressure.

Now we describe the construction of the ALE mapping. We assume that the inlet and outlet are straight segments given by the conditions $X_1 = a$ and $X_1 = b$, respectively, where $a,\ b \in \mathrm{R},\ a < b$ and the walls are represented by the graphs of smooth functions

$$x_2 = \phi(X_1, t),\ X_1 \in [a, b], t \in [0, T] \ \text{(upper wall)},$$

$$x_2 = \varphi(X_1, t),\ X_1 \in [a, b], t \in [0, T] \ \text{(lower wall)},$$

[1]The research of M. Feistauer and P. Sváček was a part of the project No. 201/05/0005 of the GACR. The research of M. Hadrava was a part of the project No. 7486/2007 of the GAChU.

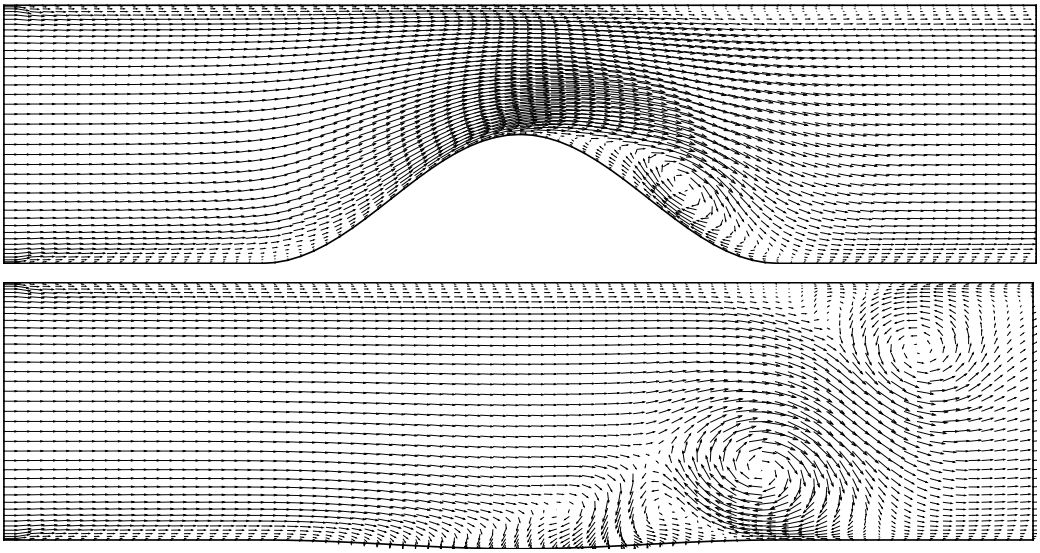

Figure 1: Velocity vectors at $t = 1.7$ and $t = 3.3$

where $\phi(X_1, t) > \varphi(X_1, t)$ for all $X_1 \in [a, b],\ t \in [0, T]$. The ALE mapping is given by the relations

$$x_1 = X_1,\ \ x_2(\boldsymbol{X}, t) = \varphi(X_1, t) + \frac{X_2 - \varphi(X_1, 0)}{\phi(X_1, 0) - \varphi(X_1, 0)}(\phi(X_1, t) - \varphi(X_1, t)). \qquad (4)$$

Discretization and results

For the time discretization we introduce a time partition $t_k = k\tau$, $k = 0, 1, \ldots,\ \tau > 0$ and use the second order backward difference formula. The space discretization is carried out by the stabilized finite element method applied over a triangular mesh and using the Taylor-Hood elements. This means that the velocity components are approximated by continuous piecewise quadratic functions and the pressure is approximated by continuous piecewise linear elements. The stabilization, which is necessary due to large Reynolds numbers, is carried out by the SUPG method according to [1]. As a result we obtain on each time level t_k a strongly nonlinear algebraic system, which is solved with the aid of the Oseen iterations, as is described in [2]. It appears that the worked out method is accurate and robust. It will be further combined with equations describing the deformation of elastic walls.

In the test problem we considered the following data: $a = -2,\ b = 2,\ \varphi(X_1, t) = \sin t\ (\cos(\pi X_1) + 1)/4, \quad X_1 \in [-1, 1], \varphi(X_1, t) = 0, \quad X_1 \in [-2, 1) \cup (-1, 2], \phi(X_1, t) = 1, \quad X_1 \in [-2, 2],\ t \in [0, T]$. Figure 1 shows the velocity field at time $t = 1.7$ and $t = 3.3$.

References

[1] T. Gelhard, G. Lube, M.A. Olshanskii, J.-H. Starcke: Stabilized finite element schemes with LBB-stable elements for incompressible flows. J. Comput. Appl. Math. 177 (2005), 243-267.

[2] P. Sváček, M. Feistauer, J. Horáček: Numerical simulation of flow induced airfoil vibrations with large amplitudes. J. of Fluids and Structures, 23 (2007), 391-411.

NONLINEAR LIFTING LINE METHOD FOR AIRPLANE WINGS

Jaroslav Hájek [1)], **Zdeněk Pátek** [1)], **Pavel Šafařík** [2)]

[1/] **Aeronautical Research and Test Institute, Prague, Czech Republic**
[2/] **Czech Technical University in Prague, Faculty of Mechanical Engineering, Prague, Czech Republic**

Introduction

An important phase in aircraft design is the evaluation of basic aerodynamic characteristics of the aircraft's wing, including lift curve, drag polar and momentum curve. This is often intended as a preliminary analysis prior to full-configuration CFD computations, or as a low-fidelity evaluation suitable for design optimization. For these purposes, full 3D viscous CFD simulations are often too costly, especially with the optimization as a goal.

The classical Prandtl wing theory is a well-known and long-established method for calculating the lift and induced drag of a slender wing. It leads to a linear system and is very fast compared to CFD. It is, however, unable to predict the nonlinear part of the wing lift curve in the area of high angles of attack (stall). An extension of the Prandtl solution is achieved by assuming a general nonlinear dependence of the local lift on the local angle of attack. This results into a system of nonlinear equations that has to be solved iteratively. Sophisticated numerical methods may be employed.

Method description

The computation proceeds as follows: first, the 2D viscous airfoil data are collected for several sections of the wing, distributed (non-uniformly) along the wing. The flowfield around the wing is then approximated by a system of horsehoe vortices, each consisting of a bound vortex segment and two free semi-infinite vortex filaments. These vortex elements are arranged in such a manner that the bound segments approximate the wing's quarter-chord line and the free segments follow the direction of freestream velocity. The unknown vortex stregths (circulations) are then determined by imposing a balance condition on the generated forces: The lift for each bound segment is calculated in two ways – first, calculating the local angle of attack (from induced velocity) and interpolating the 2D viscous data, and second, using the Kutta-Joukowski law. The balance condition requires these two quantities to be (approximately) equal on each bound segment. This in turn translates into a set of rather complicated nonlinear equations for the circulations (involving the interpolated 2D viscous data). These can be solved using appropriate iterative numerical methods. Furthermore, to obtain the whole wing lift curve, it is necessary to perform this computation repeatedly for

varying angle of attack.

The method allows for evaluation of the total lift, induced drag, viscous drag and momentum of the aircraft wing, provided that the appropriate quantities are supplied for the 2D viscous data. Also available are spanwise distributions of these quantities, which can be useful in material analysis and design, or to determine if fall-safety criteria are satisfied. Even when a fine stepping of the angle of attack is used (necessary in the stall area), the method is still by orders of magnitude faster than 3D vsicous CFD analysis of the wing. An attractive property from a technical perspective is the possibility to employ experimental (e.g. wind-tunnel) data for the 2D viscous part. For these reasons, we consider this method an useful tool for slender wing aerodynamics.

Example

An example comparing a linear method (Glauert solution of Prandtl's problem) with the described nonlinear method on a simple trapezoidal wing is shown in Illustration 1. Plotted are the lifting lines, i.e. dependencies of wing lift coefficient on the angle of attack.

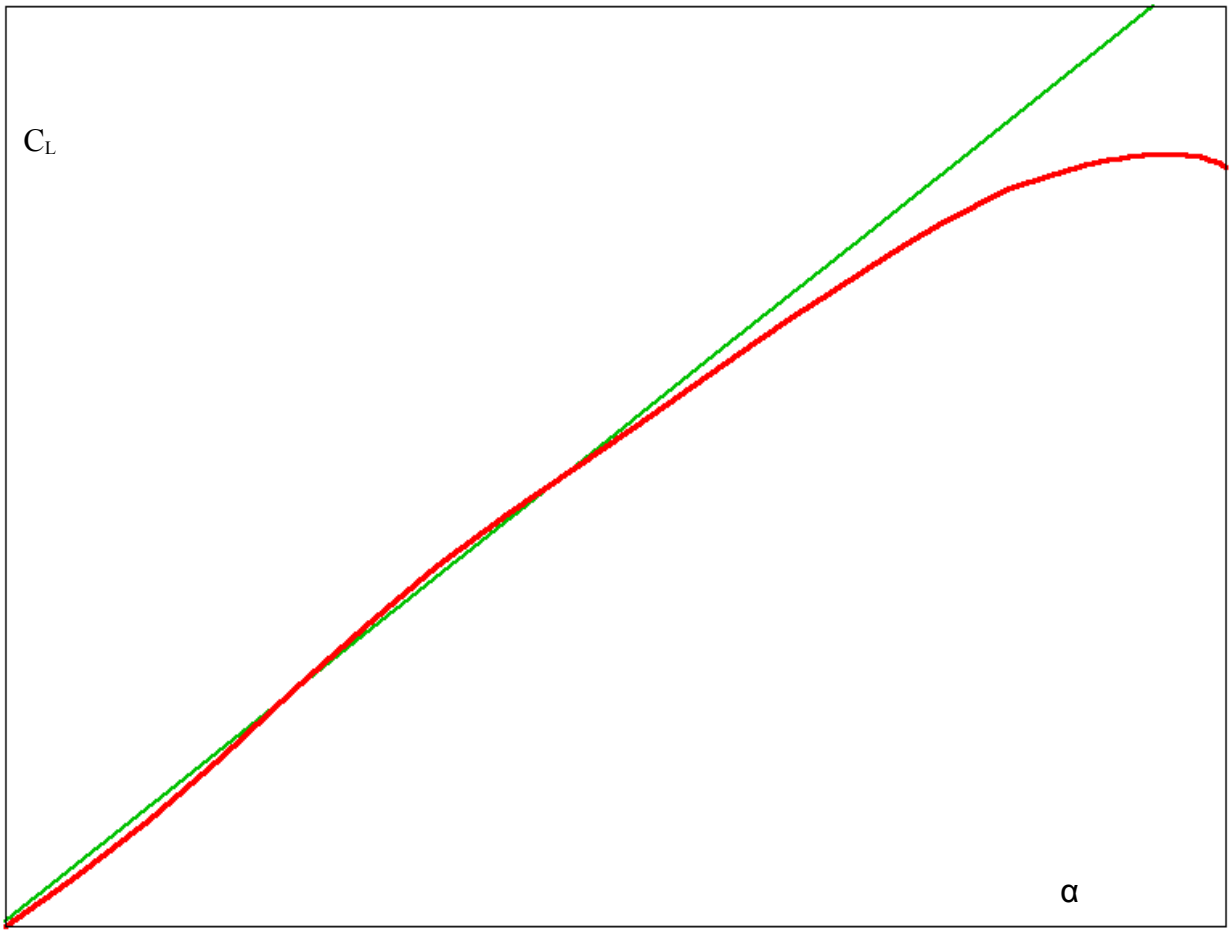

Illustration 1: Scheme of linear and nonlinear lifting line

NUMERICAL SOLUTION OF COMPRESSIBLE TURBULENT FLOWS USING EARSM MODEL

J. Holman, J. Fürst
CTU in Prague, Faculty of Mechanical Engineering, Department of Technical Mathematics, Prague

Introduction

This article deals with the numerical solution of compressible turbulent flows in aerodynamics. Compressible turbulent flow is described by the system of Favre averaged Navier-Stokes equations, which are closed by the explicit algebraic Reynolds stress model (EARSM) of Wallin and Johansson. The averaged Navier-Stokes equations together with EARSM model of turbulence are discretized by the finite volume method based on HLLC Riemann solver with piecewise linear WENO reconstruction and explicit two-stage TVD Runge-Kutta method. Source terms in transport equations of turbulence model are treated by point implicit method for better stability of explicit scheme. The numerical method is validated by comparison to theoretical results for the subsonic flow around the flat plate and experimental results for the transonic flow around the RAE 2822 airfoil.
From test cases is clear, that EARSM model improve prediction accuracy in comparison to the two equation eddy-viscosity models. EARSM model archived similar results as Kok's TNT model in case 9 (flow around the RAE 2822), but in the case 10, where separation of boundary layer occurs, EARSM model predicted much better shockwave position then TNT model.

References

[1] Batten, P., Leschziner, M. A., Goldberg, U. C.: Average-State Jacobians and Implicit Methods for Compressible Viscous and Turbulent Flows, Journal of computational physics 137, 1997

[2] Fořt, J., Kozel, K., Fürst, J., Halama, J., Dobeš, J.: Numerická simulace proudění I, skriptum ČVUT FS, 2005

[3] Holman, J.:Numerické řešení stlačitelného turbulentního proudění ve vnější a vnitřní aerodynamice, Diplomová práce ČVUT FS, 2007

[4] Kok, J. C.: Resolving the Dependence on Freestream Values for $k-\omega$ Turbulence Model, AIAA Journal, Vol. 38, No. 7, 2000

[5] Příhoda, J., Louda, P.: Matemetické modelování turbulentního proudění, skriptum ČVUT FS, 2006

[6] Wallin, S.: Engineering turbulence modeling for CFD with focus on explicit algebraic Reynoldes stress models, Ph.D. these, Royal Institutte of Technology, 2000

[7] Wilcox, D. C.: Turbulence modeling for CFD, DWC Industries, 1994

Acknowledgement: The work was supported by the Research Plan No. 6840770010 of the MSMT CR.

Transonic turbulent flow around the RAE 2822 airfoil

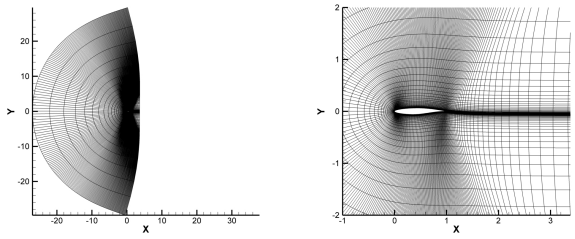

(a) Computational domain and mesh (b) Detail of mesh in the area of profile

Figure 1: Computational domain and mesh for the flow around the RAE 2822 airfoil

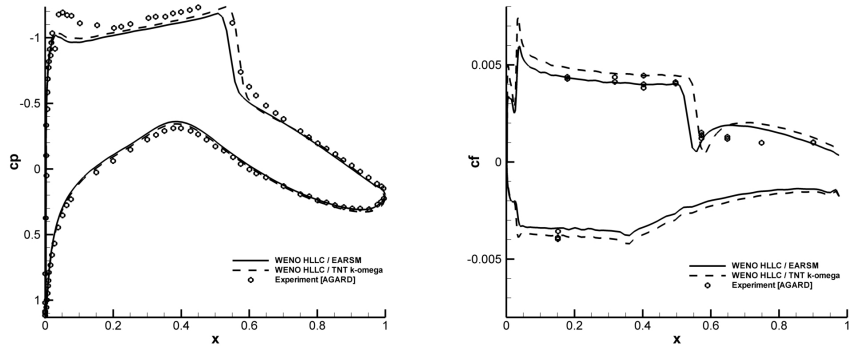

(a) Distributions of pressure coefficient (b) Distributions of friction coefficient

Figure 2: Case 9 ($M_\infty = 0.734, \alpha_\infty = 2.54°, Re = 6.5 \cdot 10^6$)

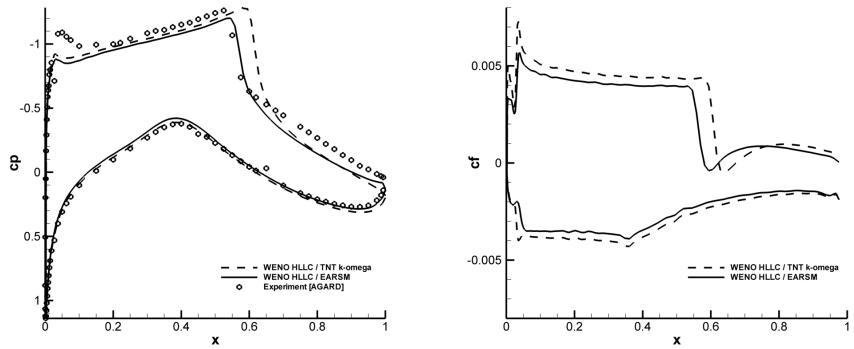

(a) Distributions of pressure coefficient (b) Distributions of friction coefficient

Figure 3: Case 10 ($M_\infty = 0.754, \alpha_\infty = 2.57°, Re = 6.2 \cdot 10^6$)

PROUDĚNÍ V KAVITĚ VYVOLANÉ SMYKOVÝM TOKEM PŘI VELKÝCH REYNOLDSOVÝCH ČÍSLECH

Shear-driven cavity flow at high Reynolds numbers

Zdeněk Chára, Bohuš Kysela, Bohumír Hoření
Ústav pro hydrodynamiku AV ČR, v. v. i., Praha 6

Abstrakt
V příspěvku jsou prezentovány výsledky měření rychlostních polí v kavitě čtvercového průřezu, kdy je proudění vyvolané smykovým tokem. Hodnoty Reynoldsových čísel jsou v rozsahu 12000-100000. Pro měření byla použita metodika PIV s kontinuálním zdrojem světla. Získané výsledky byly ve vybraných profilech porovnány s měřeními pomocí LDA. Současně byly pro stejné rozsahy Reynoldsových čísel prováděny numerické simulace proudění pomocí standardního turbulentního modelu k-ω, SST.

Experimentální zařízení
Experimenty byly realizovány na hydraulickém uzavřeném kanálu a rozměrech 2 x 20 cm. Dálka kanálu byla 2 m. Voda byla oběhovým čerpadlem dopravována do zásobní nádrže, kde byla pomocí stavitelného přepadu udržována konstantní hladina. Ve vzdálenosti 1.5 od vtoku byla přes celou šířku dna umístěna kavita o rozměrech 10 x 10 cm. Schématický řez kavitou je ukázán na obr. 1. Celý model byl zhotoven z plexiskla. Pro vlastní měření byly použity dvě optické metody. Jednak byl použit dvousložkový systém LDA, s jehož pomocí je možné proměřit strukturu turbulentního proudu v jednotlivých bodech.

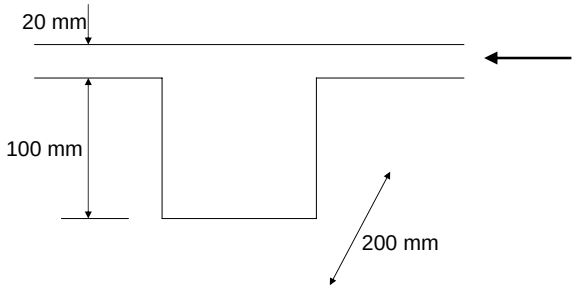

Obr. 1 Schématický řez kavitou

Vedle LDA byl také použit zjednodušený systém PIV. V současné době je k dispozici pouze rychlá kamera Redlake MotionPro X III. Místo pulzního laseru byl použit kontinuální světelný zdroj LEICA KL2500 (výkon 250W) s optickým kabelem se štěrbinou vybavenou válcovou čočkou, která umožňuje fokusovat výstupní paprsek (minimální šířka paprsku je cca 3 mm). Pro vyhodnocení PIV snímků byl použit program GPIV – GNU General Public License (GPL) s využitím implementovaných algoritmů (Gauss - pixel interpolace, Validita- normalizovaný medián), [1]. Velikost vyhodnocovaných oblastí byla nastavena na 32 x 32 s překrytím 50%.
Numerické simulace byly prováděny v prostředí Fluent 6.3, kde bylo simulováno 2D proudění v kanále a kavitě. Délka vstupního úseku byla zvolena 1 m. Byla použita nestrukturovaná síť, která byla zahuštěna v okolí stěn a na rozhraní kanálu a kavity. Pro

vlastní výpočet byl použit turbulentní model k-ω, SST v nestacionárním režimu. Výpočty probíhaly na počítači IBM se 4 procesory Power 5 a 32 GB RAM.

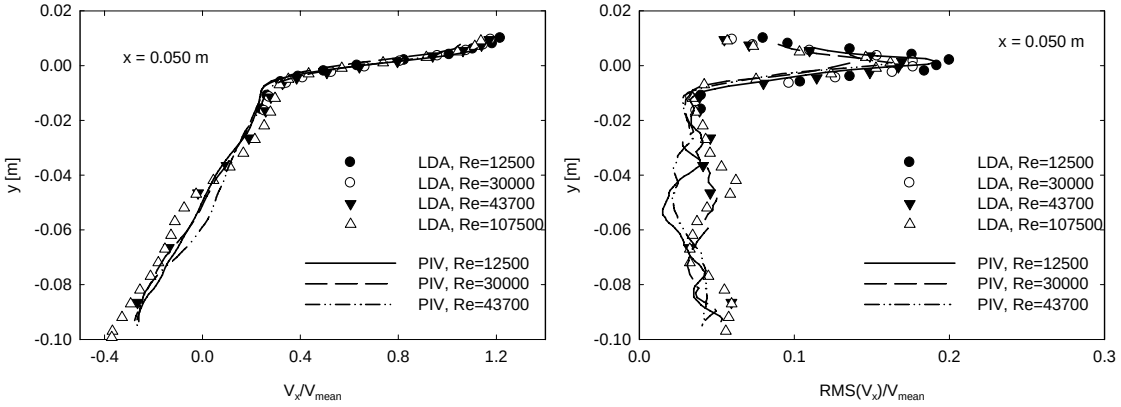

Obr. 2 Průběhy podélné složky rychlosti a RMS hodnot na svislé ose kavity

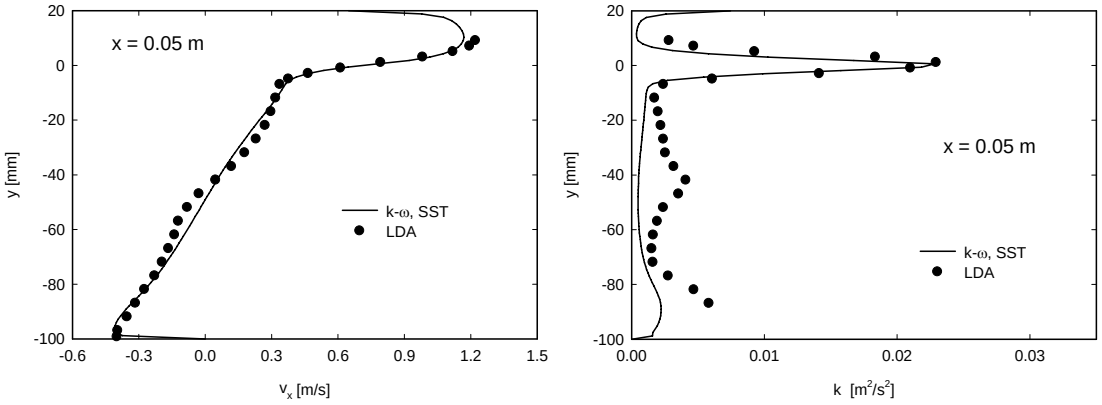

Obr. 3 Porovnání měřených a vypočtených hodnot podélné složky rychlosti a kinetické energie na svislé ose kavity (Re=107500)

Závěr

Byly měřeny rychlostní profily pomocí LDA a zjednodušené metody PIV. Současně byly provedeny numerické simulace pomocí standardního modelu k-ω, SST. Z porovnání obou experimentálních technik se ukazuje, že i zjednodušená metoda PIV dává uspokojivé výsledky a rozdíly mezi PIV a LDA se pohybují do cca 12%, obr.2. Shoda testované numerické simulace s experimentálními daty byla v měřených profilech velice dobrá, a to i v případě průběhů kinetické energie, obr. 3. Přehled dosažených výsledků je prezentován v plné verzi na CD.

Poděkování

Projekt byl řešen za finanční podpory projektů Grantové agentury ČR č. 101/05/0675 a 103/07/0136 a výzkumného záměru č. AV0Z20600510.

Literatura

[1] http://gpiv.sourceforge.net/dac.html

ON TURBULENT SPOTS DURING BOUNDARY LAYER BY-PASS TRANSITION

Pavel Jonáš* , Witold Elsner[+] , Oton Mazur*, Václav Uruba*, Marian Wysocki[+]
***Institute of Thermomechanics AS CR, v.v.i., Praha**
[+]Institute of Thermal Machinery, TU Czestochowa

The transition from laminar to turbulent flow structure depends on the specific type of flow and on the type of the acting disturbances that influence the process. Regardless to this fact, the final phase of laminar boundary layer transition starts with the occurrence of first turbulent spots. Emmons [1] first reported spots as isolated regions of strong fluctuations that are stream-wise carried, growing in size and coalescing with neighbours. Spots appear irregularly in time and at arbitrary locations of the boundary layer. Spots are an essential feature of transition to turbulence; they appear as the building blocks of boundary layer turbulence, they control the length of the transition region etc. The turbulent spots followed by calmed regions are defined structures that dominate the last stage of transition. Spots production controls the length of transition region e.g. Narasimha [2]. The spot creation rate, growth characteristics and the merger of turbulent spots lead to fully developed turbulent flow. A brief summary on turbulent spot and calmed region was compiled in [3].
The effect of the free stream turbulence (FST) level *Tu* on the location of transition onset is known as very important since forties of 20th century [4]. The authors clearly proved (Jonáš et al. [5, 6]) that the length scale L_e of the FST also influences the start of boundary layer by-pass transition. Later also Roach and Brierley [7] and Brandt et al. [8] emphasized the importance of both FST scales, of the velocity scale and the length one, on the laminar boundary layer receptivity and transition onset. But a clear physical notion on the role of the FST length scale in transition process is not elaborated yet. The authors believe that the investigation of the spots behaviour during transition at various FST scales can contribute to the problem explanation. They linked up the experiences of instantaneous wall-friction, $\tau_w(t)$ measurement and conditional analysis (Jonáš et al. [9, 10],) with the experience of the spot detection procedure by using the wavelet transform (Elsner et al. [11]) to perform a preliminary study. The initial results are presented in this contribution.
The flat plate boundary layer was investigated experimentally in the close circuit wind tunnel IT Prague (0.5 x 0.9) m^2 on a smooth wooden plate (zero pressure gradient) 2.75 m in length. Boundary conditions correspond to the ERCOFTAC Test Case T3A+: free stream velocity U_e = 5 m/s and the FST level *Tu* = 0.03 with different length parameters L_e = 3.8, 5.9 and 33.4 mm respectively in the leading edge plane (x = 0). Plane grids of different geometry (cylindrical rods and square holes) placed across the flow produce homogeneous nearly isotropic turbulence. The applied CTA measuring method and procedures allow determine digital records (25 kHz, 750000 samples) of the instantaneous velocity *U (t, x, y)* and wall-friction τ_w *(t)* rows and carry out relevant statistical analyses. Valuable information on turbulent spots role in transition process can be deduced with regard to Emmons ideas and Narasimha concept of intermittency. The flow intermittency analysis was based on digital records of $\tau_w(t)$. The procedure is very similar to that one described by Hedley and Keffer [12] and Elsner and Kubacki [13]. Finally the conditionally averaged distributions of the wall friction during periods with turbulent character and the laminar can be determined as was demonstrated in e.g. [10] and the transitional intermittency factor $\gamma(x)$ is calculated

$$\gamma\left(Re_x\right) = 1 - exp\left[-\left(Re_x - Re_{x_{tr}}\right)^2 n^* \sigma\right]; \quad Re_x = xU_e/\upsilon; \quad n^*\sigma = n\sigma\upsilon^2/U_e^3$$

here the parameter $n^*\sigma$ stands for the dimensionless spot production rate. Next n denotes the spot production rate, σ stands for the Emmons's non-dimensional propagation parameter, ν and U_e are kinematic viscosity and external flow velocity.

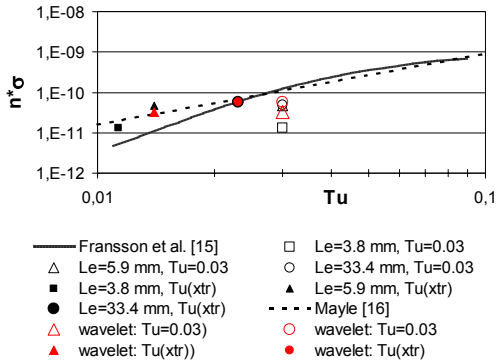

Figure 1 Dimensionless spot production rate versus turbulence level.

Other approach to the investigation of turbulent spots during boundary layer transition represents the application of wavelet transform of digital records $\tau_w(t,x)$. Elsner et al. [11] derived an original detection procedure employing the wavelet analysis. The spot could be identified based on the frequency contents because much finer turbulence scales than the surrounding flow characterize the spot's interior. The wavelet transform is able detect particular frequency components and localize the investigated event in time. Elsner et al. [11] selected the Morlet wavelet transform and all calculations performed with the Wavelet Toolbox of Matlab software [14]. Using this procedure it was possible determine the dimensionless spot production rate $n^*\sigma$ and distributions of reduced number and mean length of the identified turbulent regions arising from turbulent spots. Results (Fig. 1) following from the application of the Narasimha's intermittency concept are in a satisfactory accord with those received from the wavelet analysis mutually and also with the results of Fransson [15] and model of the spot production rate proposed by Mayle [16] if the local turbulence level – at the location of transition start is considered. The observed maximum of the spot occurrence was near $\gamma = 0.25$ because later the spot production is effectively inhibited due to calming (see Ramesh and Hodson [17]).

Acknowledgement: This work was supported by the Grant Agency of the Academy of Sciences of the Czech Republic (A200760614), by Ministry of Education, Youth and Sports CR (KONTAKT No. 37) as well as by Polish State Committee for Scientific Research under the statutory funds BS-01-103-301/2004/P.

References:

[1] Emmons H.W. (1951) J. Aero Sci. 18, 490-498.
[2] Narasimha R. (1985), Prog. Aerospace Sci., 22, 29-80.
[3] Jonáš P. (2007) Engng. Mechanics, May 14-17 2007, Svratka (ISBN 978-80-87012-06-2), 109-110 (full text CD ROM).
[4] Schubauer G.B. and Skramstad H.K. (1948), NACA–TR-909.
[5] Jonáš P. (1997), ZAMM 77, S145-S146.
[6] Jonáš P., Mazur O. and Uruba V. (2000), Eur.J.Mech. B 19, 707-722.
[7] Roach P.E. and Brierley D.H. (2000), ASME Paper 2000-GT-0278.
[8] Brandt L., Schlatter P. and Henningson D.S. (2004), J. Fluid Mech. 517, 167-198.
[9] Jonáš P., Mazur O. and Uruba V. (2000), ZAMM 79, S691-S692.
[10] Jonáš P., Mazur O. and Uruba V. (2006) Colloquium Fluid Dynamics Proc., October 25-27, (ISBN 80-87012-01-1), 67-70.
[11] Elsner W., Wysocki M. and Drobniak S. (2006), Chemical and Process Engineering, 27, 935-950.
[12] Hedley T.B. and Keffer J.F. (1974), J. Fluid Mech. 64, 625-644.
[13] Elsner W. and Kubacki S. (2000) Application of intermittency in boundary layer analysis. ITM TU Czestochowa.
[14] Misiti M.,Misiti I., Oppenheim G. and Poggi J.M.(2000) *MATLAB*. The MathWorks Inc.
[15] Fransson J.H.M., Matsubara M. and Alfredsson P.H. (2005), J. Fluid Mech. 527, 1-25.
[16] Mayle R.E. (1991) J. Turbomach. 113, 509-537.
[17] Ramesh N. and Hodson H.P. (1999) ImechE Conference Transactions C557/084.

MAGNUS AND DRAG FORCES ACTING ON GOLF BALL

A. Kharlamov, Z. Chara, P. Vlasak
Institute of Hydrodynamics AS CR, v.v.i., Prague

The paper describes the results of experiments with a rotating golf ball moving quasi-steadily in calm water. The dimensionless drag force coefficient and Magnus force coefficient were determined for ranges of translational and rotational Reynolds numbers: $1.2 \cdot 10^4 < Re < 1.6 \cdot 10^4$ and $3.8 \cdot 10^3 < Re_\omega < 2.7 \cdot 10^4$, respectively.

The ball accelerated in a special chute with gravity, and then it continued its motion in a vessel with water along approximately straight line. The motion of the ball was recorded by a digital video camera. From the video frames the Cartesian coordinates *x(t)*, *y(t)* of the ball centre and the angle of ball rotation *φ(t)* as a functions of time were read using the free software Graph2Digit.

From the equation of ball motion

$$\Omega\rho\frac{d\vec{u}}{dt} = \vec{F}_d + \vec{F}_g + \vec{F}_M + \vec{F}_H + \vec{F}_m\,, \tag{1}$$

and directions of the forces (see Figure 1) the formulae for calculation of dimensionless drag force coefficient and Magnus force coefficient can be derived:

$$C_d = \frac{\left\{\vec{F}_g + \vec{F}_H - \Omega\left(\rho + C_m\rho_f\right)\frac{d\vec{u}}{dt}\right\}\vec{\tau}}{\frac{\pi d^2}{4}\rho_f\frac{u^2}{2}},\quad C_M = \frac{\left\{\Omega\left(\rho + C_m\rho_f\right)\frac{d\vec{u}}{dt} - \vec{F}_g - \vec{F}_H\right\}\vec{n}}{\Omega\rho_f\left[\vec{\omega}\times\vec{u}\right]\vec{n}}, \tag{2}$$

where Ω is the ball volume, ρ is the ball density, u is the ball velocity, F_d, F_g , F_M, F_H, F_m are drag force, submerged gravitational force, Magnus force, history force, added mass force, $C_m = 0.5$ is the dimensionless added mass coefficient, ρ_f is the water density, $\vec{\tau}$ is the tangent unit vector to the ball trajectory, d is ball diameter, $\vec{n}$ is the normal unit vector to the ball trajectory, ω is the angular velocity of the ball.

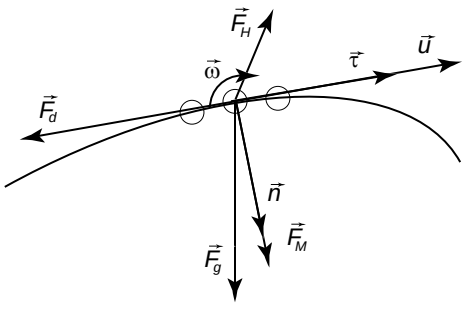

Figure 1 The forces acting on the rotating ball moving translationally in calm water.

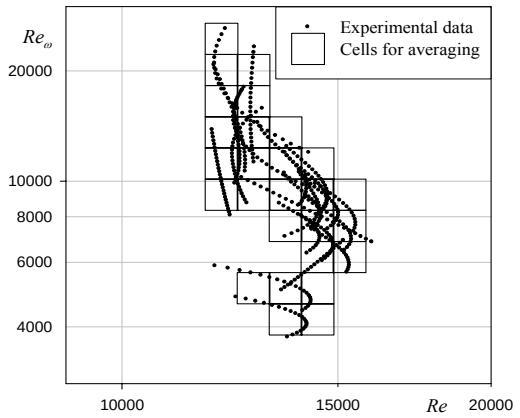

Figure 2 The $Re \times Re_\omega$ map of the experimental data and the cells for averaging.

Experimental data $x(t)$, $y(t)$ and $\varphi(t)$ were fitted using the least square method with simple functions. Then the first and the second time derivatives of the functions were calculated. The coefficients of interest and the corresponding values of Re and Re_ω were calculated numerically for each frame of a particle trajectory, using formulas (2). The experimental area Re vs. Re_ω was split into 5x10 cells. For a cell the coefficients C_d and C_M were calculated as an arithmetic mean of all data points in the cell, see Figure 2.

The plots of drag and Magnus coefficients compared with data of other authors (Davies (1949), Briggs (1959), Bearman & Harvey (1976), Watts & Ferrer (1987)) are presented on Figures 3 and 4. As can be seen from the comparison, the values of the coefficients and its trends are in a good accordance with data of the other authors. Within the accuracy of such investigations, it can be said that the results of the Magnus force on baseball do not differ much from that on golf balls.

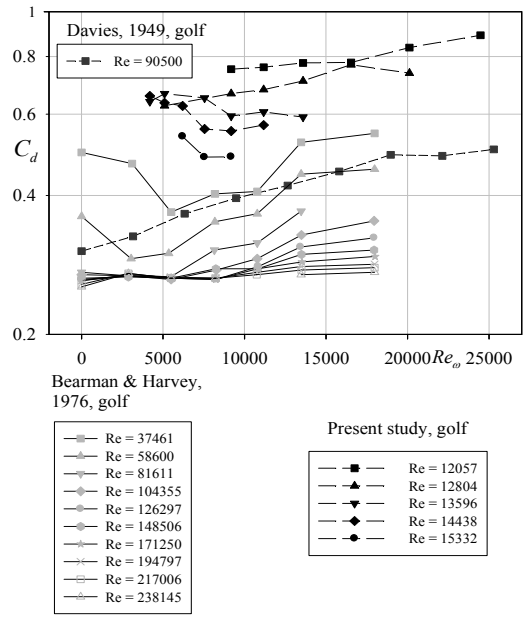

Figure 3 Drag force coefficient.

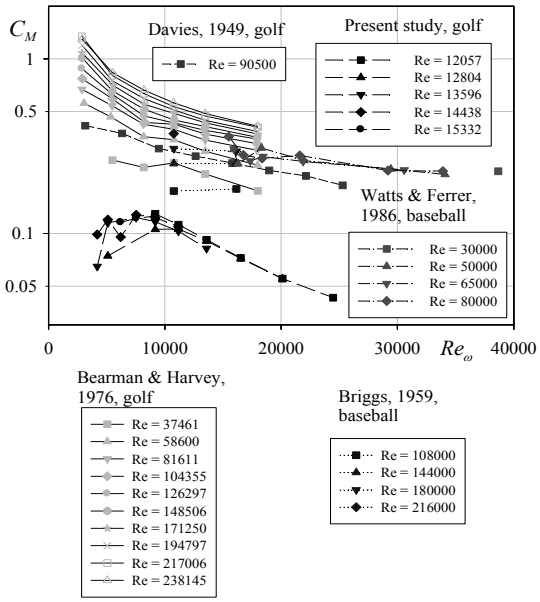

Figure 4 Magnus force coefficient.

Acknowledgements

The support under the project No. A200600603 of the Grant Agency of Academy of Sciences of the Czech Republic and under Institutional Research Plan No. AV0Z20600510 of Academy of Sciences of the Czech Republic is gratefully acknowledged.

References

Bearman, P.W. & Harvey, J.K. (1976) Golf ball aerodynamics. *Aeronautical Quarterly*, May, pp. 112-122.

Briggs, L.J. (1959) Effect of spin and speed on the lateral deflection(curve) of a Baseball; and the Magnus effect for smooth Spheres. *American Journal of Physics,* 27, pp. 589-596.

Davies, J. M. (1949) The aerodynamics of golf balls. *J. Appl. Phys.,* 20, pp. 821-828.

Watts, R.G. & Ferrer, R. (1987) The lateral force on a spinning sphere: Aerodynamics of a curveball. *Am. J. Phys.,* 55 (1), pp. 40-44.

Symmetry of Turbulent Characteristics Inside Urban Intersection

Radka Kellnerová[1,2] Zbyněk Jaňour[1]

[1] Institute of Termomechanics, Academy of Science of the Czech Republic, Prague, Czech Republic *
[2] Department of Meteorology and Environment Protection, Charles University, Prague, Czech Republic
radka.kellnerova@email.cz

Introduction

In wind-tunnel modeling a lot of embarrassments are related to the central symmetry. Even a small asymmetry in flow field leads to a significant change in pollutant dispersion. The asymmetry of flow field inside the symmetrical model is often caused by one of two reasons: inappropriate inlet conditions or non-symmetric set-up of model. The aim of this research was to estimate flow processes inside the wind-tunnel, mainly to investigate the symmetry over all working space and the influence of dimension of model relative to the dimension of working section.

Experimental Set-up

The experiment have been conducted in open-circuit low-speed aerodynamic tunnel belonging in to Institute of Thermomechanics in Nový Knín, Czech Republic. The flow measurements were carried out using two-dimensional fibre-optic laser Doppler anemometry (LDA). For "empty tunnel" arrangement, only roughness elements were put on the testing floor with the same sequencing as the one we used in the developing zone (Figure 1 - left).

The model setting was designed after the typical inner-city area with 20 m high apartment houses with a pitched roof (see scheme on Figure 1). Model has been scaled down to 1 : 200 according to criterium of Snyder (1985)[1].

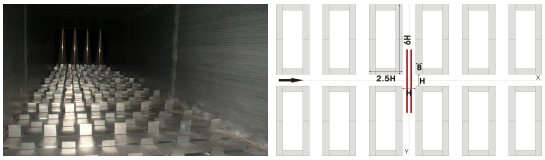

Figure 1: Left: roughness elements in testing section. Right: Scheme of model.

*Dolejškova 1402/5, Praha 8, 182 00

[1]Snyder, W. H.: Guideline For Fliud Modeling Of Atmospheric Diffusion (1981). Meteorology ond Assessment Division Enviromental Sciences, U.S. Enviromental Protection Agency.

Flow characteristics inside the tunnel

The vertical profile of turbulent characteristics was measured with three different reference velocities: 1 $m.s^{-1}$, 2.5 $m.s^{-1}$ and 4 $m.s^{-1}$. The experiment was conducted with reference velocity 4 $m.s^{-1}$, when the validity of Thowsend hypothesis was confirmed.

The measurements at Z/H=3 show that w-component velocity has on the sides significant positive values. The right side of tube has stronger upward motion near the wall than the left side. The symmetry is maintained within the fetch Y/H=4.5 from the center. This is confirmed on the base of the same results for root mean squares and for turbulence intensities of u and w components.

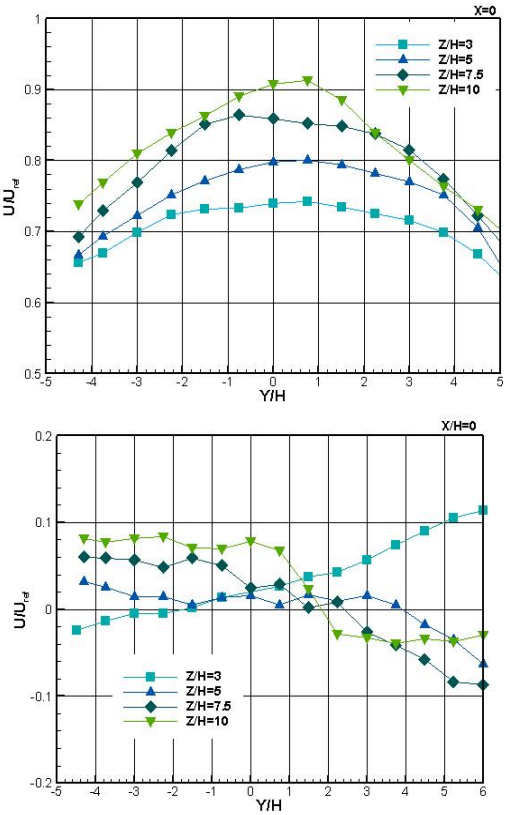

Figure 2: U- and v- components of velocity along lateral axis.

From flow measurement in horizontal plane (Figure 2 - down), the lowest level Z/H=3 suggests a large outflow on the right side. Next levels upward is situation inverse. Considering the updraft on the outside location at heights Z/H=3, we can suppose that the vertical vortices (vortex with horizontal axis) are merged between lowest level and upper level. The overall displacement of center of symmetry is 14% to the right side.

Flow characteristics inside the model

The lateral profile of flow characteristics is displayed in Figure 3. For both components the right side has slightly higher values, then the left side. It can be explained from the Figure 2, the inlet conditions have stronger longitudinal velocity and more significant outflow on the right side. The approaching flow have certain influence on the condition in the canopy layer, although the model has a dominant role up to the Z/H=1.5.

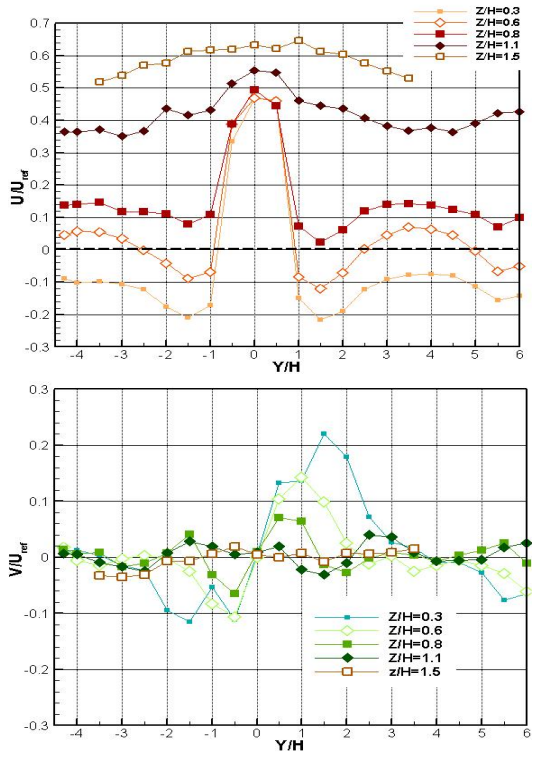

Figure 3: Lateral profiles at various level. Upper: u-component. Lower: w-component.

The measurement of w-component velocity was done. Surprising results are shown in the Figure 4. The values are strongly asymmetrical.

This asymmetry was investigated with great effort. The first was researched if the asymmetry correspond to the angle between model axis and approaching flow. The influence of model's orientation was detectable, but still very soft to be able to explain such a difference. Further, the model was widened just to the walls of tunnel in order to suppress the lateral flow. The widening induced the amplification of the asymmetrical effects, since the flow dominantly flushed through the central street.

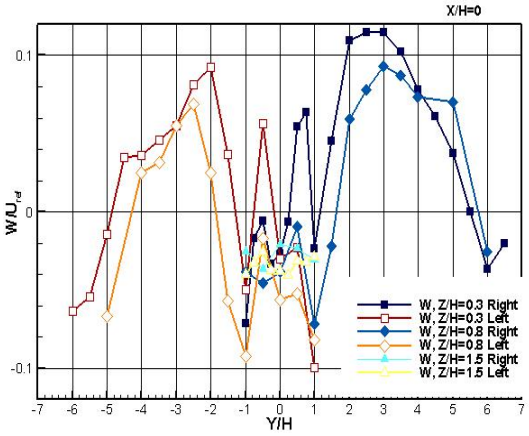

Figure 4: Velocity w along the lateral axis at various hight. Left means that probe is looking to the left side, right means inverse direction.

Finally, it was discovered that with the probe on the left side the results are strictly symmetrical to them with the probe in the right side.

With increasing height the influence of probebody on the circumfluence becomes weaker. The presence of the body near the rooftop level forces the air flow into central street essentially differently.

Conclusion

The flow quality in aerodynamic low-speed tunnel was investigated. Main objective was the central symmetry. The area proper for a experimental purpose is located within inner 60% of tunnel width. Nevertheless, although the model has dominant force for flow character up to the level Z/H=1.5, the asymmetrical inlet conditions have an influence on experimental results. In our case, the right side of tunnel indicates higher longitudinal velocity and lateral outflow. And data sets from model measuring inside the canopy layer confirmed the enhanced value of these quantities.

The biggest discrepancies in w-component and $< u'w' >$ charts was explained like a dependence of the vertical flow field on the position of measuring LDA facility. This finding makes the reliability of LDA measurements problematic in terms of physical modeling method.

Acknowledgements: This project is supported by AVOZ20760514.

THE UNSTEADY VORTICAL STRUCTURE IN A JET IMPINGING INTO A TROUGH CAVITY

Martin, Knob/ Václav, Uruba
Institute of Thermomechanics, Czech Academy of Sciences, v.v.i., Prague

In a blind, retcangular, trough- like cavity subject to a jet impingement, the jet-switching phenomenon has been known for decades. This is caused by the double-Coanda effect: at the very beginning, as the jet starts to blow the fluid into the cavity, the fluid is bent towards one of the sidewalls due to the Coanda effect. Then the jet is divided into two different wall jet- like streams, one of which flows straight to the cavity opening ("upwards"), the other flows "downwards" along the sidewall toward the cavity bottom wall. As the second wall jet reaches the bottom wall, it turns in the right angle along it and continues toward the opposite sidewall, along which it turns again and flows "upwards", i.e. towards the cavity opening. However, at this moment it starts to interact with the jet, placed on the top of the cavity. Since both the free jet and the wall jet entrain their surrounding fluid, in the region between them, a region of low pressure is created, which then causes the jet to swing to the other side. After the jet is swung, the process is repeated in the same manner on and on.

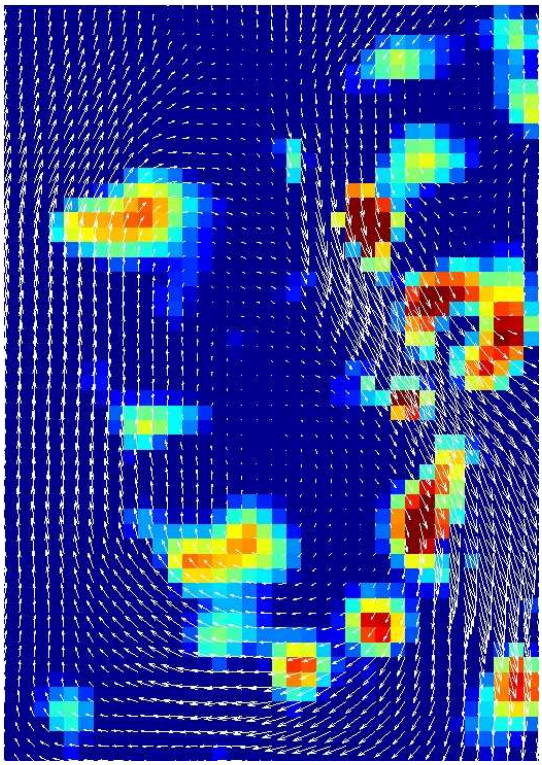

Fig. 1: The instantaneous flowfield with visualized vortical structure; the Kelvin-Helmholtz instability is clearly visible

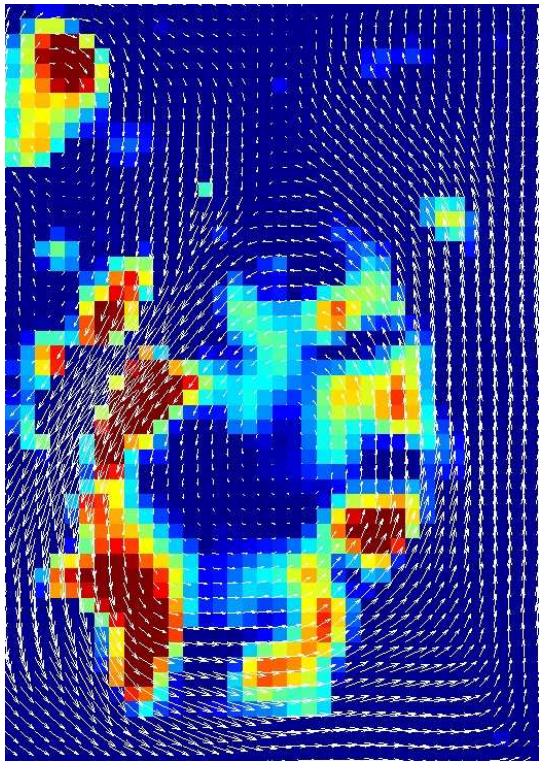

Fig. 2: The instantaneous flowfield with visualized vortical structure; the vortex loop just formed

In the reported research, the TR PIV system was used for the investigation of the vortical structure, visualized using the Δ- criterion. On the results obtained, several phenomena are observed. First, on the edges of the jet, the Kelvin- Helmholtz instability forms “large” vortices, which are further entrained by the fluid and grow in size (see Fig. *1*). Second, after the impingement on one of the cavity walls, the flow together with the vortices is bent in the direction towards the cavity opening. At the moment, the vortices start to interact with the just- formed vortices on the edge of the impinging jet- following the basic rules of vortex dynamics, the pathlines are changed, and the vortices are bent back into the cavity, forming a kind of closed vortex loop (see Fig. *2*). During this process, the fluid between the impinging jet and the quasi- wall- jet is entrained and, therefore, the low- pressure area is created and the jet is swung.

As may be understandable from the text and pictures above, the vortex paths are of high interest. These, however, can be observed only manually- although the authors have their own method to do that. This procedure is based on the secondary application of the PIV algorithm on the succesive images of the instantaneous vortical structures, and thereby evulating the vortices displacements; the following steps are straightforward. It should be mentioned here, that the above mentioned procedure requires at least five times faster PIV system than that available at the institute and, consequently, is not applied here.

From the mainly visual analysis of the given set of successive vortical structures, it can be said, that the vortices, formed by the Kelvin- Helmoholtz instability, can be divided into three different groups. In the first group, the vortices, which are formed by the K-H instability and, after the impingement onto the appropriate sidewall, turimmediately leave the cavity. In the second group, the vortices, which are entrained deep into the cavity, can be found. These vortices leave the cavity, following the cavity bottom wall and one of the sidewalls. The third group contains vortices, which, similarly to the second group, are entrained deep into the cavity, however, they turn back as a result of the vortex- vortex intaraction and thereby form the vortex loop.

References:

[1] Knob, M., Uruba, V.: A Brief Survey of Vortex Identification Methods with Application to 2D PIV data, Symposium on Anemometry, 2007

[2] Knob, Martin - Antoš, Pavel - Adamec, J.: Experimental and Numerical Investigation of Unsteady Behaviour of a Jet Impinging into a Trough- like Cavity. Experimental Fluid Mechanics 2006, Liberec 2006

[3] Knob, M. - Šafařík, P. - Adamec, J.: The Unsteady Behavior of a Plane Jet Impinging into a Through Cavity, Topical Problems of Fluid Mechanics 2007

OPTIMALIZACE EJEKTORU PRO NADZVUKOVÝ AERODYNAMICKÝ TUNEL

Optimalization of ejector for supersonic wind tunnel

J. Kolář
Technická univerzita Liberec, Katedra energetických zařízení, Liberec

The paper not supplied.

NUMERICAL AND EXPERIMENTAL STUDY OF THE FLOW OVER A SIMPLE BUILDING

Tomáš Kopáček* and Luděk Beneš$^+$ and Milan Jirsák$^-$

*** ČVUT, Faculty of Mechanical Engineering, Department of Technical Mathematics, Karlovo nám. 13, Praha 2, 12135**
+ Institute of Thermomechanics AS CR, Dolejškova 5 , Praha 8, 18200
- ARTI a.s, Department of Low Speed Aerodynamics, Beranových 130, Praha-Letňany

Introduction

This contribution presents a study of turbulent flow over a simple building. We considered a building with a flat roof and a building with a double pitched roof. The main goal was to compare our numerical results computed at the Department of Technical Mathematics with experimental data measured in a wind tunnel at ARTI.

Mathematical and numerical method

To model incompressible viscous turbulent flow over a complex geometry in 2D, the system of RANS equations completed by the $k-\omega$ TNT model was considered. Using the method of artificial compressibility, we start with the two dimensional system

$$\Gamma W_t + F_x + G_y = \nu(R_x + S_y),$$

where $\nu = \nu_M + \nu_T$, ν_M and ν_T denotes molecular and turbulent viscosity, respectively. $W = (p, u, v)^T$ is the vector of unknowns, $\Gamma = diag(1/\beta^2, 1, 1)$ is a diagonal matrix, F and G are two-dimensional flux vectors and R, S are viscous fluxes, i.e.

$$\begin{aligned} F &= (u, u^2 + p, uv)^T, \quad R = (0, u_x, v_x)^T, \\ G &= (v, uv, v^2 + p)^T, \quad S = (0, u_y, v_y)^T. \end{aligned}$$

The $k-\omega$ TNT model is based on two transport equations for k (turbulence kinetic energy) and ω (specific dissipation rate) which are coupled with the RANS equations. Numerical discretization has been done by the finite volume method with the AUSM scheme used for the numerical fluxes and piecewise linear reconstruction limited by Barth–Jespersen limiter.

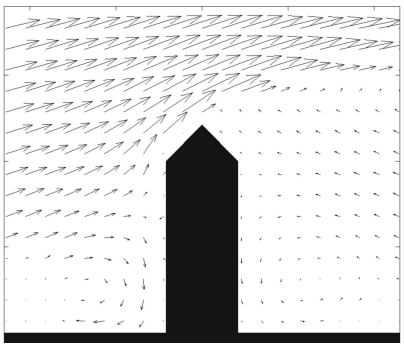

Figure 1: PIV measurement–velocity flow field close to the double piched building

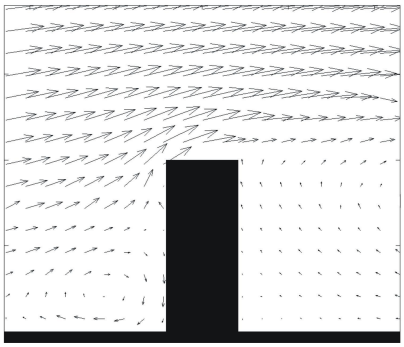

Figure 2: PIV measurement–velocity flow field close to the flat building

Numerical and experimental results

The main goal of this work was to obtain numerical results and to compare them with the experimental data measured by the ARTI. The experiment was carried out in a tunnel for simulation of the turbulent boundary layer (BLWT). Several measurements for flows over different geometries were undertaken, namely flow over the double pitched roof and the flat roof.

Nowadays we have done numerical simulation over the flat roof building. The streemlines and the absolut velocity obtained by numerical simulation are shown in fig. 4.

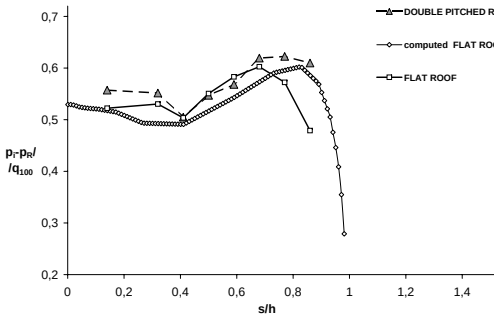

Figure 3: The comparison of the computed and measured presure distribution on the front face of building

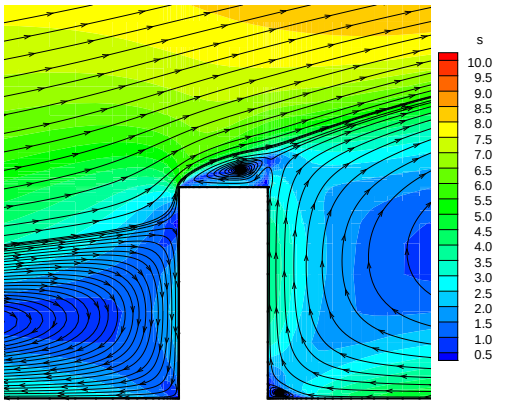

Figure 4: The Flat roof building - the streamtraces and the absolute velocity s

Conclusion

In Figure 3, a comparison of the pressure coefficients obtained by numerical and experimental methods shows good agreement so we can say, that the used numerical schema is propper for this type of tasks. However distorted mesh and complex phenomena arising near the building influence negatively convergence of the method, therefore we had to decrease the CFL coefficient to 0.1.

Acknowledgment

The financial support for the present project is partly provided by the Research Plan MSM No.6840770003 and the project of the Grant Agency of the Czech Republic No. 205/06/0727.

References

[1] Wilcox D.C. Turbulence Modeling for CFD, *DCW Industries*

[2] Kopáček T.: Numerické řešení vazkého nestlačitelného proudění,*Diploma thesis (in czech) ČVUT, 2007*

[3] Jirsák M., Zachoval D., Kopáček T.: Wind Tunnel Modelling of Ventilation and Infiltration Boundary Condition, *ARTI in Prague, 2006*

[4] Fuka V., Brechler J.: 2D model interakce proudění s pevnými překážkami. *Colloqium FLUID DYNAMICS 2006 (Jonas, Uruba, eds.), Inst. of Thermomechanics, Acad. of Sci., Prague, 2006,35–38.*

[5] Bodnár T., Fraunié Ph., Kozel K., Sládek I.: Numerical simulation of Comlex Atmospheric Boundary Layer Problems,*ERCOFTAC Buletin No.60, March 2004, p.5-12*

NUMERICAL SIMULATION OF FLOW AND POLLUTION DISPERSION OVER OBSTACLES IN COMPLEX TERRAIN

K. Kozel[1)], T. Bodnár[1)], E. Gulíková[2)] and V. Píša[2)]
1) Department of technical mathematics, Faculty of mechanical engineering, Czech Technical University in Prague
2) ECOPROGRESS a.s., Most

Introduction

This paper presents some of the results of numerical simulation of flow and pollution dispersion in the proximity of significant terrain obstacles. The mathematical model is based on Reynolds averaged Navier-Stokes equations for incompressible flows. Turbulent closure of the model is obtained by simple algebraic turbulence model. The numerical solution is carried out by the semi-implicit finite-difference scheme. The results of simple tests are presented and summarized. Model sensitivity has been studied with respect to simulated obstacle size and shape.

The complex terrain profile used in this study represents a part of the opencast coal mine where is placed a coal storage. This storage acts as a source of coal dust which is drifted by the wind. The detailed orography profile was obtained by a combination of data from several geographical resources. In order to get maximum of realistic details a laser scan of the terrain was performed and included into the orography profile. The aim of this study is to give both qualitative and quantitative guidelines for the evaluation of the environmental impact of artificial obstacles placed downwind from the coal storage.

Mathematical Model

The flow in atmospheric boundary is turbulent in most simulations. The fluid motion can be thus described by the Reynolds averaged Navier-Stokes equations (RANS). The non-conservative form of the RANS system is represented by the following equations:

$$u_x + v_y + w_z = 0 \tag{1}$$

$$V_t + uV_x + vV_y + wV_z = -\frac{\nabla p}{\rho} + [KV_x]_x + [KV_y]_y + [KV_z]_z \tag{2}$$

Here $V = col(u, v, w)$ is the velocity vector, p is pressure, ρ is density.

The same form as the momentum equations take also the transport equations for concentration of passive pollutants.

$$C^i_t + uC^i_x + vC^i_y + wC^i_z = \left[K\frac{C^i_x}{\sigma_{C^i}}\right]_x + \left[K\frac{C^i_y}{\sigma_{C^i}}\right]_y + \left[K\frac{C^i_z}{\sigma_{C^i}}\right]_z \tag{3}$$

Here C^i is the concentration of i-th pollutant and σ denotes the turbulent Prandtl's number.

The turbulence model is based on the Boussinesq hypothesis on the turbulent diffusion coefficient $K = \nu + \nu_T$ which is expressed as a sum of molecular and eddy viscosity.

Numerical Simulation

Numerical experiments were performed in a 3D domain of the size 500×250×400 meters. The bottom boundary represents a complex terrain orography. The height difference between highest and lowest point of the terrain profile is about 70 meters. The coal storage is represented by a rectangular surface source of pollution. The dimension of this source is about 40×20 meters and is centered at position x=125, y=120. The wind flow in the model domain is forced by the prescribed velocity profile at the inlet (x=0). The maximum velocity $10m/s$ is achieved at the upper boundary of the domain.

Conclusions, remarks

From the presented tests it is possible to draw the following conclusions:

- The selected mathematical model is able to describe properly the pollution dispersion problems in complex terrain.
- The numerical method used to solve the set of governing equations seems to be sufficiently robust and efficient for the appropriate resolution of given class of problems.
- The presented numerical simulations have shown that the effect of simulated obstacles on the flow and pollution dispersion has only local impact on both velocity and concentration field. This is caused mainly by the complexity of the terrain, where the orography profile involves height changes with scales much larger than the maximum height of the simulated obstacles. Thus the orography effect is dominant in this case.
- More detailed study of dust sedimentation should be performed in order to quantify the effects of obstacles on deposition of particles of different sizes.

Acknowledgment

The financial support for the present project was partly provided by the *Grant No.1ET400760405* and by the Research Plan *MSM 6840770010* of the *Ministry of Education of Czech Republic*.

References

[1] BENEŠ, L., BODNÁR, T., FRAUNIÉ, P., & KOZEL, K.: Numerical Modelling of Pollution Dispersion in 3D Atmospheric Boundary Layer. In: *Air Pollution Modelling and Simulation* (edited by B. SPORTISSE), (pp. 69–78). Springer Verlag (2002).

[2] BODNÁR, T., KOZEL, K., FRAUNIÉ, P., & BENEŠ, L.: Numerical Modelling of Pollution Dispersion in Complex Terrain. In: *Air Pollution IX.*, (pp. 85–94). WIT Press (2001).

[3] BODNÁR, T., KOZEL, K., FRAUNIÉ, P., & JAŇOUR, Z.: Simulation of Flow and Pollution Dispersion in 3D Atmospheric Boundary Layer. *Computing and Visualization in Science*, vol. 3, no. 1–2.

NUMERICAL SOLUTION OF COMPRESSIBLE FLOW IN A CHANNEL WITH MOVING WALLS

V. Kučera, M. Feistauer and J. Prokopová
Charles University Prague, Faculty of Mathematics and Physics

Introduction

This work is considered with the numerical solution of inviscid compressible fluid flow through a channel with moving walls. The governing Euler equations written in the ALE (Arbitrary Lagrangian-Eulerian) form are discretized by the discontinuous Galerkin method. We apply a semiimplicit linearization with respect to time. Currently, the movement of the wall must be prescribed by a given formula.

Formulation of the problem

We consider the flow in a bounded 2D domain Ω_t depending on time t with boundary $\partial\Omega_t = \Gamma_I \cup \Gamma_O \cup \Gamma_{W_t}$, where Γ_I and Γ_O represent the inlet and outlet and Γ_{W_t} represents moving impermeable walls.

The dependence of the domain on time is taken into account with the aid of a regular ALE mapping $\mathcal{A}_t : \overline{\Omega}_0 \to \overline{\Omega}_t$, i.e. $\boldsymbol{X} \mapsto \boldsymbol{x} = \boldsymbol{x}(\boldsymbol{X}, t)$. Further, we define the ALE velocity: $\tilde{\boldsymbol{z}}(\boldsymbol{X}, t) = \frac{\partial}{\partial t}\boldsymbol{x}(\boldsymbol{X}, t) = \frac{\partial}{\partial t}\mathcal{A}_t(\boldsymbol{X})$, $\boldsymbol{z}(\boldsymbol{x}, t) = \tilde{\boldsymbol{z}}(\mathcal{A}_t^{-1}(\boldsymbol{x}), t),\ t \in [0, T],\ \boldsymbol{x} \in \overline{\Omega}_t$ and the ALE derivative of a function $f = f(\boldsymbol{x}, t)$: $\frac{D^A}{Dt} f(\boldsymbol{x}, t) = \frac{\partial \tilde{f}}{\partial t}(\boldsymbol{X}, t)|_{X=\mathcal{A}_t^{-1}(x)}$, where $\tilde{f}(\boldsymbol{X}, t) = f(\mathcal{A}_t(\boldsymbol{X}), t),\ \boldsymbol{X} \in \Omega_0$.

It is possible to show that

$$\frac{D^A f}{Dt} = \frac{\partial f}{\partial t} + \boldsymbol{z} \cdot \nabla f = \frac{\partial f}{\partial t} + \mathrm{div}(\boldsymbol{z} f) - f \mathrm{div} \boldsymbol{z}. \tag{1}$$

This leads to two different formulations of the Euler equations in ALE form:

$$\begin{aligned} 1) \quad & \frac{D^A \mathbf{w}}{Dt} + \sum_{s=1}^{2} \frac{\partial \boldsymbol{f}_s(\mathbf{w})}{\partial x_s} - \boldsymbol{z} \cdot \nabla \mathbf{w} = 0, \\ 2) \quad & \frac{D^A \mathbf{w}}{Dt} + \sum_{s=1}^{2} \frac{\partial \mathbf{g}_s(\mathbf{w})}{\partial x_s} + \mathbf{w} \mathrm{div} \boldsymbol{z} = 0 \end{aligned} \tag{2}$$

where $\boldsymbol{f}_s$, $s = 1, 2$, are the *inviscid fluxes* and

$$\begin{aligned} \mathbf{w} &= (\rho, \rho v_1, \rho v_2, e)^{\mathrm{T}} \in \mathbb{R}^4, \\ \boldsymbol{f}_i(w) &= (f_{i1}(\mathbf{w}), \dots, f_{i4}(\mathbf{w}))^{\mathrm{T}} = (\rho v_i, \rho v_1 v_i + \delta_{1i} p, \rho v_2 v_i + \delta_{2i} p, (e + p) v_i)^{\mathrm{T}} \end{aligned} \tag{3}$$

and $\mathbf{g}_s$, $s = 1, 2$, are modified inviscid fluxes

$$\mathbf{g}_s(w) := \boldsymbol{f}_s(w) - \mathrm{z}_s \mathbf{w}. \tag{4}$$

[1]This work is a part of the research project No. 7486/2007 of the GAChU. The work of V. Kučera is supported by the Nečas Center for Mathematical Modelling, project LC06052, financed by MSMT.

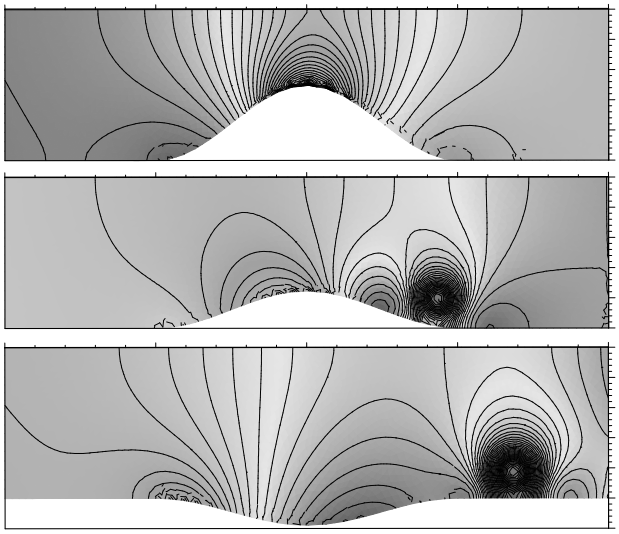

Figure 1: Pressure isolines.

This system is equiped with standard inlet and outlet boundary conditions. On the moving wall we impose the impermeability condition $\mathbf{v} \cdot \mathbf{n} = \mathbf{z} \cdot \mathbf{n}$, where $\mathbf{n}$ is the unit outer normal to Γ_{W_t}. The discretization of equations 1) and 2) in (2) is carried out by the discontinuous Galerkin finite element method, which uses piecewise polynomial function spaces without the assumption of interelement continuity, e.g. [2].

Discretization in time is carried out using the semi-implicit linearization of the backward Euler method used in [1]. Additional terms which are a result of the ALE formulation of (2) do not require special treatment, since they are linear with respect to the unknown state vector $\mathbf{w}$ and therefore can be taken implicitly.

Now we describe the construction of the ALE mapping. We assume that the inlet and outlet are straight segments given by the conditions $X_1 = -2$ and $X_1 = 2$, respectively. In our first results we assume that the upper wall is given by the condition $X_2 = 1$ and that the ALE mapping is equal to the identity in the sets $[-2, -1] \times [0, 1]$ and $[1, 2] \times [0, 1]$. Otherwise we construct the ALE mapping so that lower wall is represented at time t by the graph of the smooth function.

$$sin(0.5 * t) * (cos(\pi * X_1) + 1)/4.$$

This movement is interpolated to the rest of the domain.

The computed solution is periodic and although the flow is inviscid, a vortex forms after the lower wall starts to descend. This vortex is then convected out of the domain through the outlet. Figure 1 shows the pressure isolines at three different time instants: before the vortex is formed, after the formation and the vortex convection.

References

[1] Dolejší V., Feistauer M.: *A Semi-Implicit Discontinuous Galerkin Finite Element Method for the Numerical Solution of Inviscid Compressible Flow*, J. Comput. Phys. 198 (2004) pp. 727746.

[2] Feistauer M., Felcman J., Straškraba I.: *Mathematical and Computational Methods for Compressible Flow*, Oxford University Press, Oxford, (2003).

MĚŘENÍ PERIODICKÉHO PROUDĚNÍ METODOU TIME-RESOLVED PIV A LDA

Time-Resolved PIV and LDA Measurements of Pulsating Flow

Jan Matěcha[1], Jan Novotný[1], Josef Adamec[1], Bohuš Kysela[2] a Zdeněk Chára[2]

[1]ČVUT v Praze, Fakulta strojní, Ústav mechaniky tekutin a energetiky, Praha
[2]Ústav pro hydrodynamiku AV ČR, v.v.i., Praha

ÚVOD

V článku jsou prezentovány výsledky z měření pulzačního proudění v kruhové trubici konstantního průřezu metodou Time-Resolved Particle Image Velocimetry (TR-PIV) a metodou Laser Doppler Anemometry (LDA). Jsou vyhodnoceny a porovnány proudové charakteristiky pro různé režimy pulzačního proudění.

EXPERIMENT

Bylo provedeno měření rychlostního pole v kruhové trubici o poloměru R = 10 mm. Pracovní kapalina byla voda. Pulzační proudění bylo generované experimentálním zařízením, které superponuje oscilační a stacionární složku proudění [1] .

Parametry testovaných režimů proudění jsou shrnuty v následující tabulce.

Stacionární proudění
Re_S = 1000, 2000, 3000
Pulzační proudění
Re_S = 1000, 2000
$\alpha = R\sqrt{2\pi f / \nu} = 6.7 - 14.4$
$\lambda = Q_{OS}/Q_S = 0.4 - 3.7$

Parametr f je frekvence pulzací, ν je kinematická viskozita kapaliny, Re_S je Reynoldsovo číslo vypočtené pro střední průtok Q_S. Q_{OS} je amplituda oscilační složky proudění.

Pro LDA měření byl použit systém sestávající z vláknové optiky Dantec s výstupní čočkou f=310 mm, argonového laserového zdroje, vyhodnocovací jednotky BSA (Burst Signal Analyzer) fi. Dantec. Měření bylo prováděno v 15 bodech po průřezu s krokem 1.33 mm. V každém bodě byla načítána časová řada v minimální délce 25 period. Z naměřených dat byla pro každou pozici na poloměru vypočtena střední hodnota rychlosti a RMS ze všech měřených period.

Pro TR-PIV měření byla použita kamera NanoSense Mklll s čipem typu CMOS 1024x1200 pixelů, velikost RAM 4GB, vysokorychlostní zesilovač signálu HAMAMATSU C9548. Pro osvětlení měřící roviny byla použita kontinuální dioda s vlnovou délkou 660 nm. Jako značkovací částice byly použity polyamidové částice o průměru 10 μm. Byla měřena oblast v rovině symetrie kanálu o rozměru 22 mm x 4.5 mm, která byla zaznamenána na aktivní ploše čipu o velikosti 1016 x 208 pixelů. Použitá snímkovací frekvence byla v rozmezí 1000 až 2000 Hz v

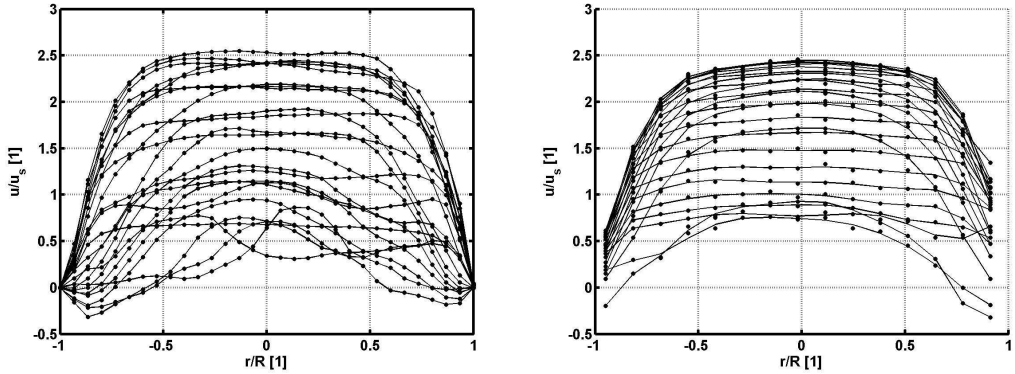

Obr. 1 Ukázka rychlostních profil pro pulzační proudění s parametry $Re_s = 2000$, $\alpha = 8.86$, $\lambda = 0.7$. Vlevo: Okamžité rychlostní profily pro jednu periodu získané metodou TR-PIV. Vpravo: Fázově profily střední rychlosti získané metodou LDA.

závislosti na měřeném režimu. Pro každý pulzační režim byla naměřena jedna perioda. Vyhodnocení snímků bylo provedeno v systému MATLAB použitím adaptivní korelace. Pro nalezení přesnější polohy signálového peaku byla použita tří bodová sub-pixelové interpolace. Velikost vyšetřované oblasti byla zvolena 128x32 pixelů a velikost překrývání 50%. Při stacionárním proudění byla vyhodnocena střední hodnota a RMS. Při pulzačním proudění byly vyhodnoceny okamžité rychlosti a střední hodnoty vypočtené pomocí klouzavého průměru pro jednu periodu.

ZÁVĚR:

V článku jsou porovnány proudové charakteristiky pro stacionární a pulzační proudění v trubce konstantního průměru získané optickými metodami TR-PIV a LDA.

Metodou TR-PIV byla měřena časová posloupnost maximálně 16000 snímků vzhledem k současným možnostem experimentálního zařízení a příslušného ovládacího programu. Z dat získaných metodou TR-PIV byla získána časová závislost rychlostních profilů při pulzačním proudění pro jednu periodu. Metodou LDA byly získány časové řady rychlosti vždy pro jednu pozici na poloměru. Při pulzačním proudění bylo vyhodnocováno 20 period.

Pro stacionární proudění byly vyhodnoceny časově střední hodnoty rychlosti, RMS a časové řady v závislosti na Re oběmi metodami. Pro pulzační proudění byly vyhodnoceny časové řady rychlosti, fázově střední rychlosti a jejich RMS z dat LDA měření, a průběh rychlostních profilů v závislosti na čase pro jednu periodu a klouzavý průměr těchto rychlostí z TR-PIV měření.

PODĚKOVÁNÍ:

Tento výzkum byl podporován grantem GA ČR 101/05/0675 *Teoretická a experimentální optimalizace cévních rekonstrukcí a hlediska hemodynamiky*.

LITERATURA

[1] Chára, Z., Hoření, B. (2007) NUMERICAL SIMULATION AND EXPERIMENTAL INVESTIGATION OF PULSATING FLOW, Inženýrská mechanika 2007, Svratka, ČR, 14.-17.5.2007, 101-102, full text CD, ISBN 978-80-87012-06-2.

Vliv syntetizovaného paprsku na hodnotu celkového ztrátového součinitele v kompresorové lopatkové mříži

Influence of Synthetic Jet to the Compressor Blade Cascade Total Loss Coefficient

Milan Matějka [1], Lukáš Popelka [2], Jiří Nožička [1]
[1] Ústav mechaniky tekutin a energetiky, Fakulta strojní, ČVUT v Praze
[2] Ústav termomechaniky, Akademie Věd České Republiky, Praha

Abstrakt: V příspěvku je presentován positivní vliv syntetizovaného paprsku (SP) na velikost celkového ztrátového součinitele kompresorové lopatkové mříže. Výstupní otvor generátoru syntetizovaného paprsku byl umístěn v boční stěně tunelu na spojnici náběžných hran lopatek. Studován byl zejména vliv budící frekvence generátoru SP, dále hodnoty Stokesova a Reynoldsova čísla výstupního otvoru generátoru SP.

1. Experimentální určení hodnoty ztrátového součinitele

Výstupní otvor (štěrbina) generátoru syntetizovaného paprsku byl umístěn v boční stěně tunelu na spojnici náběžných hran 6 a 7 lopatky lopatkové mříže. Šířka výstupního otvoru generátoru je rovna rozteči lopatkové mříže, tj. s = 36 mm. Pro budící frekvence f = 0, 600, 800, 1000 Hz budiče generátoru syntetizovaného paprsku a výšce štěrbiny h = 0,2, 0,5 a 1 mm byly experimentálně získány hodnoty celkového a sekundárního ztrátového součinitele. Jejich změna je vyjádřena v Tab. 1 a 2.

štěrbina \ f [Hz]	0	600	800	1000
0,2	0	-0,88	-1,49	-1,81
0,5	0	1,64	0,43	-0,33
1	0	1,14	-0,36	-0,27

Tab. 1 *Změna hodnoty celkového ztrátového součinitele v %*

štěrbina \ f [Hz]	0	600	800	1000
0,2	0	-3,94	-5,29	-5,72
0,5	0	2,14	-0,62	-2,51
1	0	0,90	-2,34	-1,94

Tab. 2 *Změna hodnoty sekundárního ztrátového součinitele v %*

2. Diskuze výsledků

Přestože řízení mezní vrstvy bylo aplikováno pouze na malé části mezilopatkového kanálu (boční stěna tunelu), byl prokázán výrazný dopad syntetizovaného paprsku na proudové pole mezilopatkového kanálu. Došlo k nezanedbatelnému poklesu hodnoty celkového i sekundárního ztrátového součinitele o 1,8 %, resp. 5,7 %.

štěrbina / f [Hz]	0	600	800	1000
0,2	0	1,87	3,14	3,82
0,5	0	-3,43	-0,91	0,69
1	0	-2,54	0,80	0,61

Tab. 3 *Efektivita syntetizovaného paprsku* η_{sp} *pro všechny případy velikosti slotu a frekvencí.*

$$\eta_{sp} = \frac{w_{us}}{w_{dod}} \tag{1}$$

Poměr přivedeného elektrického příkonu P a hmotnostního toku proudu tekutiny v mezilopatkovém kanále určuje velikost měrné přivedené práce. Z poměru měrné uspořené a přivedené práce lze definovat efektivitu syntetizovaného paprsku η_{sp} na proudové pole tekutiny, rov. (1). Efektivita syntetizovaného paprsku tak vyjadřuje, kolikrát více vložené energie bylo uspořeno. V tab. 3 jsou uvedeny hodnoty efektivity syntetizovaného paprsku pro jednotlivé případy velikosti štěrbiny a budící frekvence. Pro štěrbinu o velikosti 0,2 mm a budící frekvenci f = 1000 Hz bylo uspořeno cca 4 krát více energie, než bylo vloženo.

3. Závěr

Z experimentálních výsledků vyplývá výrazný vliv budící (resp. bezrozměrné) frekvence a Stokesova čísla výstupního otvoru generátoru syntetizovaného paprsku na hodnotu ztrátového součinitele.

Protože na boční stěně tunelu došlo k ovlivnění nejen mezní vrstvy, ale také vírových struktur, jeví se volba charakteristického rozměru (paprskem ovlivněné oblasti) pro výpočet bezrozměrné frekvence poněkud problematická.

Na snížení hodnoty ztrátového součinitele má také výrazný vliv umístění výstupního otvoru generátoru syntetizovaného paprsku, který byl v tomto případě umístěn v boční stěně tunelu, kdy došlo zejména k poklesu hodnoty sekundárního ztrátového součinitele. Je zřejmé, že pokud by se podařilo zabudovat generátor syntetizovaného paprsku přímo do lopatky (podél celého rozpětí lopatky) došlo by k výraznějšímu poklesu profilových ztrát a následně tak celkového ztrátového součinitele.

Mnohem vhodnější metodou snížení profilových ztrát je použití pokročilejší metody řízení mezní vrstvy, řízení plazmatem. Použití této metody k řízení mezní vrstvy na lopatce je z technologických důvodů mnohem jednodušší než v případě syntetizovaného paprsku.

Poděkování

Tato práce vznikla za podpory grantového projektu GA ČR 101/05/2537 a Výzkumného centra MŠMT 1M06059. Zvláštní poděkování za podmětné připomínky patří Prof. Ing. Pavlu Šafaříkovi, CSc.

Literatura

Glezer, A., Amitay, M. (2002): *Synthetic Jet.* Annual Revision Fluid Mechanics 2002.

Greenblatt D., Wygnanski I. J. (2000): *The Control of Flow Separation by Periodic Excitation.* Aerospace Science 36, pp. 487-554.

Matějka, M., Součková, N. Popelka, L., Nožička, J. (2007): *Active flow control on the simplified flapped airfoil.* 1st CEAS European Air and Space Conference, Berlin, p. 237–241.

Uruba, V. (2004): *Flow Control Using Synthetic Jet Actuators.* Inženýrská Mechanika 2004, Praha.

GIS BASED MAPPING FOR MODELLING OF THE FLOWFIELD ABOVE THE SURFACE OF MINING AREAS

Luboš Matějíček[1], Tomáš Bodnár[2], Luděk Beneš[2], Eva Gulíková[3]

[1]Inst. for Environmental Studies, Charles University in Prague, Czech Republic
[2]Inst. of Thermomechanics, Academy of Sciences, Prague, Czech Republic
[3]ECOPROGRESS, Most, Czech Republic

For simulation of wind flows above the complex terrain, the spatial model based on surface mapping in a few scales is needed to provide numerical calculation in a more precise way. Each map scale can be supported by a different spatial data sources. Thus, many software tools are mostly used to solve individual tasks focused on processing of satellite images, aerial photographs, GPS data, laser scans and standard digital map layers. In this case, geographic information systems (GISs) are used to manage complex data structures, to carry out spatial analyses and to visualize results. In order to integrate the flowfield simulation, two concepts of modelling are merged. In spatial modelling, the basic concept is one of spatial distribution and spatial relationship. In temporal modelling represented by numerical models of the flowfield, the basic concept is one of state, determined in terms of wind speed, wind direction or concentration of the pollutant. The resulting projects bring together spatial data and simulation inputs/outputs, which promotes new ways in processing and interpretation. A number of applications are discussed in the book "GIS and Environmental Modeling: Progress and Research Issues" edited by Goodchild (Goodchild et al., 1996).

The attached case study demonstrates GIS mapping of the opencast coal mining areas that are used to support modelling of the flowfileds and dispersion of dust emissions from mining activities. In addition to GIS analysis, the map layers extended by simulation outputs assist to identify the dominant dust emission sources and their influence on surrounding areas. Thus, the GIS spatial data can be utilized by environmental scientists and local authorities in the field of environmental protection.

The basic schema in Figure 1 illustrates the processing of spatial data, terrain measurements and modelling inputs/outputs in the framework of GIS. The upper part represents the spatial data sources. The bottom part contains the key data integration module-GIS, which is extended on the left side by the data connection to modelling tools, environmental statistics and other available spatial data sources. The standalone modules on the right part represent extensions dedicated to the presentation of the GIS data outputs by printed documents or digital data.

The time series of meteorological measurements are pre-processed and included into geodatabase to generate wind rose statistics and plots for several meteorological data formats. In order to improve accuracy of the GPS measurements, the data from reference stations (CZEPOS) are included into estimates of positional data that contain coordinates for georectification of satellite images and aerial images, and locations of surface objects (mining excavators, transport routes, temporary repositories and meteorological stations).

Satellite images from Landsat 7 ETM+ are selected to display and classify the surface of the whole opencast mine at the resolution of 30 meters. The bands 3-2-1 (red, green, blue) create a true colour composite that displays surface objects similar to a colour image. The bands 4-3-2 (near IR: 0.77-0.90 μm, red, green), 5-4-2 (mid IR: 1.55-

1.75 μm, near IR, green), and 7-4-2 (mid IR: 2.09-2.35 μm, near IR, green) are transformed into the visible light spectrum and create a pseudo colour composite. The middle infrared bands can be used for discrimination of geologic rock types, soil boundaries and soil moisture content, which significantly influence the rate of surface emission sources (bare soil, mining areas and larger coal repositories). The aerial images support mapping of local emission sources and surface objects at the resolution of 0.5 meters. All the images are draped onto the digital terrain model (DTM) that is based on terrain measurements and laser scanning.

Laser scanning together with terrain measurements form the input data for building of the DTM in the format of the triangulated irregular network (TIN).

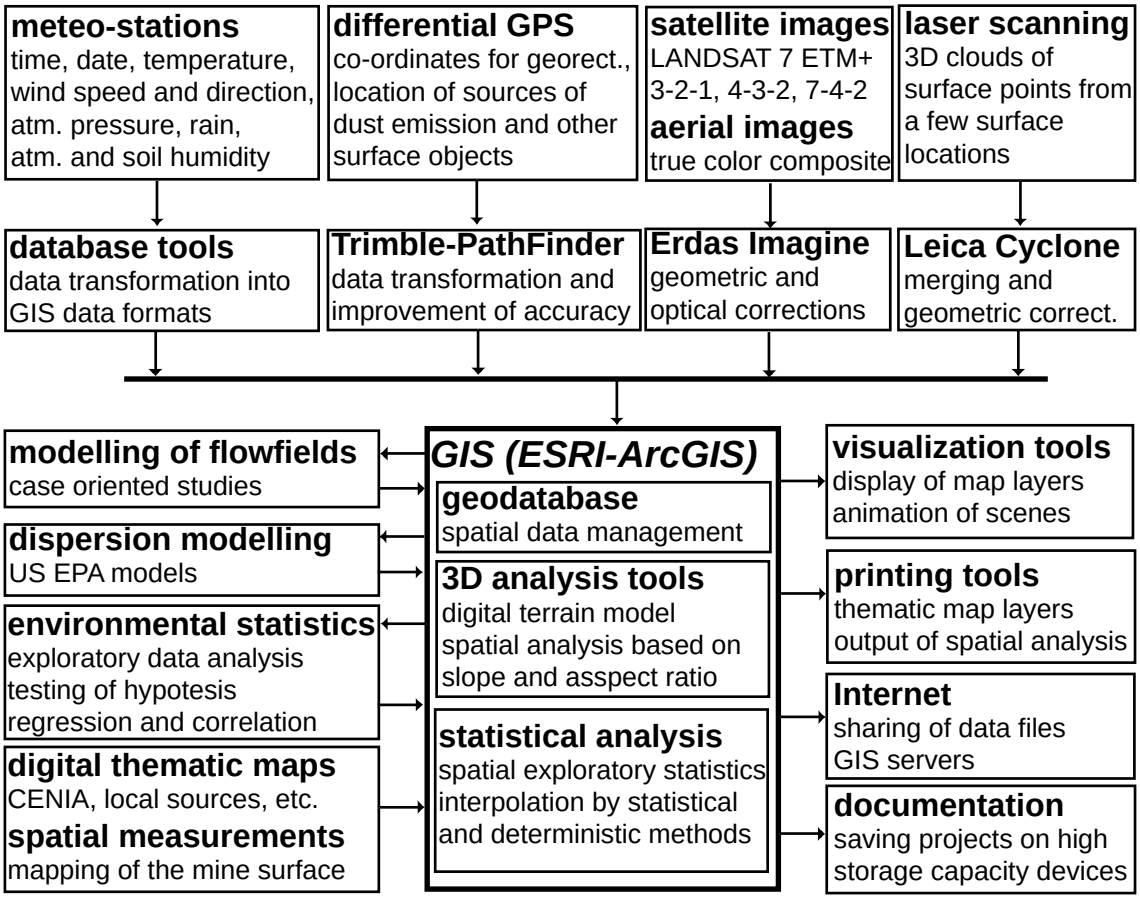

Figure 1. Processing of spatial data and simulation inputs/outputs in the framework of the GIS project (ESRI's ArcGIS)

Acknowledgements

The contribution was supported by the grant No. 1ET400760405 and the Research Plan MSM 6840770003. The spatio-temporal data have been processed by ArcGIS, Erdas Imagine and other programming tools in the GIS Laboratory, Faculty of Natural Science, Charles University in Prague.

References

M.F. Goodchild, L.T. Steyaert, B.O. Parks (Ed.), 1996. GIS and Environmental Modeling: Progress and Research Issues. Fort Collins: GIS World, Inc.

GIS BASED VISUALIZATION FOR TERRAIN MEASUREMENTS AND DUST DEPOSITION IN THE AREA OF COAL MINES

Luboš Matějíček[1], Tomáš Bodnár[2], Luděk Beneš[2], Eva Gulíková[3]

[1]Inst. for Environmental Studies, Charles University in Prague, Czech Republic
[2]Inst. of Thermomechanics, Academy of Sciences, Prague, Czech Republic
[3]ECOPROGRESS, Most, Czech Republic

In order to support simulation of wind flows and to estimate dust deposition in the neighbourhood of coal mining areas, the geographic information systems (GISs) are used to create complex data structures, to solve advanced spatial analysis and to visualize the results. GISs, formerly utilized by cartographers, are often used for mapping and spatial analysis in environmental science and other research disciplines. Using of new computer technology enables more complex displays for thematic mapping using animation and multimedia (Goodchild, 1996). Environmental issues, like simulation of flowfields and dust deposition, incorporate temporal as well as spatial phenomena that lend themselves to dynamic display. New trends in GIS research empower users to use interactive applications in the framework of visualization, which brings new possibilities into spatio-temporal modelling.

The GIS project in the environment of ESRI's ArcGIS is developed to integrate all the spatial data and simulation outputs in the geodatabse. In addition to the spatial data management, a huge range of ArcGIS extensions is used to provide spatio-temporal analysis and to make up data inputs for flowfield simulation and final visualization.

In case of the GIS project, the digital terrain model (DTM) forms the basic map layer. A few data sources are used to create DTM. The contour lines support mapping of the whole mining area. The terrain measurements with GPS and the data from geodetic survey are used for visualization of a part of the mining area, which contain the temporary coal repository near the residential zones. Finally, the laser scanning enables to obtain clouds of the 3D spatial points. The laser scanning is focused on selected parts that need higher density of terrain measurements. Thus, the zone between the temporary coal depository and a nearest part of the residential area is selected to obtain the highest density of the 3D spatial points with the highest accuracy. The created DTM represents the key spatial data structure that improves accuracy of flowfield modelling in the framework of the developed standalone software tools. In case of GIS visualization, the DTM is used for draping of satellite images, aerial images and thematic map layers.

The image from Landsat 7 ETM+ supports display of the mining areas at the resolution of 30 meters. A true colour composite and pseudo colour composites combine the bands 1-7. The aerial images enable more precise mapping of the local surface objects including the dust emission sources represented by transport routes, temporary repositories and mining excavators. Spatial identification of these surface objects is complemented by the differential GPS measurements.

The basic schema of the GIS project is in Figure 1. All data are included into the GIS project. The visualization methods included mainly in the ArcGIS extensions (ArcScene, ArcGlobe) provide enhanced display of map layers extended by symbols based on the map attributes, Figure 2. Besides visualization, the digital map layers and reports are generated to document all the results and to share selected data structure via Internet.

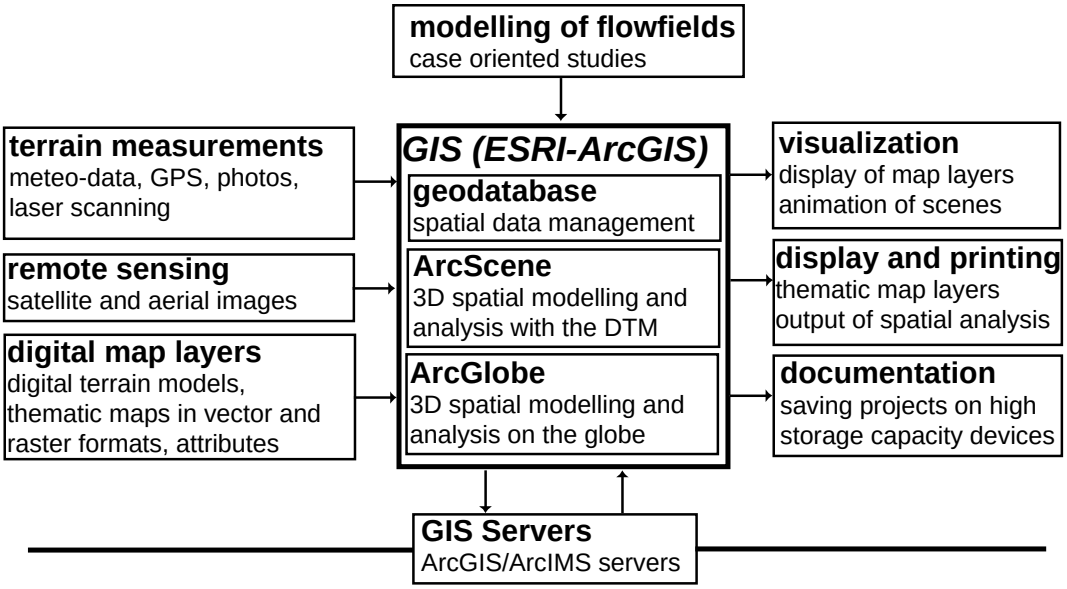

Figure 1. Processing of spatial data and flowfield simulation in GIS

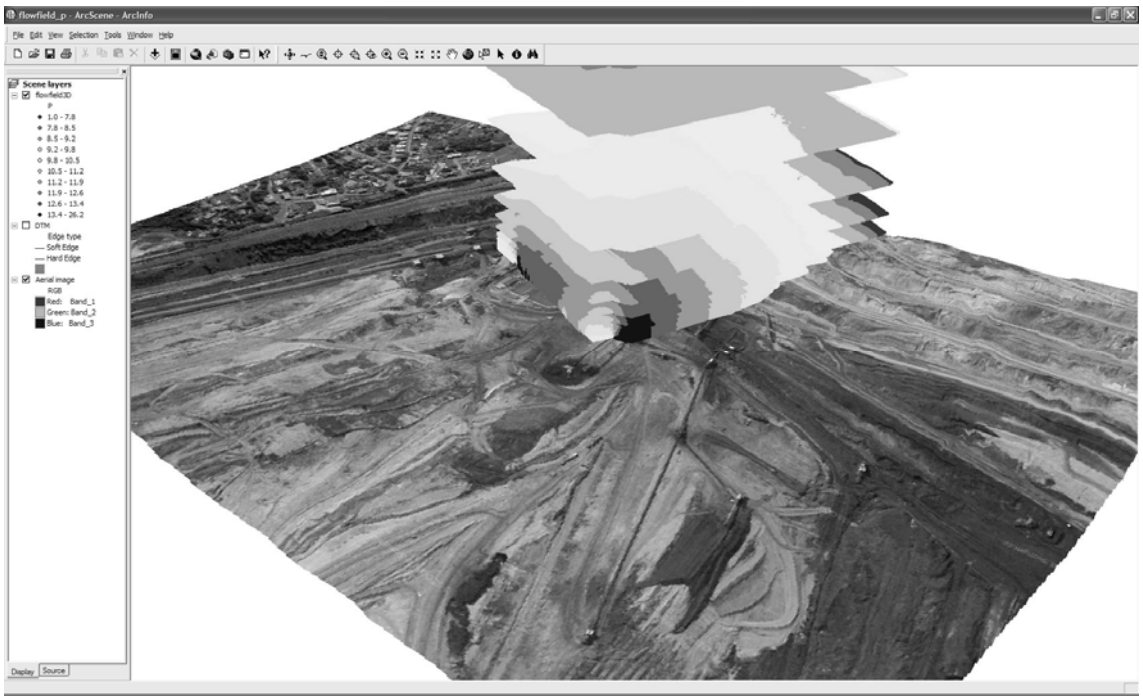

Figure 2. Local visualization of spatial data and flowfield simulation in ArcGIS

Acknowledgements

The contribution was supported by the grant No. 1ET400760405 and the Research Plan MSM 6840770010. The spatio-temporal data have been processed by ArcGIS, Erdas Imagine and other programming tools in the GIS Laboratory, Faculty of Natural Science, Charles University in Prague.

References

M.F. Goodchild, L.T. Steyaert, B.O. Parks (Ed.), 1996. GIS and Environmental Modeling: Progress and Research Issues. Fort Collins: GIS World, Inc.

SONDA SE TŘEMI ŽHAVENÝMI DRÁTKY PRO SOUČASNÉ MĚŘENÍ KONCENTRACE A DVOU SLOŽEK RYCHLOSTI VE SMĚSI DVOU PLYNŮ

The three hot-wire probe for simultaneous measurement of concentration and two velocity components in a binary gas mixture

Oton Mazur, Pavel Jonáš, Václav Uruba
Ústav termomechaniky, v.v.i., Akademie věd ČR, Praha

Úvod

Pro úplný popis turbulentní difúze v okolí daného bodu pole proudění směsi dvou plynů je třeba znát okamžité hodnoty všech tří složek vektoru rychlosti, hodnoty koncentrace, a pokud proudění směsi není izotermické, také hodnoty teploty. To je pět nezávislých veličin, takže intuitivní úvaha vede v tomto případě k závěru, že pro současné měření těchto veličin by bylo třeba rozmístit v těsném okolí měřeného bodu nejméně pět žhavených čidel různého tvaru a žhavených na rozdílné teploty. To však je tak náročná technologická úloha, že ji dosud nevyřešil žádný výrobce termoanemometrických sond ani žádná laboratoř zabývající se měřením proudění tekutin. Proto bylo v ÚT AV ČR přikročeno k pokusu o zhotovení vlastní sondy se třemi žhavenými drátky, jejichž konfigurace a provozní podmínky by umožnily měřit kromě koncentrace složek směsi alespoň dvě složky rychlosti proudění.

Popis sondy

Ke konstrukci těla třídrátkové sondy byla použita válcová keramika o průměru 5,8 mm, kterou prochází rovnoběžně s její osou 6 kanálků o průměrech 0,8 mm rozmístěných v rovných vzdálenostech na kružnici o průměru 3,5 mm. Těmito kanálky jsou prostrčeny a zalepeny přívodní jehly z ocelové struny tloušťky 0,7 mm, které vyčnívají z keramiky proti proudu zhruba 17 mm a na závětrné straně 8-10 mm. Jehly jsou na návětrné straně kuželově zbroušeny asi na polovině své délky na koncový průměr cca 0,3 mm. Zároveň jsou jehly mírně ohnuté k ose keramiky tak, aby jejich špičky tvořily požadovanou konfiguraci bodů z pohledu proti jejich hrotům. Schéma uspořádání jehel třídrátkové sondy je patrno z obr.1.

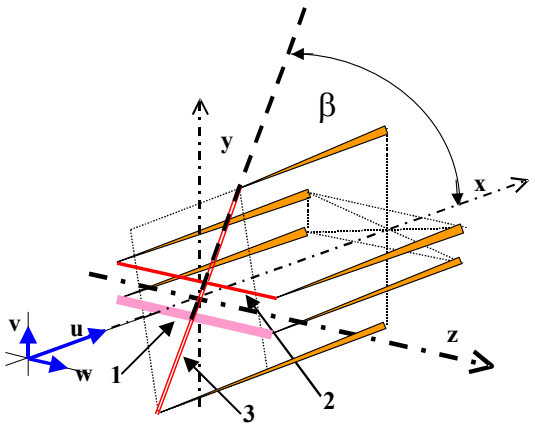

Obr. 1 Schéma sondy ÚT AV ČR, v.v.i. se třemi žhavenými drátky.

Na vnější dvojice jehel jsou přivařeny dva rovnoběžné drátky, které leží v rovině kolmé na podélnou osu sondy, jíž definuje osa keramiky. Jeden drátek z této dvojice je ze slitiny platiny (90 %) a rhodia (10%) , má průměr 0,010 mm a délku 1,28 mm. (označen na obr. jako č.1). Druhý drátek (č. 2) z této dvojice je z wolframu, má průměr 0,0025 mm a délku 1.15 mm. Šikmý drátek (č.3) leží v rovině, která obsahuje osu sondy a je kolmá na dvojicí rovnoběžných drátků. Je z poplatinovaného wolframového drátku o tloušťce 0,005 mm, má délku 1.56 mm a prochází středem mezery mezi rovnoběžnými drátky. Jeho sklon k ose sondy je 48^0.

Na konce jehel vyčnívajících na závětrné straně keramiky jsou přiletované stíněné přívodní kabely o celkové tloušťce 1.8 mm dlouhé zhruba 1 m, které jsou zakončené koaxiálními konektory o vnějším průměru 3 mm. Letované spoje kabelů a jehel jsou chráněny mosazným pláštěm zalitým pryskyřicí aby nedošlo k jejich poškození při manipulací se sondou.

Postup měření třídrátkovou sondou v proudu binární směsi a způsob jejího cejchování

Popsaná sonda je schopná ve spojení s tříkanálovým anemometrem měřit střední i okamžité hodnoty koncentrace v proudu binární směsi plynů a při její vhodné orientaci také dvě složky rychlosti za předpokladu, že střední proudění směsi je buď dvourozměrné, nebo symetrické vůči určité rovině. V prvém případě je nutno sondu orientovat tak, aby šikmý drátek ležel v rovině středního proudění a ve druhém případě v rovině symetrie středního proudu. Přesnosti měření středních i okamžitých hodnot zejména podélné a příčné složky rychlosti budou při tom tím vyšší, čím menší úhel bude svírat podélná osa sondy s vektorem střední rychlosti proudění.

Kardinální podmínkou pro to, aby popsaná sonda umožňovala změřit výše vyjmenované veličiny, je její pečlivá a podrobná kalibrace při měnící se koncentraci směsi, při změně rychlosti proudění i při změně směru obtékání šikmého drátku vždy alespoň v rozsahu příslušné veličiny, který může přicházet v úvahu při vlastním měření. Nadto je třeba všechny drátky cejchovat při řadě hodnot jejich žhavících teplot při vybraných hodnotách koncentrací a rychlostí. Podrobný popis této procedury pro sondu se dvěma žhavenými drátky, které jsou ve stejné konfiguraci jako drátky 1 a 2 u současně popisované sondy, je uveden v literatuře Moryń-Kucharczyk aj. (2003). Metodika měření koncentrace a podélné složky rychlosti s takto ocejchovanou dvoudrátkovou sondou a její aplikace při měření v kruhovém paprsku CO_2 vyfukovaném paralelně do homogenního vzdušného proudu je popsána v literatuře Jonáš aj. (2006) a Moryń-Kucharczyk aj. (2006). Tuto metodiku lze beze zbytku aplikovat na dvojici drátků 1 a 2 popisované sondy a určit tak koncentraci směsi a velikost U té složky rychlosti, která leží v rovině šikmého drátku.
K určení příčné složky ležící v rovině šikmého drátku potřebujeme pak ještě jeho směrovou kalibraci vyjádřenou zpravidla tzv. směrovou funkcí, což je čtverec poměru efektivní rychlosti ochlazování drátku $\mathrm{U}(\alpha)$, když ten svírá s vektorem rychlosti úhel α k téže efektivní rychlosti při kolmém ofukování drátku $\mathrm{U}(\alpha = 90^0)$. Je zřejmé, že efektivní rychlost při kolmém ofukování drátku musí být rovná velikosti rychlosti U určené z údajů dvojice rovnoběžných drátků. Na základě toho a z údajů šikmého drátku najdeme hodnotu směrové funkce a na základě toho určíme úhel α. Při známé pevné orientaci sondy v poli proudění již pak snadno určíme příčnou složku rychlosti proudění směsi v daném bodě.

Závěr

V článku je popsána nová sonda se třemi žhavenými drátky, která umožní měřit současně koncentraci a dvě složky vektoru rychlosti ve dvourozměrném nebo osově symetrickém (ve smyslu středních hodnot) proudu směsi dvou plynů.

Poděkování

Tato práce byla vykonána v rámci projektu COST OC 114 akce 732 s finanční podporou Ministerstva školství, mládeže a tělovýchovy České republiky.

Literatura

Moryń-Kucharczyk, E., Jonáš, P., Mazur, O. & Uruba V. (2003) *Preliminary investigation of the features of a probe with hot-wires pair at measurement in an air/CO_2 mixture stream*. In: Proc. Fluid Dynamics 2003 (P.Jonáš, V.Uruba eds.), IT AS CR Prague, 22.-24.10.2003,
pp. 89-92.

Jonáš, P., Mazur, O., Moryń-Kucharczyk, E., Podolski, M. (2006) *The spreading of a carbon dioxide gas round jet into a collateral air flow.* CMFF'06, The 13th International Conference on Fluid Flow Technologies, Budapest, Hungary, September 6-9, 2006 , pp. 297-303.

Moryń-Kucharczyk, E., Jonáš, P., Mazur, O., Podolski, P. (2006) *Zastosowanie techniki termoanemometrycznej w badaniach modelowych nad rozprzestrzenianiem się zanieczyszczeń gazowych.* Systems, 2006, Vol. 11, No. 1 (Appendix), pp. 247-354.

Mazur, O., Jonáš,P., Uruba, V. (2007) *Hot-wire probes for simultaneous measurement of concentration and velocity component in a binary gas mixture flow.* (in Czech), Proc. 21st Symposium on anemometry, May 29-30, 2007,Holany-Litice, ed.: Chára, Z., Klaboch, L., ISBN: 987-80-87117-01-9, pp. 111-11

AERODYNAMICKÝ ODPOR PŘI OBTÉKÁNÍ GOLFOVÉHO MÍČKU

Aerodynamic Drag at Flow past a Golf Ball

Martin Miczán, Jiří Nožička, Pavel Šafařík
České vysoké učení technické v Praze, Fakulta strojní, Ústav mechaniky tekutin a energetiky, Odbor mechaniky tekutin a termodynamiky, Praha, Česká Republika

Cílem této práce bylo ověřit charakteristiku součinitele odporu C_D na Reynoldsově čísle při obtékání golfového míčku a hladké koule.
V teoretické části je zpracována metoda řešení výpočtu volného pádu a letu golfového míčku a hladké koule ve vzduchu tj. řešení parametrů volného pádu a trajektorie letu s odporem prostředí. Po zadání počátečních podmínek je metoda [1] připravena k řešení letu golfového míčku nebo hladké koule a k vyhodnocení vypočtených hodnot a určení balistické křivky. Lze měnit počáteční rychlost, úhel odpalu golfového míčku nebo hladké koule a zjistit tak výšku letu nebo dráhu letu.

Při volném pádu s odporem prostředí $\frac{dv}{dt} = g - K\,v^{2-n}$ se pohybuje golfový míček nebo hladké koule pohybem rovnoměrně zrychleným do své max. rychlosti (= asymptotické rychlosti), v této práci je uveden vztah pro výpočet asymptotické rychlosti $v_{\max}$, $v_{\max} = \sqrt{\frac{8\,m\,g}{\pi\,C_D\,\rho\,d^2}}$. Golfový míček dosáhne své asymptotické rychlosti za čas t = 38,5 s a hladké koule za čas t = 26,5 s. Asymptotická rychlost koule je tedy o 30% menší oproti golfovému míčku.
Při výpočtu trajektorie letu golfového míčku a koule je zanedbáván vztlak, tj. rotace míčku nebo koule. Pro výpočet balistické křivky jsou použity vztahy $\ddot{x} = -K_1\left(\dot{x}^2 + \dot{y}^2\right) C_D \cos\delta$ a $\ddot{y} = -K_1\left(\dot{x}^2 + \dot{y}^2\right) C_D \sin\delta - g$, kde $K_1 = \rho\,\frac{\pi d^2}{4}\,\frac{1}{2m}$.
Za předpokladu nižšího součinitele odporu C_D u golfového míčku je dolet golfového míčku o 20 % větší než u koule a maximální výška letu o 15 % větší než u koule, při počáteční rychlosti v_0 = 57,9 m/s a úhlu odpalu 10˚.
Při řešení volného pádu a letu golfového míčku a koule je pro výpočet diferenciálních rovnic použita metoda Runge-Kutta 4. řádu.
V části experimentu byla navržena velmi jednoduchá metodika měření součinitele odporu C_D [1] při obtékání golfového míčku nebo koule v závislosti na Reynoldsově čísle. Metodika spočívala v měření odporové síly v aerodynamickém tunelu na základě posunutí obtékaného tělesa a následném přepočtení na skutečnou hodnotu odporové síly. Byla navržena metoda zavěšení měřeného tělesa v aerodynamickém tunelu a metodika výpočtu součinitele odporu z měření. Metoda výpočtu součinitele odporu C_D z měření nakonec spočívala v silové rovnováze tíhy, aerodynamické odporové síly a výsledné síly v závěsu lanka.
Byl odvozen matematický popis řešení součinitele odporu na Reynoldsově čísle pro navrženou metodiku zavěšení – metodika posunu míčku v rovině – posun v ose *x* vztažený k délce zavěšení *R* golfového míčku nebo koule v závislosti na odporové síle

$F_D = \frac{1}{2}\rho v^2 A C_D$ a tíze míčku nebo koule $G = m g$. $\frac{x}{R} = \frac{1}{\sqrt{\left(\frac{2 m g}{\rho v^2 C_D A}\right)^2 + 1}}$.

Byl určen i matematický vztah pro určení teoretického vychýlení golfového míčku nebo koule $\gamma = arctg\left(\frac{C_D \rho v^2 A}{2 m g}\right)$ $\left[^\circ\right]$ a vztah pro výpočet součinitele odporu C_D při posunu míčku v ose *x* v závislosti na délce zavěšení *R*. $C_D = \frac{\frac{x}{R}}{\sqrt{1-\left(\frac{x}{R}\right)^2}} \frac{2 m g}{\rho v^2 A}$.

Metoda se prokázala být dosti spolehlivá pro možné budoucí použití v praxi.
Bylo připraveno měření součinitele odporu C_D na Reynoldsově čísle pro golfový míček a kouli v aerodynamických tunelech. Pro jedno z měření v aerodynamickém tunelu byly vyrobeny i modely těžšího golfového míčku a hladké koule.

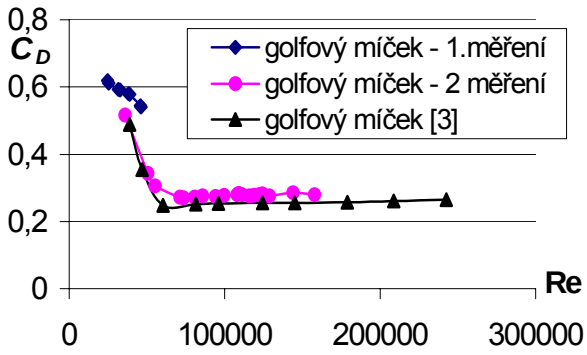

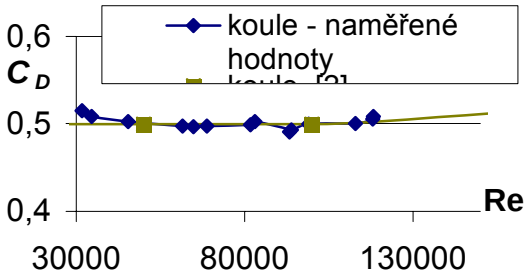

V této práci bylo prokázáno, že golfový míček je za určitých podmínek z hlediska velikosti aerodynamického odporu výhodnější (tj. má nižší součinitel odporu C_D), součinitel odporu C_D se sníží v důsledku snížení tlakového odporu až o polovinu, než je hodnota součinitele odporu pro hladkou kouli.
Snížení je dosaženo účinkem důlků na povrchu golfového míčku, na předčasný přechod mezní vrstvy na turbulentní a tím na oddálení místa odtržení proudu od povrchu míčku.

Literatura

[1] M.Miczán : Aerodynamický odpor při obtékání golfového míčku, bakalářská práce, ČVUT v Praze, Fakulta strojní, Praha, 2007
[2] E.Achenbach : The Effects of Surface Roughness and Tunnel Blockage on the Flow past Spheres, Journal of Fluid Mechanics, Vol.65, 1974, str.113-125
[3] P.W.Bearman, J.K.Harvey : Golf Ball Aerodynamics, Aeronautical Quaterly, May 1976, str.112-122

Práce byla podpořena v rámci projektu Grantové agentury AVČR reg.č. IAA200760504 a činnosti Výzkumného centra MŠMT reg.č. 1M06059 PTSE.

NUMERICKÉ MODELOVÁNÍ OBTÉKÁNÍ DESKY DVĚMI NEMÍSITELNÝMI TEKUTINAMI VE VRSTVĚ

Numerical Modelling of Flow of Two Immiscible Fluids in Layer Past a Flat Plate

T.Mužík, J.Nožička, P.Šafařík
České vysoké učení technické v Praze, Fakulta strojní, Ústav mechaniky tekutin a energetiky

1. ÚVOD

Stékání tenkého vodního filmu je problém vyskytující se v řadě inženýrských aplikací. Například na lopatkách turbinových mříží může kondenzující a stékající voda způsobit i mimořádné komplikace. Proto je třeba tento jev zkoumat a z tohot důvodu se jím zabývá tato práce. Byla tedy zformulována a řešena 2D úloha obtékání desky vzduchem, na níž vstupuje vrstva vody. Řešené téma představuje úvodní studii řešení vývoje kapalných vrstev a interakce nemísitelných tekutin při obtékání těles.

2. NUMERICKÉ MODELOVÁNÍ PROUDĚNÍ

V generátoru sítí Gambit byly vytvořeny dvě varianty geometrií desky se vstupem vody a následně v oblastech byly vygenerovány výpočtové sítě.
Proudění nestlačitelné tekutiny bylo řešeno CFD programem Fluent 6.3, který řeší soustavu Navierových–Stokesových [1] rovnic pomocí metody konečných objemů. Soustava se stává z

rovnice kontinuity: $$\frac{\partial u_i}{\partial x_i} = 0\,, \tag{1}$$

a rovnice bilance hybnosti: $$\frac{\partial u_i}{\partial t} + \rho \frac{\partial \left(u_i u_j\right)}{\partial x_j} = -\frac{\partial p}{\partial x_i} + \frac{\partial \tau_{ij}}{\partial x_j} + F_i\,. \tag{2}$$

Pro výpočet mezifázového rozhraní, které lze popsat následující rovnicí:

$$\frac{1}{\rho_q}\left[\frac{\partial}{\partial t}\left(\alpha_q \rho_q\right) + \nabla \cdot \left(\alpha_q \rho_q \vec{v}_q\right) = S_{\alpha_q} + \sum_{p=1}^{n}\left(\dot{m}_{pq} - \dot{m}_{qp}\right)\right], \tag{3}$$

byl použit explicitní model VOF (Volume of Fluid):

$$\frac{\alpha_q^{n+1}\rho_q^{n+1} - \alpha_q^n \rho_q^n}{\Delta t} V + \sum_f \left(\rho_q U_f^n \alpha_{q,f}^n\right) = \left[S_{\alpha_q} + \sum_{p=1}^{n}\left(\dot{m}_{pq} - \dot{m}_{qp}\right)\right] V\,, \tag{4}$$

který je vhodný pro výpočet proudění dvou (nebo i více) nemísitelných látek. Pro výpočet fázového rozhraní bylo použito schéma Geo – Reconstruct.

2.1 NASTAVENÍ PARAMETRŮ PROUDĚNÍ V PROGRAMU FLUENT

Proudění je uvažováno jako laminární, vazké, nestlačitelné, nestacionární. Rychlost vzduchu byla na vstupu zadána homogenně 40 $m.s^{-1}$ a rychlost vody byla $1m.s^{-1}$ ve variántách úhlu vstřiku 0° a 90°. Ostatní parametry byly nastaveny tak, aby simulovaly reálné prostředí.

3. VÝSLEDKY VÝPOČTU PROUDĚNÍ

Výsledky řešení ukazují vývoj koncentrace kapalné fáze od počátku vstřiku do ustálení proudové vrstvy vody. Na následujících Obr. 1 a 2 jsou zobrazeny hmotnostní podíly jednotlivých tekutin pro obě řešené varianty, v již ustáleném stavu.

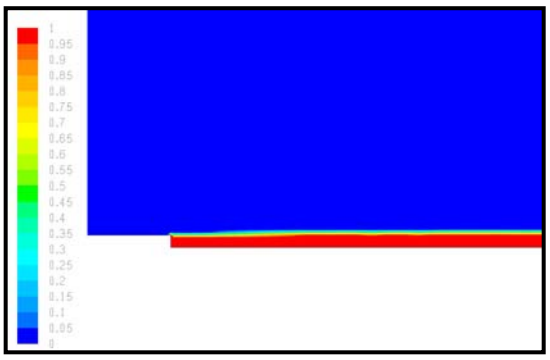

Obr. 1. Hmotnostní podíl vody a vzduchu u varianty se vstupem 0°.

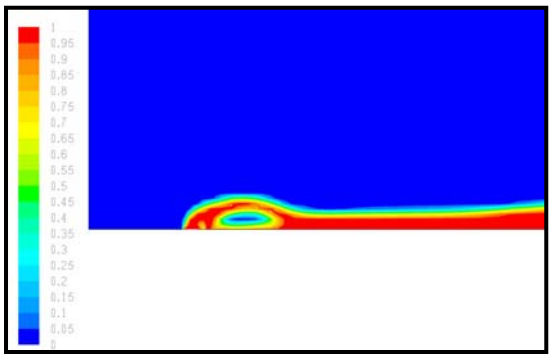

Obr. 2. Hmotnostní podíl vody a vzduchu u varianty se vstupem 90°.

Je vidět, že proud vody vstupující do oblasti z desky pod úhlem 90° nepřilne k desce hned po vstupu. Vytvoří se zde oblast obsahující vzduch pod oblastí vody. Výsledky výpočtu ukazují dále, že na vodním filmu a zvláště v úplavu za deskou vznikají vlny. Ve fázi rozběhu kapalné fáze lze pozorovat podle výsledků výpočtu rozpad kapalné fáze, který je vyjádřen zřejmým rozptylem koncentrace a který v postupu řešení v čase se posune přes výstupní okrajovou podmínku a proudění v řešené oblasti se ustálí. Tento výsledek je uveden v [1].

4. LITERATURA

[1] Fluent 6.3 Documentation, Fluent Inc., 2006
[2] T.Mužík, J.Nožička, P.Šafařík**:** Numerické Modelování obtékání desky dvěmi nemísitelnými tekutinami ve vrstvě, In: Dynamika tekutin 2007, CD-ROM, Praha, 2007

Poděkování
Práce byla podpořena v rámci činnosti Výzkumného centra MŠMT reg.č.1M06059 PTSE.

ENERGY DISSIPATED AT THE SHOCK WAVE DURING ITS PROPAGATION IN WATER

Miloš, Müller
Technical university of Liberec, Department of Power Engineering equipment, Hálkova 6, 461 17 Liberec 1.

Abstract
The shock wave propagation in liquids is usually calculated without considering the energy dissipation. However in some situations, when the initial shock wave pressure is in order of 1000 MPa, the dissipation effect can be important. This paper presents the possibility of calculation of the energy dissipated at the shock wave during its propagation in water. The dissipated energy and the temperature increase at the shock wave are expressed as a function of shock wave peak pressure. The NIST data [2] are used for the fitting of coefficients of the equation of state, which is applied for the calculation of the shock wave energy dissipation.

The equation of state
The most common equation of state (EOS) for liquids is Tait´s equation, which represents the dependence between the liquid density and the pressure. In the presented case, it is convenient to use the EOS in isentropic form [3] as

$$\frac{\rho(p,s)}{\rho(p=0,s)} = \left(\frac{B(s)+p}{B(s)+p_0} \right)^{\frac{1}{n}}, \; B(s) = \frac{\rho_0 c_0}{n}. \tag{1}$$

where $n=7$, p is the shock wave peak pressure, $\rho(T, p_0)$ is the liquid density and $c(T, p_0)$ is the speed of sound. The last two variables depend on temperature and are evaluated at the initial pressure p_0 = 1 atm.

Enthalpy dissipated at the shock wave
If the shock wave passes a position in liquid, which has the temperature T_0 and pressure p_0, the temperature and pressure in that place increase up to the values p and T. The specific enthalpy increment experienced by the fluid ΔH is given in from Rankine-Hugoniot conditions. Having passed the shock wave the pressure in the liquid reaches again the pressure p_0 along the adiabatic curve but the temperature returns to a higher value T_1 due to the dissipation process. Based on the consideration, the enthalpy increment ΔH can be evaluated as a sum of undissipated and dissipated enthalpy as

$$\Delta H = h + h_{dis} = \frac{2c_1^2}{n-1}\left(\left(\frac{\rho}{\rho_1} \right)^{\frac{1}{n}} - 1 \right) + \int_{T_0}^{T_1} c_p(T_0, T_1)\, dT \; . \tag{2}$$

The estimation of the temperature T_1 is the key for obtaining the dissipated energy. Its evaluation has following consequence. First, ΔH is obtained using Rankine-Hugoniot conditions at the shock wave [1] and specific heat c_p is expressed as function of

T_0=293K	NIST			Richardson[3]
p [MPa]	ΔT_1 [K]	T_1 [K]	h_{dis} [J/kg]	h_{dis} [J/kg]
0	0.0	293.0	0.0	0.0
250	0.2	293.2	1046.0	x
500	1.2	294.2	5152.0	5570.0
1000	5.4	298.4	22480.0	23450.0
1500	11.5	304.5	47978.0	49350.0
2000	18.8	311.8	78484.0	80050.0
2500	26.9	319.9	112547.0	115000.0
3000	35.6	328.6	148720.0	152500.0
3500	44.7	337.7	186806.0	192000.0
4000	54.0	347.0	225771.0	233000.0

Tab. 1. Dissipated enthalpy calculated as a function of the pressure at the shock wave.

temperature *T*. The Eq. 2. is then an implicit function of the shock wave peak pressure and the temperature T_1. The value of T_1 can be obtained for given pressure from the equation Eq. 2. using an appropriate iterative method. This temperature is then used in the calculation of dissipated enthalpy. The data obtained from the calculation are given in Tab. 1. The explicit formula for energy dissipated at the shock wave as function of pressure has the form

$$h_{dis}(p) = 3.0917x10^{-2}\,p^4 - 4.7538p^3 + 2.8574x10^2\,p^2 - 1.5626x10^2\,p\,. \qquad (3)$$

Conclusion

This paper presents the possibility of calculation of shock wave energy dissipated at the shock wave in water. For the solution, the dissipated enthalpy was derived based on the new material data obtained from NIST material database. The comparison between the dissipated energy calculated by Richardson in [2] and the presented data shows very good agreement.

Acknowledgement

This work is supported by grant no. 4674788501 of the Ministry of Education and by grant no. 101/07/1612 of the Grant Agency of the Czech Republic.

References

[1] R.H. Cole, Underwater explosion, Princeton Univ. Press, Princeton, 1948

[2] P. J. Linstrom, W. G. Malard, NIST Chemistry WebBook, NIST Standard Reference Database Number 69, National Institute of Standards and Technology, Gaithersburg MD, 2005, (http://webbook.nist.gov).

[3] J. M. Richardson, A. B. Arons, R. R. Halverson, Hydrodynamic Properties of Sea Water at the Front of a Shock Wave, The Journal of Chemical Physics 15 (11) (1947) 785-794.

SOME RESULTS OF COHERENT STRUCTURES IDENTIFICATION IN PLASMA JETS

Václav Něnička, Jiří Šonský
Institute of Thermomechanics AS CR, v.v.i., Dolejskova 5, CZ-182 00 Prague 8

In the experiment, plasma jet image is projected by objective lens onto ends of optical fibres coupled to the photodiodes, which converts the light into the electrical current. Attached electronic amplify the current, digitalize it and record. The total 128 fibres are divided into four independent directions of observation indexed by angle of 45 degrees. Each of the observation direction subsystem consists of two rows with sixteen fibres. Cross section perpendicular to the axis of the plasma jet can be reconstructed from these records. For scheme of the experiment see Figure 1 [1].

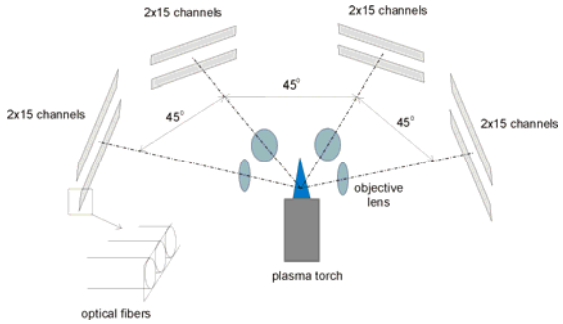

Figure 1. Experimental layout schematic.

The time development of radiation intensity in the cross sections perpendicular to the axis of a plasma jet yields basic information on dynamics of structures propagation along the flow axis. These diagnostic cross sections can be constructed along the flow axis and perpendicular to axis of plasma jet. An important influence on the resultant plasma jet dynamics rests also with impact of dynamic effects of the surroundings, that cooperate in installing un-equilibrium dynamic system of the plasma jet core with surrounding medium. The balance relations of un-equilibrium open thermodynamics make it possible to study the time evolution of such arrangement, using experimental data of the radiation intensity variations scanned in several planes adjusted perpendicularly to the plasma jet axis. Each of these planes contains information on the time evolution of radiation intensity for plasma jet in both its spatial and time disposal.

Hence, the problem rests with identifying the structures that iterate in the plasma jet core, using as the basis the information scanned from four separate directions that are dislocated inside two parallel planes. To determine the time intervals of the recurrences, the maximum of radiation intensity will be scanned, obtaining four components of the vector. The time evolution within two selected time intervals is compared using the correlation analysis for determining the correlation coefficients. The sequence of the values of the correlation coefficients yields information concerning the mutual orientation of such structures.

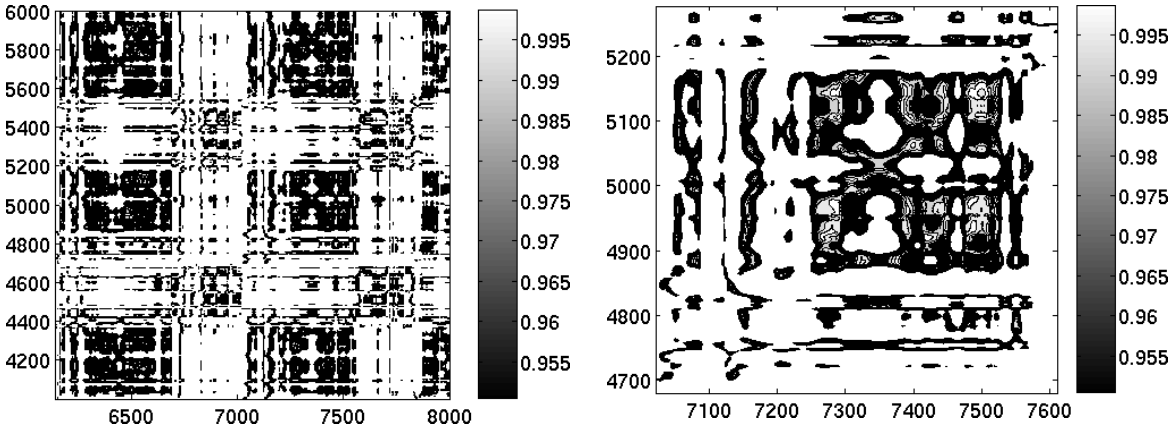

Figure 2. Graphic representation of correlation coefficients matrices.

Within time intervals of significant mutual resemblance, the correlation coefficients are approaching to the value one. Such approach allows constructing rectangular matrices. The rows and columns of these matrices correspond to the monitored time intervals, see figure 2 left. If there exists a significant resemblance of the monitored signals, the values of the elements in the matrices are approaching to one, see Figure 2 right. As we can assume relatively equal relaxation intervals of heat energy transfers in radial direction for the two monitored configurations in free plasma flow, the resemblance of the monitored structures suggests the possibility of their coherence see Figure 3. The recurrence in the regions whose values approaching to one represents an important characteristic of the structures in plasma jet. In this way the monitored record represents structures with features of coherent behaviour in the plasma jet.

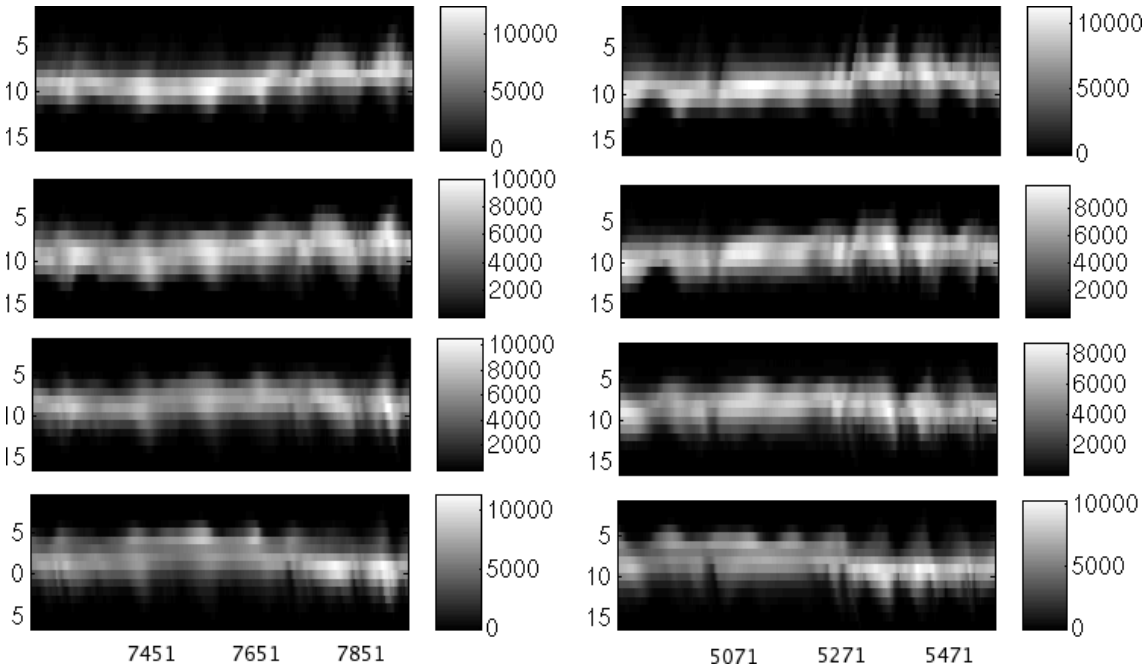

Figure 3. Time evolution of source signal corresponding to right matrix in figure 2.

[1] Jiří Šonský, *Applying of fibre optics to plasma jet diagnostics*, Acta Technica CSAV 52 (2007), 15-31

This work was supported by project PP-07-07011.

POHYB ZNAČKOVACÍCH ČÁSTIC V NESTACIONÁRNÍM PROUDOVÉM POLI

Behavior of Seeding Particles in the Unsteady Flow Field

Jan Novotný, Jiří Nožička
České vysoké učení technické v Praze, Fakulta strojní, Ústav mechaniky tekutin a energetiky, Praha

Úvod

Principem měření metodou PIV (Particle Image velocimetry) je určit posunutí obrazů značkovacích částic za zvolený časový interval. Přesnost takového měření je ovlivněna způsobem výpočtu „korelační roviny“, dále pak metodou použitou při vyhledávání přesné pozice signálového peaku a v neposlední řadě na schopnostech značkovacích částic sledovat nestacionární chování kapaliny. Způsobům vyhodnocení posunutí včetně nalezení polohy maxima a jejich vlivu na přesnost měření se v tomto článku nebudeme věnovat. Zaměřili jsme se na rozbor schopností značkovacích částic sledovat proud a s tím spojenou otázku použitelnosti značkovacích částic příslušných parametrů pro měření nestacionárního proudění. V závěru jsme se pokusili poskytnout čitateli tohoto článku stručný návod, jak postupovat při volbě vhodných značkovacích částic při měření nestacionárního proudění, kdy je cílem
zachytit fluktuace o vysoké frekvenci.

BBO rovnice

Pohyb částic je popsán rovnicí označovanou podle svých autorů jako Basset-Boussinesq-Ossen, BBO rovnice.

$$m_p\frac{du_p}{dt}=\frac{18\mu_F}{\rho_p d_P^2}m_p(u_F-u_P)-m_F\frac{Du_F}{Dt}+\frac{1}{2}m_F\left(\frac{Du_F}{Dt}-\frac{du_p}{dt}\right)+9\sqrt{\frac{\rho_F\mu_F}{\pi}}\frac{m_p}{\rho_p d_P}\int_{t_0}^{t}\frac{\frac{Du_F}{D\tau}-\frac{du_p}{d\tau}}{\sqrt{t-\tau}}d\tau+(m_p-m_F)g$$

kde:

m_p	hmotnost částice
u_p	rychlost částice
ρ_p	hustota částice
d_p	průměr částice
μ_F	dynamická viskozita kapaliny
u_F	rychlost tekutiny
m_F	hmotnost kapaliny o objemu
t	čas
g	gravitační zrychlení
τ	časový interval od počátku akcelerace

Řešení BBO rovnice pro pohyb částice v proudovém poli vyjádřené pomocí Fourierova integrálu uvádí Hjelmfelt i Sommerfeld [1, 2] pro různá Stokesova čísla. Jak ale vyplynulo z našich rozborů, pro měření metodou PIV není rozsah uváděných závislostí poměru amplitud výchylek na Stokesově čísle dostatečný. Hjemfeld [1] uvedl řešení rovnice BBO pro průběh rychlosti kapaliny u_F a rychlosti částice u_P vyjádřené pomocí Fourierova integrálu:

$$u_F=\int_0^{\infty}(\zeta\cos\omega t+\lambda\sin\omega t)d\omega$$

Řešením je rovnice popisující pohyb částice jejíž fáze je zpožděná o úhel β a původní amplituda je přenásobena koeficientem η.

$$u_P=\int_0^{\infty}\eta\left[(\zeta\cos(\omega t+\beta)+\varphi\sin(\omega t+\beta))\right]d\omega$$

Vyneseme-li průběh poměru amplitud v závislosti na velikosti Stokesova čísla,

které nám udává bezrozměrnou frekvenci rozruchů v proudu, získáme následující průběh:

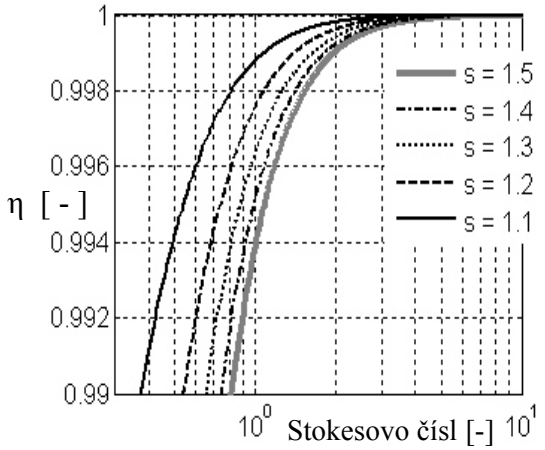

Obr.1 Závislost poměru amplitud na Stokesově čísle pro několik poměrů hustot částice a kapaliny používaných při měření ve vodě o 20°C.

Z uvedeného je zřejmé, že pokud se budeme pohybovat v poměrech hustot kapaliny a částice do hodnoty 1.5, pak při hodnotě Stokesova čísla vyšším než 2 bude pokles amplitudy menší než jedna desetina procenta. Tato shoda je již dostatečná a za daných podmínek je možné považovat proudění tekutiny a pohyb částice za totožné. Obdobnou závislost je možné vynést pro fázové zpoždění a samozřejmě pro libovolný poměr hustot vyskytující se v reálné praxi. Při vynesení obdobné závislosti pro poměry hustot vyskytující se při měření ve vzduchu dojdeme k závěru, že při stejné požadované shodě v amplitudě je nutné se pohybovat v oblasti Stokesových čísel větších než cca 30 při poměru hustot do 1000. Zůstává však nezodpovězena otázka jakých dosahujeme hodnot Stokesova čísla při použití jednotlivých druhů značkovacích částic o různých průměrech a v tekutinách s rozdílnou viskozitou. Z těchto závislostí je pak možné odečíst pro jaké druhy značkovacích částic a pro jakou požadovanou maximální frekvenci je Stokesovo číslo větší nebo menší než hodnota stanovená z Obr.-1.

Závěr

Vhodnost použití jednotlivých druhů značkovacích částic při měření nestacionárního proudění metodou PIV je nutné kontrolovat pomocí hodnoty Stokesova čísla pro maximální předpokládané frekvence rozruchů. Je-li hodnota Stokesova čísla vypočtená pro danou částici, tekutinu a frekvenci menší než mez stanovená pro maximální povolenou odchylku, není možné zvolený druh částic použít pro měření zvolených frekvencí a je nutné použít buď částic stejných vlastností ale menšího poloměru nebo částic s hustotou bližší hustotě tekutiny, kterou sledujeme.

[1] Hjelmfelt A. T., Mockros L. F., Motion of Discrere Particles in a Turbulent Fluid, Appl. Sci. Res. Vol. 16, 149-161, 1966

[2] Sommerfeld M., Theoretical and Experimental Modelling of Particle Flows, lecture series 2000-2006, von Karman Institute for Fluid Dynamics, 2000

[3] Hesham M. El-Batsh., Modeling Particle Deposition on Compressor and Turbine Blade Surfaces, dissertation, Vienna University of Technology, Vienna, 2001

[4] Crowe C., Sommerfeld M., Tsuji Y., Multiphase Flows with Droplets and Particles, ISBN 0-8493-9469-4, CRC Press, USA, 1998

Poděkování:

Tento projekt je financován z prostředků VCJB

PERFORMANCE OF PRESSURE AND EFFERVESCENT ATOMIZERS

Jan Otahal, Jan Fiser, Miroslav Jicha
Department of Thermodynamics and Environmental Engineering
Faculty of Mechanical Engineering, Brno University of Technology
Brno, Czech Republic

Abstract

The article deals with an evaluation of the efficiency of atomization for two different types of atomizers. The comparison between efficiency of the pressure and the effervescent atomization may help decide which type of the atomizer is suitable for a particular application. The evaluation of both types of atomization principles is based on experiments. The PDA (Phase Doppler Analyzer) was used to acquire information about the spray quality in particular measurement points within the spray cone. The experiments were carried out on a model of an effervescent atomizer and three small pressure atomizers.

Introduction

If there is a need to decide which type of atomizers is suitable for an application, it is needed to determine a comparable characteristic, which describe the produced spray or the construction parameters of the nozzle. One of the comparable characteristic is efficiency of the atomization process.

According Bayvel & Orzechowski the efficiency of atomization for all traditionally used atomizers is very small, namely $\eta < 0.1\%$. Improvement of atomization is related to the energy demand, i.e. increased energy demand corresponds to a decrease of the atomization efficiency. The efficiency of the atomization process of pressure atomizers is higher then of the pneumatic atomizers. Effervescent atomizers should generate droplets of particular size with greater efficiency then other types of twin-fluid atomizers.

Nozzles description

For the experiments, there were three small pressure nozzles (Fig. 1) and one effervescent nozzle (Fig. 2) used. In order to compare the two atomization processes, two factors were determined and kept comparable for both the atomization processes. The first one was the injection pressure and the second one was the flow rate of the atomized fluid. The atomizers were operated at the maximal injection pressure of 0.5 MPa and the flow rates ranged from 0.3 to 6 kg/min.

Fig. 1 Unijet nozzle

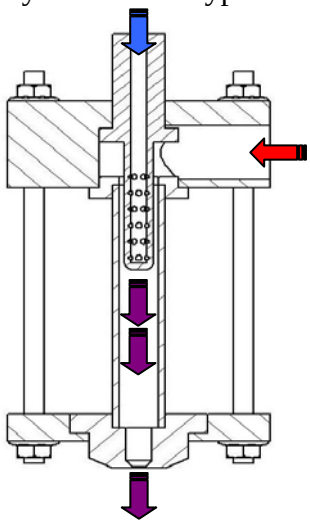

Fig.2 Effervescent nozzle

Atomization efficiency

Total energy E_i required to generate a spray using pneumatic atomizer consists of two energies; firstly E_g, the energy introduced by the compressed gas and, E_l, energy introduced by the liquid.

Transformation of bulk liquid into fine droplets is associated with enormous increase of surface. If bulk liquid with the volume V_l is subdivided into droplets having all the same radius IR_{20} (so called Integral surface radius), then the area of the droplet system will be $A = 3 \cdot V_l / IR_{20}$.

The corresponding surface energy increase neglecting the original surface energy of bulk liquid reads $E_a = A \cdot \sigma$. The efficiency of the atomization process finally is:

$$\eta = \frac{E_a}{E_i} = \frac{3 \cdot V_l \cdot \sigma / IR_{20}}{E_i} = \frac{3 \cdot \sigma / IR_{20}}{p_l + GLR \cdot \frac{\rho_l}{\rho_g} \cdot \left(p_g + p_b\right) \cdot \ln\left(\frac{p_g + p_b}{p_b}\right)} \tag{1}$$

Results

In Fig. 3, there is the efficiency of the pressure and the effervescent atomization against the water flow rates plotted. It is clear the efficiency of the pressure atomization is higher for pressure nozzles than for effervescent ones over the same range of flow rates and pressure levels. High values of the efficiency were reached at the low pressure (0.1 MPa). Increasing the pressure level results the deterioration of the atomization efficiency. The efficiency of pressure atomization achieves a quite high value (3%) which is a consequence of decrease in the injection pressure to the minimal possible pressure level and small diameter of the final orifice.

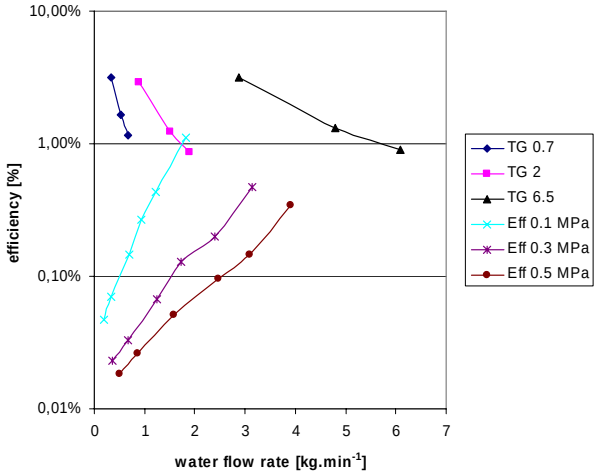

Fig. 3 Atomization efficiency against flow rates

Conclusion

Spray characteristics of pressure and effervescent atomizers have been assessed by means of PDA measurement. The pressure level of the atomized fluid has the main effect on value of the atomization efficiency.

Although the efficiency of atomization of effervescent atomizers is lower than that of the pressure atomizers, their main advantage can be seen in the possibility to produce the spray of the same quality at much lower pressure.

Acknowledgement

The support of this research from Development fund FRVS no. 172/2007 of the Ministry of Education of the Czech Republic, and project no. GA 101/06/0750 from Czech Science Foundation is gratefully acknowledged.

POMĚRNÝ ÚTLUM JEDNODUCHÉHO TĚLESA V PROUDU VZDUCHU
Damping factor of a simple body in an air flow

Aleš Pacák[1,2], Klára Matoušková[2], Ladislav Tajč[2], Jiří Linhart[1]
[1] Západočeská univerzita v Plzni, Fakulta strojní
Katedra energetických strojů a zařízení
[2] ŠKODA POWER a.s., Plzeň

Abstrakt

Hlavním úkolem prezentované studie je prvotní prověření dynamického chování jednoduchého modelu v proudícím prostředí. Je uveden základní popis experimentálního zařízení pro vyšetřování aeroelastických vazeb, princip měření výchylky pružně uloženého modelu s tlumením a postup při kalibraci výchylky. Studie popisuje experimentální stanovení poměrného útlumu a vlastní frekvence v závislosti na rychlosti proudícího média. Cílem je získat poznatky o průběhu těchto závislostí, identifikovat případné změny v průběhu či lokální extrémy funkcí, a dále navrhnout vhodné náměty a úpravy pro další experimenty.

Experimentální zařízení pro vyšetřování aeroelastických vazeb

Experimentální zařízení sestává z nízkorychlostního aerodynamického tunelu, na jehož výstupu je připojen měřící prostor s pružně uloženým modelem, dále ze senzorů pro snímání změny polohy modelu, měřícího zařízení a z programů pro zaznamenávání a vyhodnocení měřeného signálu. Schematické znázornění aerodynamického tunelu je na obr. 1, uspořádání měřícího prostoru se zkoumaným modelem ukazuje obr. 2.

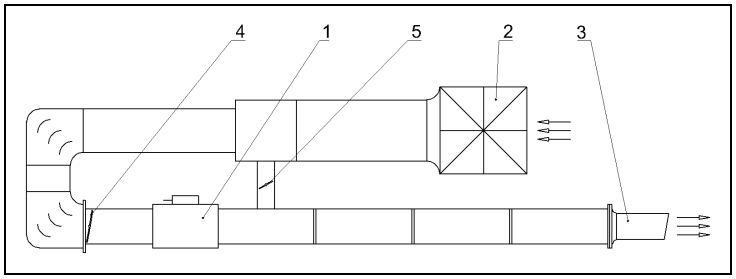

Obr. 1: Nízkorychlostní aerodynamický tunel.

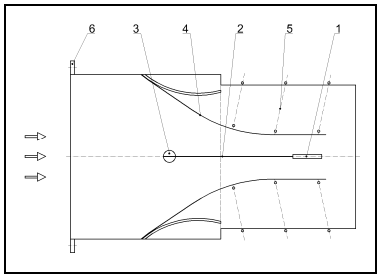

Obr. 2: Měřící prostor.

Výchylka je měřena nepřímo, prostřednictvím dvojice tenzometrů. Závislost snímaného poměrného prodloužení krajních vláken planžety a výchylky modelu se určí kalibrací. Naměřená data ukazují, že závislost je v celém rozsahu předpokládaných výchylek lineární.

Matematický model

Pohybovou rovnici popisující dynamické chování zkoumaného systému předpokládáme ve tvaru (1). Uvažujme, že působící aerodynamické síly mají charakter lineárních tlumících sil a jejich účinek se projeví pouze ve změně konstanty tlumení b. Konstanta tlumení b^* ve vztahu (1) zahrnuje vliv materiálového i aerodynamického tlumení.

$$m\ddot{q}(t) + b^{*}\dot{q}(t) + kq(t) = 0 \qquad (1)$$

Stanovení poměrného útlumu

Poměrný útlum lze vyjádřit jako

$$D = \frac{\delta}{\sqrt{4\pi^2 + \delta^2}}, \qquad (2)$$

kde δ je logaritmický dekrement útlumu, který představuje přirozený logaritmus podílu výchylek tlumených kmitů vzdálených od sebe právě jednu periodu.

Během experimentu je zaznamenáván časový průběh výchylek kmitů. Program pro vyhodnocení dat identifikuje lokální maxima tlumených kmitů a z jejich hodnot stanoví logaritmický dekrement útlumu. Výpočtem dle vztahu (2) se určí poměrný útlum.

Výsledky

Pro každou řešenou variantu bylo provedeno přibližně dvacet měření při různých rychlostech proudění vzduchu. Finálním výstupem každého měření je hodnota poměrného útlumu a vlastní frekvence tlumené soustavy. Závislost těchto veličin na rychlosti proudění ukazují obr. 3 a obr. 4.

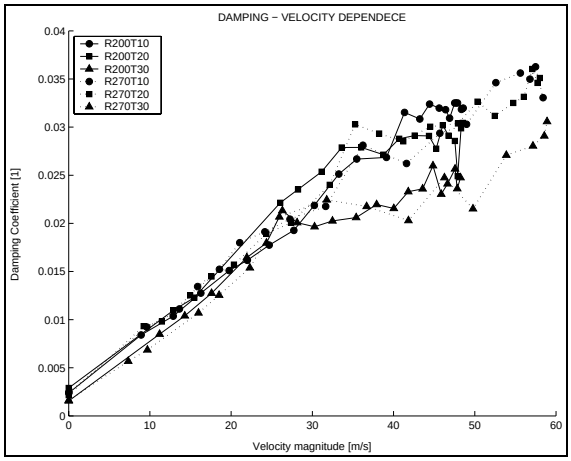

Obr. 3: Závislost poměrného útlumu na rychlosti proudění.

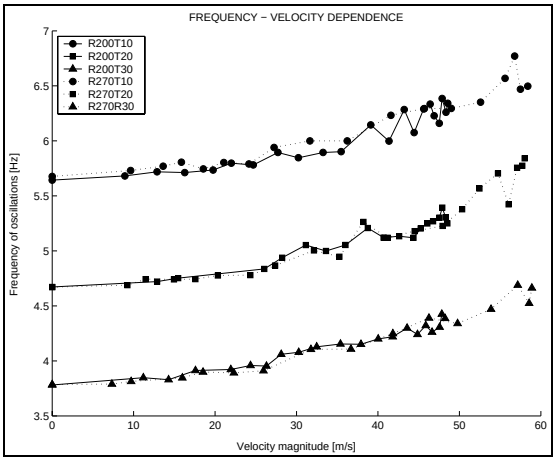

Obr. 4: Závislost vlastní frekvence tlumené soustavy na rychlosti proudění.

Poměrný útlum dle předpokladů se stoupající rychlostí proudění roste. Zajímavá je změna charakteru průběhu závislosti, kdy se při stoupající rychlosti proudění vzduchu prakticky lineární průběh s velmi podobnými hodnotami poměrného útlumu mění. Dochází ke zlomu charakteristiky, naměřené hodnoty za tímto zlomem vykazují větší rozptyl. Tyto změny jsou pravděpodobně způsobeny změnou charakteru proudění v oblasti testovaného modelu. Přesnější vysvětlení jevu není ze získaných dat možné.

Závislost vlastní frekvence na rychlosti proudění proti očekávání roste. Tento trend nedokáže sestavený matematický model popsat. V navazujících pracích by měla být pozornost soustředěna především na úpravu matematického modelu a nalezení vhodného popisu řešeného problému.

NUMERICAL SIMULATION OF TURBULENT FLOWS AROUND SINUSOIDAL HILLS

Luboš Pirkl and **Tomáš Bodnár**

Czech Technical University of Prague, Faculty of Mechanical Engineering, Department of Technical Mathematics

Introduction

Prediction of wind field over terrain plays an important role in many engineering applications. A numerical investigation of the flow over sinusoidal hill is presented in this work. We assume two-dimensional, steady, turbulent flow of incompressible fluid. We have computed four test cases with different geometries. The model is set-up for the wind flow according to Kim [1]. The introduced test cases were experimentally measured [1] and comparison with experiment and with other numerical simulations was made. The numerical method we have used is based on solving Reynolds Averaged Navier-Stokes equations with help of Finite Volume Method. We have implemented two models of turbulence. Mixing Length Model (T.B.) and Spalart-Allmaras turbulence model (L.P.) was used.

Computational domain

According to data published in [1] we have chosen 2D domain with four different sinusoidal single-hill terrain profiles having the following parameters:

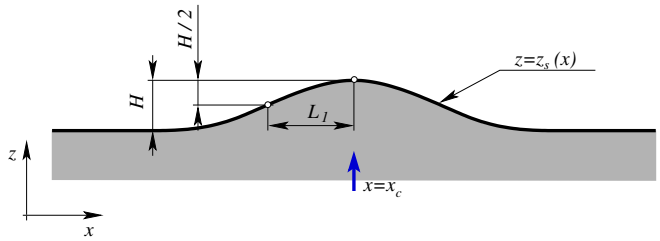

Figure 1: Hill geometry

Hill	**slope**	**height** H	**length** L_1
S3H4	0.3	4 cm	6.67 cm
S3H7	0.3	7 cm	11.67 cm
S5H4	0.5	4 cm	4.0 cm
S5H7	0.5	7 cm	7.0 cm

Table 1: Hill setup

The notation we use here to distinguish between hills with different slopes and heights is the same as in [1]. It means the SxHy stands for the hill with maximum slope $0.x$ and height $y\ cm$. The height of the whole computational domain is $0.5m$ and the length is $2.0m$.

Boundary conditions

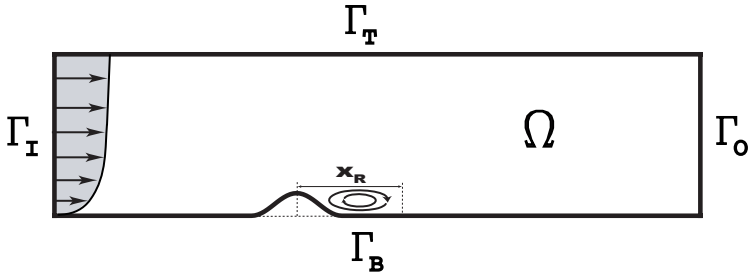

Γ_I ... Logarithmic velocity profile $u(y) = \frac{u_t}{\kappa} ln \frac{y}{y_0}$, $u_t = 0.33m/s$, $y_0 = 0.0005mm$ for $y < 0.25m$ and $u(y) = 7.0m/s$ for $y > 0.25m$.
Γ_B ... $u, v = 0.0$,
Γ_T ... $\frac{\partial \vec{u}}{\partial \vec{n}} = 0.0$,
Γ_O ... $p = const.$

Figure 2: Computational domain

the rest of variables are extrapolated from the inside of the computational domain.

Numerical method

Governing system are Reynolds Averaged Navier-Stokes equations, solved with help of Finite Volume Method. We have used two turbulence models. **Spalart-Allmaras** one-equational model and **Mixing Length Model** are used. For computation we have used MacCormack scheme and non-orthogonal, wall-fitted mesh.

Results

For $S3Hx$ (gentle-sloped) test cases we all obtained small separation zones near the wall, but mentioned experiment obtained none. The comparison of $S5Hx$ (sharp-sloped) test cases is shown in following table:

Hill	**Experiment**	**Standard** $k-\epsilon$	**RNG** $k-\epsilon$	**Low-Re model**	**MLM**	**S-A**
S5H4	**5.25** $\pm$ **0.5**	2.5	3.42	4.55	**5.0**	**5.8**
S5H7	**4.30** $\pm$ **0.3**	-	3.97	4.42	**4.7**	**5.7**

Table 2: Reattachment point position (x_R/H)

Results from first four columns are presented in [1], the last two columns are results from both authors.

Acknowledgement

The financial support for the present project was partly provided by the *Czech Grant Agency* under the *Grant No.205/06/0727* and by the Research Plan *MSM 6840770010* of the *Ministry of Education of Czech Republic*.

References

[1] Kim, H. G., Lee, C. M., Lim, H. C., and Kyong, N. H.: An experimental and numerical study on the flow over two-dimensional hills. Journal of Wind Engineering and Industrial Aerodynamics, vol. 66, no. 1:(1997) pp. 17-33.

[2] Dvořák R., Kozel K.: Matematické modelovaní v aerodynamice. Vydavatelství ČVUT, 1996.

[3] Bodnár T., Numerical Simulation of Flows and Pollution Dispersion in Atmospheric Boundary Layer. CTU Thesis, 2003

[4] Wilcox D.C. Turbulence Modeling for CFD, DCW Industries

[5] Příhoda J., Louda P., Matematické modelování turbulentního prodění,Vydavatelství ČVUT, 2007.

[6] Pirkl L., Numerical Simulation of Incompressible Flows with Variable Viscosity, Diploma Thesis, CVUT FS MMT , Prague, 2007.

[7] Spalart P.R., Allmaras S.R., A One-equational Turbulence Model for Aerodynamic Flows, AIAA, Paper 92-0439, (1992).

FLOW CONTROL OF BOUNDARY LAYER TRANSITION AND SEPARATION ON AIRFOILS AND BODIES IN FREE ATMOSPHERE CONDITIONS

Lukáš Popelka, Lubor Zelený
Institute of Thermomechanics AS CR, Prague, Aeroclub Přibyslav

Summary
The paper deals with visualisation of uncontrolled and controlled cases of boundary layer transition and separation carried out during in-flight measurements. Oil flow and tuft techniques have been applied. Influence of passive flow control devices to the performance of the entire aircraft has been established and importance of active and adaptive approach shown.

1. Measurement methodology

Self-launching TST10a sailplane OK-A631 /LZ/ was used as test aircraft. Oil flow visualisation on two positions along wingspan was prepared. Oil was applied on surface prior to the take-off, and flight of 10 minutes duration was carried out. Airspeed V = 100 km/h IAS was held constant during whole flight, even during climb and approach to landing.
Array of tufts was applied to the wing root area and video recording acquired for airspeed V = 85, 100, 130 and 160 km/h IAS. Extent of separation was studied in these conditions in straight flight.
Detailed measurement of TST10a saiplane speed polar was based on GPS methodology, *Popelka (2006)*, which was further refined. Every measurement programme was started at altitude of 2000m MSL or higher, for each airspeed 4 individual straight flight sequences were used. Flight track of 300m altitude loss in each sequence was recorded.
Expenses for numerous required test flights were covered by Mr. Zelený, the owner of TST10a OK-A631 /LZ/.

2. Results

Region of separation bubble was determined, Fig. 4. Based on previous findings on Standard Cirrus sailplane, leading to 10.7% glide ratio L/D improvement of OK-7077 /CX/ at 115 km/h IAS, Zig-zag type turbulators were applied along the wingspan.
Visualization in the transition wing-fuselage geometry have been done by tufts, Fig 1, on four airspeeds covering the common competition range. Region of separated flow has been determined, counter-rotating vortex generator of height h = 3mm (denoted as VG1) applied on chordwise location x/c = 0.48 and separation suppression observed. Effect on performance of sailplane have been consequently established by measuring both uncontrolled and controlled speed polar of the test sailplane.
Installation of wing-root VG1 resulted to L/D improvement in low-speed range. Compared to the theoretical curve, *Popelka (2006)*, it can be stated that notable shift towards TST10 performance potential utilization has been reached. The remaining difference can be accounted to the drag of fixed main undercarriage.

Fig. 1 Tuft visualization on left wing root of TST10a, V = 85km/h IAS. Left figure – uncontrolled case, note large region of separated flow. Right figure – VG1 applied, attached flow till the proximity of wing trailing edge

On the other hand, substantial decrease of L/D has been observed for typical interthermal glide airspeed. Unacceptable deterioration of high-speed sailplane performance has lead to the new layout of vortex generator VG2 currently installed on test aircraft.

3. Conclusions

Methodology of flow visualisation feasible for in-flight investigation on airfoils and bodies was developed. Sailplane speed-polar measurement with use of GNSS FR was further improved.

Two types of passive flow control devices were used. For boundary layer transition control the optimum turbulator location was established. The case of separation control have shown potential of performance improvement. The need of off-design detrimental effect minimization has been demonstrated. In given wing-fuselage geometry, application of acoustic-driven synthetic jet is feasible. Such active device could be optimized to supress separation on V = 85 km/h IAS. For higher airspeeds the jet intensity should be lowered, with dynamic pressure as trigger and hence adaptive control can be reached.

4. Acknowledgment

The work has been supported by the grant projects GA AS CR No. IAA2076403 and No. IAA200760614 and by Ministry of Education, Youth and Sports of the Czech Republic within project No. 1M06031.

5. Literature

Popelka, L.: *Aerodynamic Optimization of Sailplane Airfoils*
Ph.D. dissertation work. Prague: Czech Technical University in Prague, FME, 2006, 166s.

EXPERIMENTAL INVESTIGATION OF STRATIFICATION BREAKING BY TURBULENT MIXING

J. M. Redondo
Departament de Física Aplicada, Universitat Politécnica de Catalunya, Barcelona

The paper will be supplied afterwards on a separate sheet.

[1]

Interaction of a channel flow and moving bodies

Martin Růžička[*)], Miloslav Feistauer[*)], Jaromír Horáček[**)] and Petr Sváček[***)]
[*)] **Charles University Prague, Faculty of Mathematics and Physics,** [**)] **Academy of Sciences of the Czech Republic, Institute of Thermomechanics,** [***)] **Czech Technical University Prague, Faculty of Mechanical Engineering**

Introduction

The subject of this paper is the numerical simulation of the interaction of two-dimensional incompressible viscous flow through a channel (wind tunnel) and a vibrating airfoil. A solid airfoil with two degrees of freedom, which can rotate around the elastic axis and oscillate in the vertical direction, is considered. The numerical simulation consists of the finite element solution of the Navier-Stokes equations coupled with the system of ordinary differential equations describing the airfoil motion. We discuss the discretization of the problem and present some computational results.

Formulation of the problem

The two-dimensional non-stationary flow of viscous, incompressible fluid is considered in the time interval $[0,T]$, where $T>0$. The symbol Ω_t denotes the computational domain occupied by the fluid at time t. The flow is characterized by the velocity field $\boldsymbol{u}=\boldsymbol{u}(x,t)$, and the kinematic pressure $p=p(x,t)$, for $x\in\Omega_t$ and $t\in[0,T]$. Further, $\alpha(t)$ and $h(t)$ denote the rotation angle and displacement of the airfoil.

The fluid flow is described by the Navier-Stokes system written in the ALE (Arbitrary Lagrangian–Eulerian) form (see, e.g. [1])

$$\frac{D^A}{Dt}\boldsymbol{u}+[(\boldsymbol{u}-\boldsymbol{w})\cdot\nabla]\,\boldsymbol{u}+\nabla p-\nu\Delta\boldsymbol{u}=0,\quad \operatorname{div}\boldsymbol{u}=0\quad \text{in } \Omega_t,$$

where $\nu>0$ denotes the kinematic viscosity of the fluid, $\frac{D^A}{Dt}$ is the ALE derivative and $\boldsymbol{w}$ is the ALE velocity. (See, e.g. [1].)

The equations for the moving profile were derived from the Lagrange equations for the generalized coordinates h and α ([1]). In the matrix calculus these equations have the form

$$\widehat{\boldsymbol{K}}\boldsymbol{d}(t)+\widehat{\boldsymbol{B}}\dot{\boldsymbol{d}}(t)+\widehat{\boldsymbol{M}}\ddot{\boldsymbol{d}}(t)=\widehat{\boldsymbol{f}}(t), \tag{1}$$

where the stiffness matrix $\widehat{\boldsymbol{K}}$, the viscous damping $\widehat{\boldsymbol{B}}$ and the mass matrix $\widehat{\boldsymbol{M}}$ have the form

$$\widehat{\boldsymbol{K}}=\begin{pmatrix} k_{hh} & k_{h\alpha}\\ k_{\alpha h} & k_{\alpha\alpha}\end{pmatrix},\quad \widehat{\boldsymbol{B}}=\begin{pmatrix} D_{hh} & D_{h\alpha}\\ D_{\alpha h} & D_{\alpha\alpha}\end{pmatrix},\quad \widehat{\boldsymbol{M}}=\begin{pmatrix} m & S_\alpha\\ S_\alpha & I_\alpha\end{pmatrix}$$

and the vector of the force $\widehat{\boldsymbol{f}}$ and the generalized coordinates $\boldsymbol{d}$ read

$$\widehat{\boldsymbol{f}}(t)=\begin{pmatrix} -L_2(t)\\ \mathcal{M}(t)\end{pmatrix},\quad \boldsymbol{d}=\begin{pmatrix} h(t)\\ \alpha(t)\end{pmatrix}.$$

[1]This research was supported by the grant No. IAA 200760613 of the GAASCR. The research of M. Růžička was also partly supported by the project No. 7486/2007 of the GAChU in Prague.

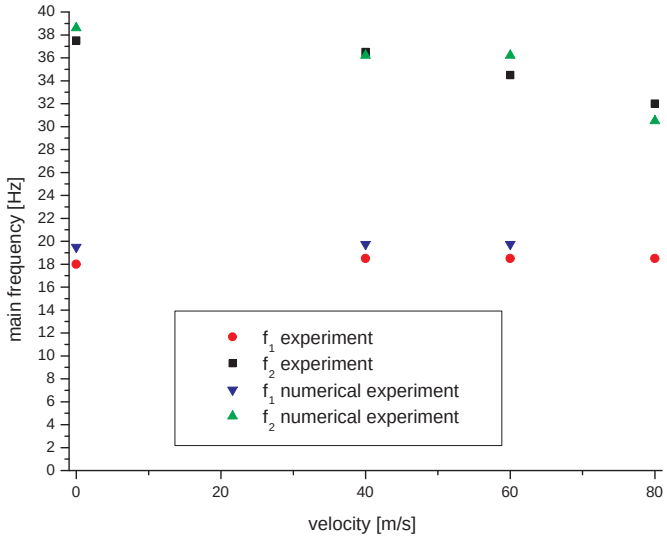

Figure 1: The main frequencies of the signals

The symbol L_2 stands for the component of the force acting on the profile in the vertical direction, $\mathcal{M}$ is the torsional moment of the force.

The above flow and structural equations are equipped by suitable initial and boundary conditions.

The time discretization of flow equations if carried out by a second order backward difference formula and the space discretization uses the finite element method stabilized by the SUPG and grad-div technique. The nonlinear discrete system is solved by the Oseen iterations. The structural system is solved numerically by the Runge-Kutta method.

Results

As a result we obtain the pressure and velocity fields and also the position of the moving profile. From this information we derive the frequency characteristics. The computational results carried out on the basis of data from [2] are compared with the experiment described in [3]. Figure 1 shows a good agreement of computational and experimental results.

References

[1] P. Sváček, M. Feistauer, J. Horáček: *Numerical simulation of flow induced airfoil vibrations with large amplitudes.* J. of Fluids and Structures, 23 (2007), 391-411.

[2] J. Horáček, J. Kozánek, J. Veselý J.: *Dynamic and stability properties of an aeroelastic model.* In: Inženýrská mechanika 2005, Svratka 9.–12.5. 2005, ÚT AVČR, Praha 2005, 121–122 (CD–ROM, 12 pages). [ISBN 80-85918-93-5]

[3] J. Horáček, M. Luxa, F. Vaněk, J. Veselý, V. Vlček: *Design of an experimental set-up for the study of unsteady 2D aeroelastic phenomena by optical methods.* Research Report of the Institute of Thermomechanics of AS CR Prague, No. Z 1347/04, November 2004 (in Czech).

THE STRUCTURE OF TURBULENT JETS

Emil Sekula and José M. Redondo
Departament de Física Aplicada, Universitat Politécnica de Catalunya, Barcelona

Abstract

Present work shows some results of research on turbulent jets and plumes, their structures and effects occurred in different configurations (free jet, wall jet, 'bubbly' jet). The proposed work is based principally on experiments but there are also made some comparisons between experimental and environmental observations. We discuss here in summary the series of detailed experiments that have been performed in laboratory utilizing visualizations methods (Particle Image Velocimetry) and Acoustic Doppler Velocimeter measurements of turbulence parameters in order to obtain a basic understanding of the turbulence phenomenon. Experimental techniques have developed very fast so we can use these new technologies that will increase our knowledge, even repeating some classical experiments under new light and improved techniques. We aim to understand the behaviour of turbulent jets incorporating the recent advances in non-homogeneous turbulence, structure function analysis, multifractal techniques and extended self-similarity.

One of the used configurations is the turbulent wall jet that occurs often in several environmental and industrial processes such as aeronautics design, heating, cooling, ventilation and environmental fluid dynamics. Other one is a 'bubbly' jet, a kind of jet 'filled' with bubbles. We used also two kinds of jet's sources: two pumps with smaller and bigger flow rate and different Reynolds numbers.

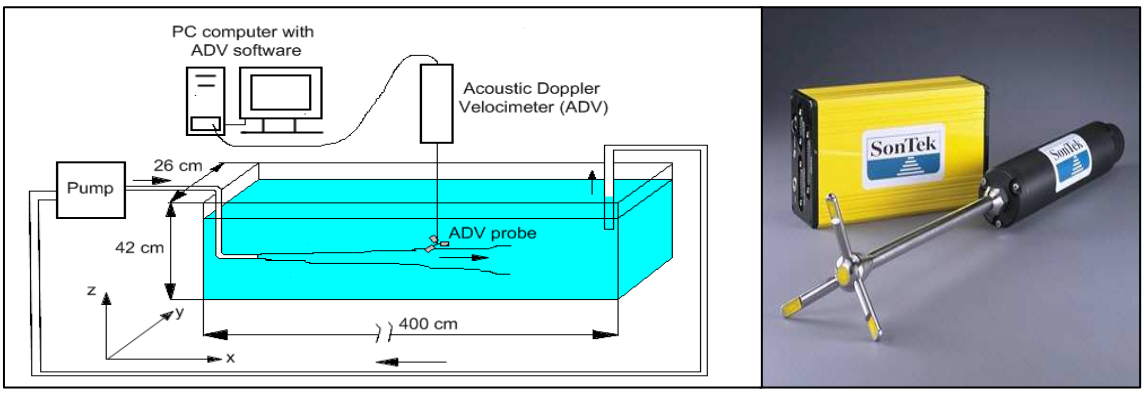

Figure 1. Scheme of workplace and Acoustic Doppler Velocimeter (ADV).

Results contain both measured (mean and fluctuation velocities, amplitudes, signal-noise-ratio, etc.) and statistical values obtained with provided and also personally created programs (correlations, covariance, kurtosis, standard deviation, skewness) and other such Reynolds number or turbulence intensity. We focus special attention on correlations and structure function which are useful for energy spectra analysis. It is interesting to investigate the convergence of performed experiments with Kolmogorov theory taking into account non-homogeneity, non isotropy, etc. and to use Extended Self

Similarity (ESS) and the third order structure functions to investigate the scale to scale transfer of energy.
With deep analysis of the performed results we can judge the adaptation of measurement methods and acquire more experience with its application.

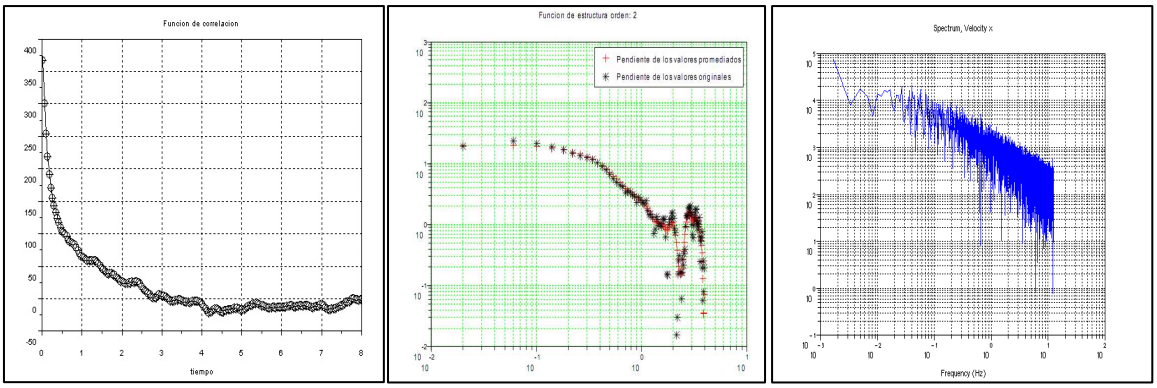

Figure 2. Correlations for one point of ADV measurements, 2-nd order structure function scaling component and Fast Fourier Transform (FFT) - Energy spectra.

An additional part of the work includes multi-fractal analysis of Synthetic Aperture Radar (SAR) images of the sea surface. The multi-fractal method allows investigating the turbulent and fractal structure of non homogeneous jets affected by different levels of turbulence. Other aims of the investigation under way are to determine the structure of ocean surface detected jets and compare coastal and boundary effects on the structure of river jets. A useful outcome is to develop further multi-fractal techniques useful for environmental monitoring in space.
We perform the box counting algorithm for the different intensities of vortices detected by SAR using special program Ima_Calc. SAR images allow us to observe convective cells and vortices formed in the sea surface.

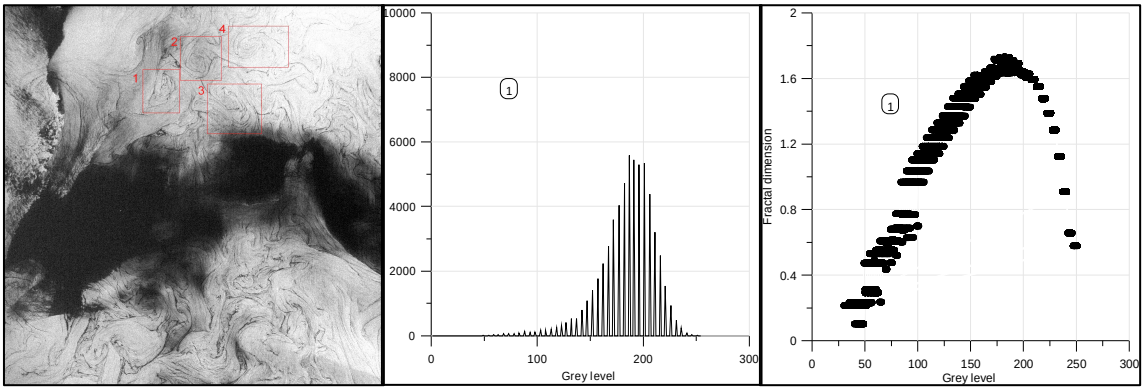

Figure 3. SAR image of the Gulf of Lions with marked sea vortices, histogram and fractal dimension of a one of the sea vortices.

MODELOVÁNÍ OBTÉKÁNÍ DVOU PRAHŮ V KANÁLU S VOLNOU HLADINOU

Modelling of flow over two transversal ribs in a channel with free surface

Aleš Sládek, Jaromír Příhoda, Jiří Stanislav,
Ústav termomechaniky AV ČR, v.v.i., Dolejškova 5, 182 00 Praha 8

1. Úvod

Kromě spojité drsnosti obtékaných stěn, která je dána výrobní technologií nebo působením provozních podmínek, je často drsná stěna tvořená výstupky, které slouží k disipaci kinetické energie proudu. Ve vodohospodářské praxi jsou příčné prahy na dně kanálu často používány při vypouštěni vody ze zemních nádrží ke zbrzdění proudu. V těchto kanálech s poměrně velkým sklonem dna je typické nadkritické proudění se značnými změnami výšky hladiny. Příspěvek se zabývá numerickým modelováním nadkritického obtékaní dvou příčných prahů na dně kanálu s volnou hladinou. Výsledky navazují na numerické řešení nadkritického proudění v kanálu s jedním prahem, viz Sládek a Příhoda [1].

2. Geometrické uspořádání

Tvar řešeného kanálu se dvěma příčnými prahy odpovídá experimentům Šulce a j. [2] a Zubíka [3], které byly prováděny v kanálu s příčným průřezem 200×200 mm, délkou 4475 mm a sklonem dna 4,77 %. V kanálu byly na dně umístěny dva příčné prahy čtvercového průřezu b×b = 10×10 mm s roztečí t = 60; 100 a 200 mm. Experimentální vyšetřování proudového pole při nadkritickém proudění bylo provedeno pomoci optických metod LDA a PIV pro střední objemovou rychlost U_m = 2,3 m/s a výšku hladiny na vstupu h = 46 mm, tj. při Reynoldsově čísle vztaženém na výšku prahu Re = 25500 a Froudově čísle Fr = 3,42.

3. Numerický model

Řešení nadkritického proudění v kanále se dvěma prahy bylo provedeno metodou VOF (Volume-of-Fluid) pomoci komerčního programu FLUENT 6.3. Metoda VOF je založena na sledování objemové frakce α_i obou tekutin v každé výpočetní buňce. Volná hladina se určuje jako rozhraní obou frakcí, kde platí $\alpha_{voda} = \alpha_{vzduch} = 0{,}5$. Pro numerické řešení středovaných Navier-Stokesových rovnic byl použit tzv. „realizovatelný" k-ε model turbulence, který navrhli Shih a j. [4]. Model se liší od standardního k-ε modelu transportní rovnicí pro rychlost disipace ε , která je odvozena z rovnice pro střední hodnotu fluktuace vířivosti a konstitučním vztahem pro turbulentní vazkost, kde C_μ je funkce $C_\mu = f(S_{ij}, \Omega_{ij}, k/\varepsilon)$ místo obvyklé konstanty $C_\mu = 0{,}09$.

Prostorová diskretizace byla provedena strukturovanou sítí s celkovým počtem cca 690000 buněk. V ose kanálu byla použita podmínky symetrie. Síť je zjemněna v oblasti volné hladiny a v blízkosti stěn kanálu. Diskretizace transportních rovnic byla provedena pomoci upwind schématu druhého řádu a v blízkosti stěn je pro aproximaci rychlostního profilu použita nerovnovážná stěnová funkce. Jako okrajová podmínka je podle experimentu zadána na vstupu výška hladiny a objemový tok, na výstupu pak je zadána výška hladiny a tlak v referenčním bodě nad hladinou.

4. Výsledky řešení

Na obr.1 je čárkovaně znázorněn průběh hladiny v kanálu se dvěma prahy s roztečí t = 100 mm získaný jako časově střední hodnota z 50 snímků PIV [3]. Plnou čarou je vyznačena hranice pásma objemové frakce vody v rozsahu α_{voda} = (0,5; 1) získaná v ose kanálu pomocí numerické simulace. Výpočet dává menší vzestup hladiny na prvním prahu a pomalejší návrat k hladině nerušeného proudu.

Vypočtené profily podélné složky rychlosti a turbulentní energie v podélné ose kanálu celkem odpovídají experimentu na prahu a v oblasti odtržení za prahem. Dále od prahu je relaxace smykové vrstvy rychlejší než podle numerické simulace, což vede k většímu rozsahu

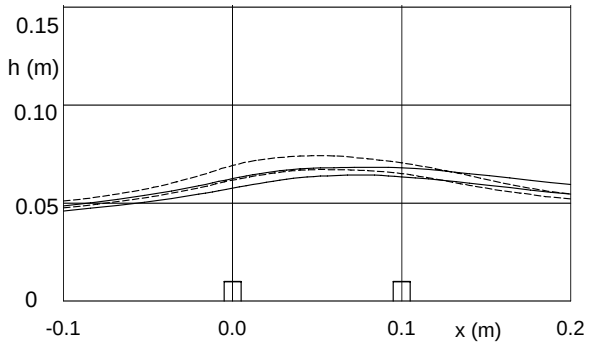

Obr.1 Průběh hladiny v kanálu se dvěma prahy s roztečí t = 100 mm

oblasti odtržení. V oblasti znovupřilnutí proudu je maximum fluktuací rychlosti blíže ke dne kanálu, zatímco při odtržení proudu leží maximum fluktuací přibližně na hranici odtržení. Podle experimentu i numerické simulace je za prahem u boční stěny kanálu dobře patrný sekundární vír, který se podobně vyskytuje při obtékání zpětného schodu. Podle experimentu je vírová struktura za prahem složitější, neboť v blízkosti prahu lze pozorovat napříč kanálem čtyři víry.

Z numerické simulace byl určen tlakový odpor jednotlivých prahů, který je vyjádřen pomocí součinitele tlakového odporu $c_d = \Delta p/(\rho U_m^2/2)$. Na obr.2 je uvedena závislost součinitele tlakového odporu obou prahů na jejich rozteči. Při malé rozteči obou prahů leží druhý práh v úplavu za prvním prahem a tlaková síla působí proti směru proudu. S rostoucí vzdáleností prahů se tlakový odpor obou prahů blíží hodnotě, určené pro jediný práh.

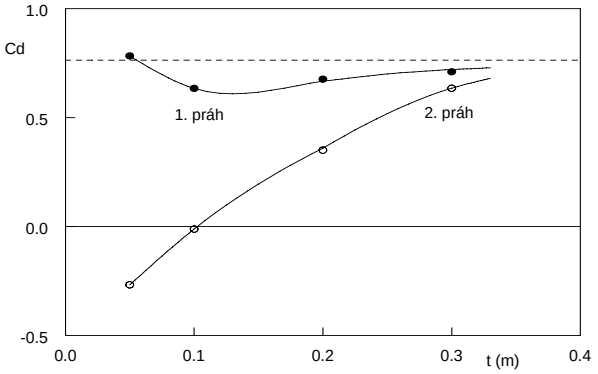

Obr.2 Závislost součinitele tlakového odporu na rozteči prahů

5. Závěr

Numerická simulace nadkritického obtékání dvou příčných prahů na dně kanálu s volnou hladinou provedená pomocí komerčního programu FLUENT dává celkem dobrou shodu s experimenty. Pomocí dvourovnicového k-ε modelu podle Shiha a j. [4] byla získána přijatelná shoda rychlostního pole i turbulentních charakteristik, i když numerická simulace v porovnání s experimentem dává menší vzestup hladiny na prvním prahu a pomalejší návrat k hladině nerušeného proudu. Nedostatkem všech modelů turbulence s turbulentní vazkostí je pomalejší relaxace proudového pole po odtržení na prahu. To vede k nadhodnocení velikosti oblasti odtržení, což se projeví i na vypočteném průběhu volné hladiny. Získaná závislost součinitele tlakového odporu na rozteči prahů umožní optimální rozložení příčných prahů při zpomalování vodního proudu vypouštěného ze zemních nádrží.

6. Poděkování

Práce vznikla s podporou grantu GA ČR č.103/06/0461 a výzkumného záměru AV 0Z20760514.

7. Literatura

[1] SLÁDEK A., PŘÍHODA J.: Modelování obtékání jednoho příčného prahu v kanálu s volnou hladinou, Sborník konference *Topical Problems of Fluid Mechanics 2007,* Praha, 157-160, 2007

[2] ŠULC J., ZUBÍK P., ŽOUŽELA M.: Měření parametrů nadkritického proudění v kanálu s příčnými prahy ve dně, Sborník konference *Hydrodynamika 2006*, Rajnochovice, 134-139, 2006

[3] ZUBÍK P.: LDA a PIV měření parametrů proudění v kanálu s příčnými prahy na dně, Sborník konference *Topical Problems of Fluid Mechanics 2007,* Praha, 199-202, 2007

[4] SHIH T.H., LIOU W.W., SHABBIR A., YANG Z., ZHU J.: A new k-ε eddy-viscosity model for high Reynolds numbers turbulent flows, *Computers Fluids*, 24, 3, 227-238, 1995

On The Validation 2D–Flow Study Over an ERCOFTAC Hill

Sládek I.[2/], Kozel K.[1/], Jaňour Z.[2/]
1/ U12101, Faculty of Mechanical Engineering, Czech Technical University in Prague.
2/ Institute of Thermomechanics, Academy of Sciences, Prague.

Abstract

The paper deals with a validation flow study performed on the mathematical/numerical model of atmospheric boundary layer flow. The mathematical model is based on the system of RANS equations closed by the two-equation $k-\varepsilon$ turbulence model together with wall functions. The finite volume method and the explicit Runge–Kutta time integration method are utilized for the numerics. The test–case is related to a neutral boundary layer 2D-flow over an isolated hill with a rough wall.

1 Mathematical formulation

The flow itself is assumed to be a turbulent, viscous, incompressible, stationary and indifferently stratified as well. The mathematical model is based on the RANS approach and the governing equations modified according to the method of artificial compressibility can be re-casted in the conservative and vector form

$$\vec{W}_t + \begin{pmatrix} u \\ u^2+\frac{p}{\varrho} \\ uv \\ uw \end{pmatrix}_x + \begin{pmatrix} v \\ vu \\ v^2+\frac{p}{\varrho} \\ vw \end{pmatrix}_y + \begin{pmatrix} w \\ wu \\ wv \\ w^2+\frac{p}{\varrho} \end{pmatrix}_z = \begin{pmatrix} 0 \\ Ku_x \\ Kv_x \\ Kw_x \end{pmatrix}_x + \begin{pmatrix} 0 \\ Ku_y \\ Kv_y \\ Kw_y \end{pmatrix}_y + \begin{pmatrix} 0 \\ Ku_z \\ Kv_z \\ Kw_z \end{pmatrix}_z \tag{1}$$

where $\vec{W} = (p/\beta^2, u, v, w)^T$ stands for the vector of unknown variables: the pressure p, the velocity vector $\vec{V} = (u, v, w)^T$ and the parameters K refers to the turbulent diffusion coefficients, see equation (4) and β is related to the artificial sound speed.

2 Turbulence model

Closure of the system (1) is performed by a standard high-Re $k-\varepsilon$ turbulence model. Two additional transport equations are added to the system (1) for the turbulent kinetic energy abbreviated by k and for the rate of dissipation of turbulent kinetic energy denoted by ε

$$(ku)_x + (kv)_y + (kw)_z = (K^{(k)}\,k_x)_x + (K^{(k)}\,k_y)_y + (K^{(k)}\,k_z)_z + P - \varepsilon, \tag{2}$$

$$(\varepsilon u)_x + (\varepsilon v)_y + (\varepsilon w)_z = (K^{(\varepsilon)}\,\varepsilon_x)_x + (K^{(\varepsilon)}\,\varepsilon_y)_y + (K^{(\varepsilon)}\,\varepsilon_z)_z + C_{\varepsilon 1}\frac{\varepsilon}{k}\,P - C_{\varepsilon 2}\frac{\varepsilon^2}{k} \tag{3}$$

where P denotes the turbulent production term $P = \tau_{ij}\frac{\partial v_i}{\partial x_j}$ for the Reynolds stress written as $\tau_{ij} = -\frac{2}{3}\,k\,\delta_{ij} + \nu_T\left(\frac{\partial v_i}{\partial x_j} + \frac{\partial v_j}{\partial x_i}\right)$ and the terms $K^{(k)}$, $K^{(\varepsilon)}$, ν_T stand for the diffusion coefficients and the turbulence viscosity

$$K^{(k)} = \nu + \frac{\nu_T}{\sigma_k}, \quad K^{(\varepsilon)} = \nu + \frac{\nu_T}{\sigma_\varepsilon}, \quad \nu_T = C_\mu\frac{k^2}{\varepsilon}. \tag{4}$$

The model closure coefficients are described in Castro (1996) [3].

3 Boundary conditions

The system (1)+(2)+(3) is solved with the following boundary conditions, Castro (1981) [3] Inlet: $u = \frac{u^*}{\kappa} \ln\left(\frac{z}{z_0}\right)$, $v = 0$, $w = 0$, $k = \frac{u^{*2}}{\sqrt{C_\mu}}\left(1 - \frac{z}{D}\right)^2$, $\varepsilon = \frac{C_\mu^{3/4} \cdot k^{3/2}}{\kappa \cdot z}$; Outlet: homogeneous Neumann conditions for all quantities; Top: $u = U_0$, $v = 0$, $\frac{\partial w}{\partial z} = 0$, $\frac{\partial k}{\partial z} = 0$, $\frac{\partial \varepsilon}{\partial z} = 0$; Wall: standard wall functions are applied at ~ 30 wall-units from wall; where u^* is the friction velocity, $\kappa = 0.40$ denotes the von Karman constant, z_0 represents the roughness parameter.

4 Validation

The reference experimental data due to Khurshudyan (1981) [1] and corrected by Trombetti (1991) [2] are also available in the ERCOFTAC database. Moreover, Castro (1996) [3] performed flow and pollution dispersion reference numerical computations.
Computational domain is $9\,m$ long and $1.6\,m$ high. A hill with the highest slope has been tested for the free-stream air velocity $U_0 = 4\,m/s$ and boundary layer depth of $D = 1\,m$. The Reynolds number based on U_0 and hill height $H = 117\,mm$ is $Re \sim 3.1 \cdot 10^4$.

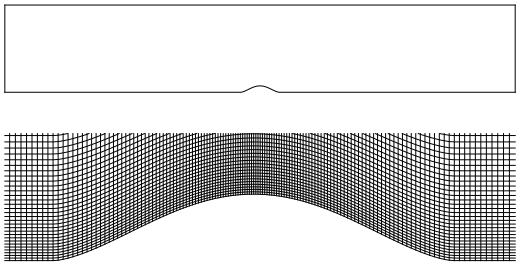

Fig 1: Computational domain 400x80 cells and zoom to non-uniform grid near hill.

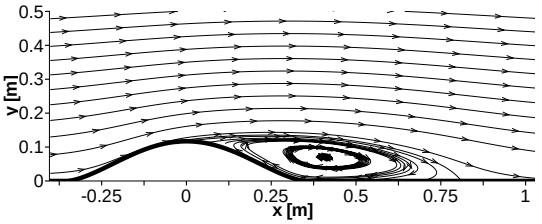

Fig 2: Zoom of separation zone behind hill.

5 Conclusion

The flow reattachment point is $x_r = 6.7H$ measured from the hill summit while the value due to Castro is $x_r = 4.1H$ for the standard $k - \varepsilon$ model and the experimentally determined value is $x_r = 6.5H$. The achieved results seems to be acceptable. The real–case 2D/3D numerical tests (*eg.* in [4]) of the implemented turbulence model will follow.

Acknowledgment

The presented work is supported by the Grant No. T400 76 04 05 – Information Society.

References

[1] Khurshudyan L.H., Snyder W.H., Nekrasov I.V. (1981): Flow and dispersion of pollutants over two-dimensional hills, U.S. EPA, Report No. EPA-600/4-81-067.

[2] Trombetti F., Martano P., Tampiery F. (1991): Data sets for studies of flow and dispersion in complex terrain: 1) the RUSHIL wind tunnel experiment, CNR Technical Report No.1, FISBAT-RT-91/1.

[3] Castro I.P., Apsley P.P. (1996): Flow and dispersion over topography: A comparison between numerical and laboratory data for two-dimensional flows, Atmospheric Environment, Vol.31, No.6.

[4] Sládek I., Bodnár T., Beneš L. Kozel K. (2004): Numerical tests on flows in coal field, In: Colloquium "Fluid Dynamics 2004", Institute of Thermodynamics, ISBN 80-85918-89-7, pp. 173–176, Prague.

ODHAD OPTIMÁLNÍ VELIKOSTI ZRN VÝPLNĚ REGENERAČNÍHO VÝMĚNÍKU S OHLEDEM NA HYDRAULICKÉ ZTRÁTY A PŘESTUP TEPLA

The Estimation of the Optimal Size of Elements in Regenerator with Respect to Hydraulic Losses and Heat Transfer

Jan Slanec
Ústav mechaniky tekutin a energetiky, Fakulta strojní, ČVUT v Praze

Abstrakt:
V příspěvku je popsán způsob, jak odhadnout vhodnou velikost částic tvořících výplň regeneračního výměníku, na který jsou kladeny specifické požadavky s ohledem na využití magnetokalorického jevu při přenosu tepla. Řešení vychází ze zjednodušeného modelu geometrie i procesu probíhajícího ve výměníku. Výsledek dává kvalitativní představu o vlivu jednotlivých veličin, vstupujících do daného problému, na velikost hydraulických ztrát a intenzitu přestupu tepla.

Chlazení s využitím magnetokalorického jevu

Existují materiály, které změní svoji teplotu, pokud jsou vystaveny silnému magnetickému poli. Tento jev se ukazuje být poměrně zajímavý pro oblast chlazení.[1] Součástí chladicího zařízení využívajícího zmíněný magnetokalorický jev je regenerační výměník vyrobený z materiálu vykazujícího výše popsanou vlastnost. Pomocí magnetického pole jsou vyvolávány změny teploty výměníku. To umožňuje střídavé odebírání a dodávání tepla teplonosné látce protékající tímto výměníkem. Při správné synchronizaci pohybu teplonosné látky a teplotních změn ve výměníku je zajištěn transport tepla požadovaným směrem. Možné uspořádání takového chladícího zařízení je na ***Obr.1***.

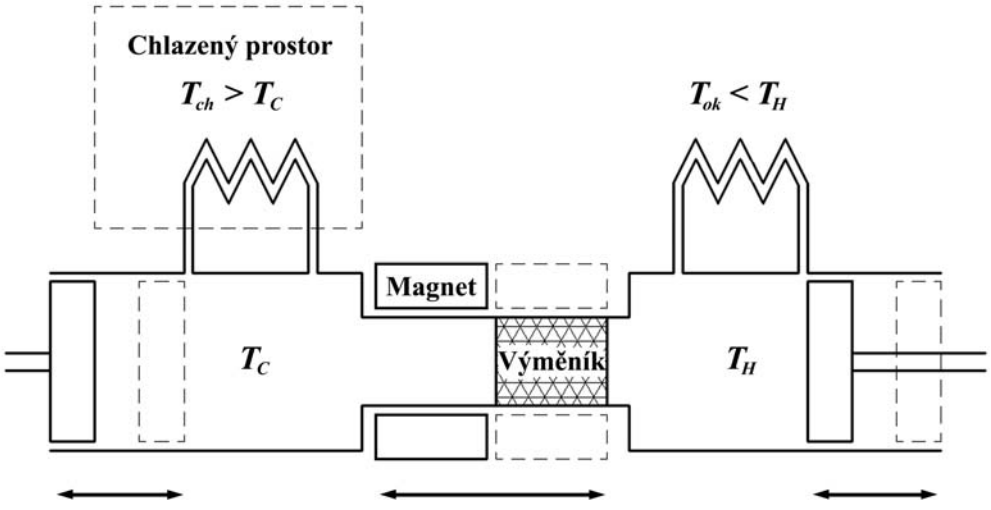

Obr. 1: Schéma uspořádání uvažovaného chladicího zařízení

Výsledky

Při určitém zjednodušení řešeného problému je možné vyjádřit maximální průměr částic tvořících výplň regeneračního výměníku:

$$d_{\max} = \left(\frac{C_2}{C_1}\right)^{\frac{1}{1,3}} = \left[\frac{3 \cdot K_1 \cdot K(\varepsilon, \mathrm{Pr}) \cdot \lambda_g}{f \cdot c_M \cdot \rho_M} \cdot \frac{\Delta T_{min}}{\Delta T_M} \cdot \left(\frac{w_0}{\nu_g}\right)^{0,7}\right]^{\frac{1}{1,3}}.$$

Protože tlakové ztráty při průtoku výměníkem závisí „nepřímoúměrně“ na průměru částic, je maximální přípustný průměr také optimálním průměrem z pohledu hydraulických ztrát. Pro výpočet tlakové ztráty lze použít například rovnici[2,3]:

$$\frac{\Delta p}{L} = \frac{(1-\varepsilon)^2}{\varepsilon^3 d} \rho_g w_0^2 \left[150 \frac{1-\varepsilon}{\mathrm{Re}_0} + 4{,}2 \cdot \left(\frac{1-\varepsilon}{\mathrm{Re}_0}\right)^{\frac{1}{6}}\right]$$

Rovnice (33) je platná v rozsahu $\mathrm{Re}_0 = 0{,}5 \cdot (1-\varepsilon) \div 40000 \cdot (1-\varepsilon)$.

Závěr

Je zjevné, že vztah pro výpočet maximální přijatelné velikosti zrn porézní vrstvy ve výměníku, vzhledem k použitým zjednodušením při jeho odvození, nemůže dát přesnou odpověď v otázce skutečně optimálních parametrů výměníku pro požadovaný pracovní režim. Poskytuje však kvalitativní představu o vlivu jednotlivých parametrů zúčastněných v daném problému a jejich vzájemných vazbách. Pro získání i kvantitativně korektního výsledku bude dále nezbytné hledat korekce, které by zohledňovaly reálné parametry, jako jsou například reálné průběhy teplot a rychlosti nebo teplotní závislost magnetokalorického jevu.

Poděkování:

Tato práce vznikla za podpory grantového projektu GA ČR 101/05/2537.

Literatura:

[1] Jílek, M., Ota, J. 2003. *Magnetokalorický jev a jeho aplikace*, Colloquium Fluid Dynamics 2003, Proceedings, Ústav termomechaniky AVČR, Praha 22.-24.10.2003, p. 43-46, ISBN 80-85918-83-8

[2] Hlavačka, V., Valchář, J., Viktorin, Z. 1980. *Tepelně technické pochody v systémech plyn-tuhé částice*. Praha : SNTL, 1980. 256 s.

[3] Viktorin, Z. 1978. *Výpočetní podklady hydrodynamických a termodynamických vlastností nehybné profukované vrstvy*. Praha : ČVTS, 1978. 52 s.

ON NUMERICAL APPROXIMATION OF AN AEROELASTIC PROBLEM

P. Sváček [1]
Czech Technical University, Faculty of Mechanical Engineering, Department of Technical Mathematics, Karlovo náměstí 13, 121 35 Praha 2

Introduction

The fluid-structure interaction play important role in many technical applications. In this paper the numerical approximation of fluid-structure interaction (FSI) problems is address. During last years, significant advances have been made in the development and use of computational methods for fluid flows with structural interactions. The arbitrary Lagrangian-Eulerian (ALE) formulations are widely used. The application of the ALE method is straightforward; however there are a number of important computational issues which needs to be properly addressed, cf. [1]. Here, the conservative ALE formulation of Navier-Stokes system of equations is employed (cf. [2]), weakly formulated and discretized by the stabilized finite element method (FEM). The structure model is described by the system of ordinary differential equations.

Mathematical model

The flow of incompressible viscous fluid is described by the Navier Stokes equations. In order to treat the moving domain case we use the Navier-Stokes system of equations written in ALE conservative form, i.e. for $i = 1, 2$

$$\frac{1}{\mathcal{J}}\frac{D^{\mathcal{A}}}{Dt}\Big(\mathcal{J}v_i\Big) + \operatorname{div}\left((\mathbf{v}-\mathbf{w}_D)v_i\right) - \nu\triangle v_i + \frac{\partial p}{\partial x_i} = 0, \qquad \operatorname{div}\mathbf{v} = 0, \text{ on } \Omega_t \subset \mathbb{R}^2, \quad (1)$$

where $\mathcal{A} = \mathcal{A}(\xi, t)$ is the ALE mapping of $\xi \in \Omega_0$ onto $x \in \Omega_t$, $\mathbf{w}_D$ denotes the domain velocity given by

$$\mathbf{w}_D(x,t) = \frac{\partial \mathcal{A}}{\partial t}(\xi, t), \qquad \text{with } x = \mathcal{A}(\xi, t),$$

$\mathcal{J}$ denotes the Jacobian of the mapping $\mathcal{A}$, $\mathcal{J} = \frac{d\mathcal{A}}{d\xi}$ and $D^{\mathcal{A}}/Dt$ denotes the ALE derivative. The system (1) is equipped with boundary and initial conditions. Now, we take a test function $\mathbf{z} = \mathbf{z}(x,t)$ in the form $\mathbf{z} = \hat{\mathbf{z}} \circ \mathcal{A}_t^{-1}$ with $\hat{\mathbf{z}} \in \mathbf{H}^1(\Omega_0)$ and formulate equations (1) weakly, i.e.

$$\frac{d}{dt}\Big(\mathbf{v},\mathbf{z}\Big)_{\Omega_t} + c(\tilde{\mathbf{w}};\mathbf{v},\mathbf{z}) + \nu(\nabla\mathbf{v},\nabla\mathbf{z})_{\Omega_t} - \Big(p,\nabla^T\mathbf{z}\Big)_{\Omega_t} + \Big(\nabla\cdot\mathbf{w}_D\,\mathbf{v},\mathbf{z}\Big)_{\Omega_t} = 0 \quad (2)$$

where $\tilde{\mathbf{w}} = \mathbf{v} - \mathbf{w}_D$, $(\cdot,\cdot)_{\Omega_t}$ denotes the dot product in $L^2(\Omega_t)$/$\mathbf{L}^2(\Omega_t)$ and the trilinear form $c(\cdot;\cdot,\cdot)$ is defined by $c(\tilde{\mathbf{w}_D};\mathbf{v},\mathbf{z}) = \int_{\Omega_t}(\tilde{\mathbf{w}_D}\cdot\nabla)\mathbf{v}\cdot\mathbf{z}\,\mathrm{dx}$. The structure model is described by a system of second order ordinary differential equations

$$\mathbb{M}\,\ddot{\mathbf{u}} + \mathbb{B}\dot{\mathbf{u}} + \mathbb{K}\,\mathbf{u} = \mathbf{f}, \quad (3)$$

[1]This research was supported under grant No. 201/05/0005 of the Grant Agency of the Czech Republic and under the Research Plan MSM 6840770003 of the Ministry of Education of the Czech Republic.

where $\mathbf{u} = (h, \alpha, \beta)^T$, $\mathbf{f} = (-L, M_\alpha, M_\beta)^T$, $\mathbb{K} = \text{diag}(k_{hh}, k_{\alpha\alpha}, k_{\beta\beta})$, $\mathbb{D} = \text{diag}(d_{hh}, d_{\alpha\alpha}, d_{\beta\beta})$, and

$$\mathbb{M} = \begin{pmatrix} m & S_\alpha & S_\beta \\ S_\alpha & I_\alpha & \widehat{\Delta} S_\beta + I_\beta \\ S_\beta & \widehat{\Delta} S_\beta + I_\beta & I_\beta \end{pmatrix},$$

where m is the mass of the airfoil, S_α, I_α are the static and inertia of the airfoil, S_β, I_β are the static and inertia moment of the control section. Furthermore, h denotes the vertical displacements, α denotes the rotation of the airfoil and β denotes the rotation of the control section, see Figure 1. L, M_α, M_β then denotes the aerodynamical forces,

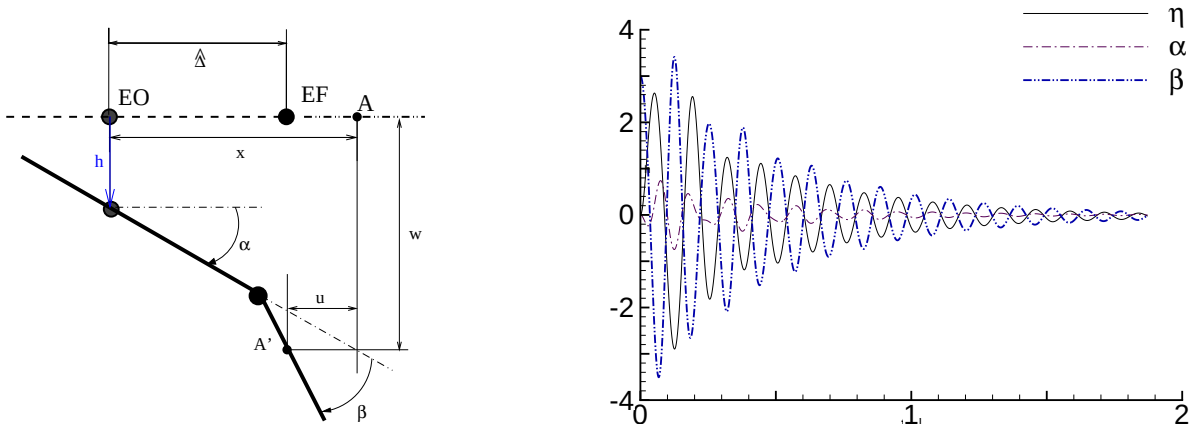

Figure 1: The 3dof structure model on the left. On the right the aeroelastic response $(h = \eta, \alpha, \beta)$ from numerical simulation for far field velocity $U_\infty = 17\,\text{m}/\text{s}$.

Space-Time discretization

In order to discretize problem (2) we consider a time step $\tau > 0$, denote $t_k = k\tau$ and at every time step t_k employ the approximation $\mathbf{v}^k \approx \mathbf{v}(\cdot, t_k)$ and $p^k \approx p(\cdot, t_k)$. The time derivative in the weak formulation (2) is approximated at time $t = t_{n+1}$ by the second order backward difference formula. The time disretized problem is then discretized with the aid of FEM: we seek for unknown functions $(\mathbf{v}, p)$ in the finite element spaces $\mathbf{v} \in \mathcal{W}_\triangle$ and $p \in \mathcal{Q}_\triangle$ such that for all test functions $\mathbf{z} \in \mathcal{X}_\triangle$ and $q \in \mathcal{Q}_\triangle$ holds

$$\Big(3\mathbf{v}/(2\tau), \mathbf{z}\Big)_{\Omega_{n+1}} + c(\tilde{\mathbf{w}}; \mathbf{v}, \mathbf{z}) + \nu(\nabla\mathbf{v}, \nabla\mathbf{z})_{\Omega_t} - \Big(p, \nabla^T \mathbf{z}\Big)_{\Omega_t} + \Big((\nabla\cdot\mathbf{w}_D^{n+1})\,\mathbf{v}, \mathbf{z}\Big)_{\Omega_t} = \mathcal{L}(\mathbf{z})/(2\tau)$$

where $\mathcal{L}(\mathbf{z}) = (4\mathbf{v}^n, \mathbf{z})_{\Omega_n} - (\mathbf{v}^{n-1}, \mathbf{z})_{\Omega_{n-1}}$ and $\mathbf{v}^{n+1} := \mathbf{v}$, $p^{n+1} := p$. In the practical implementation the stabilized finite element method is considered and Taylor-Hood couple of finite elements $(\mathcal{W}_\triangle, \mathcal{Q}_\triangle)$ is employed, which satisfies Babuška-Brezzi inf-sup condition.

References

[1] D. Boffi and L. Gastaldi. Stability and geometric conservation laws for ALE formulations. *Computational Methods in Applied Mechanical Engineering*, 193:4717–4739, 2004.

[2] F. Nobile. *Numerical approximation of fluid-structure interaction problems with application to haemodynamics*. PhD thesis, Ecole Polytechnique Federale de Lausanne, 2001.

DYNAMICS RESPONSE OF ELASTIC TUBE ON PULSATILE LOADING

V. Štembera
Ústav termomechaniky AV ČR, v. v. i., Praha

The paper not supplied.

INVESTIGATION OF CHARACTERISTICS OF A BLOWER USED AS AN AIR SOURCE IN AN EXPERIMENTAL RIG FOR STUDIES OF HELICAL INSTABILITIES IN FLOWING FLUIDS

Václav Tesař, Libor Kukačka, Radka Kellnerová
Institute of Thermomechanics of the Academy of Sciences of the Czech Republic v.v.i.

After the initial step, mechanics of fluid flow with rotational motion, teaching engineering students a course on turbomachines mostly continue by discussing the details of the fluid flow in the machines. This flow is complex—three-dimensional and unsteady—and as a result the course soon reaches a level at which it becomes rather difficult to follow. Moreover, the details of the complex flowfield are useful for only an extremely small number of the students, those who are likely in their career to actually design turbomachines. The largest percentage of mechanical engineers are just turbomechine users. What they need to know is mainly how the machine operates when connected into a fluidic circuit. Teaching this aspects requires mainly discussing the characteristics and their use.

Such course oriented towards users was introduced at ČVUT already in 1983 [1]. Behaviour of a pump or blower and its operation in a system was explained using a "black box" approach. The machine behaviour was modelled by a simple quadratic model, Fig.1, consiting of two components.

An opportunity to test this model arose recently in building a rig for investigations of aerodynamic properties of helical instabilities. The blower used as the air source, Fig. 2, was delivered without loading characteristics. It was to be operated at very low Reynolds numbers where one has to expect deviation from characteristics obtained under standard conditions.

Fig. 3 presents an example of the measured characteristic at a small speed. Apart from the stalled flow regime at very small flow rates (in which the blower will be not operated) the representation by the quadratic model discussed above is found to be extremely useful. It is fully characterised by two parameters: the specific work a [J/kg] transferred to the fluid inside the turbomachine, and the dissipance Q [m^2/kg^2], which characterises the hydraulic losses taking place inside the machine.

Present paper describes the procedure for evaluating these parameters. Then it applies a non-dimensionalisation – practically equivalent to those discussed in [1] – very useful for obtaining a universal loading curve, valid for any rotational speed.

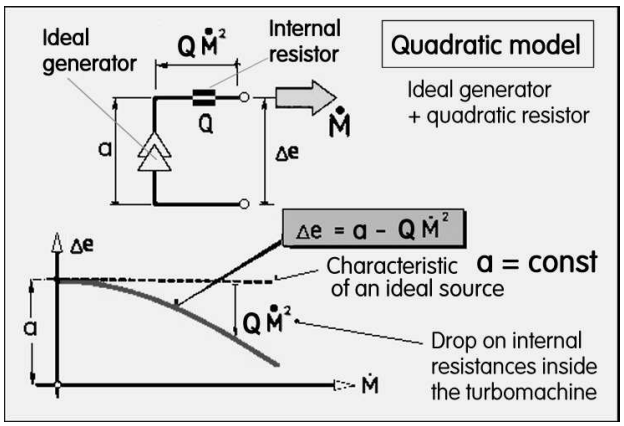

Fig. 1 **Quadratic model of the blower behaviour.**

Fig. 2 **Photograph (taken by Mr. J. Šafář) of the rotor of the investigated blower.**

practically,. The paper shows a way of presenting the characteristics, Fig. 4, converted them so that they are fitted by a simple straight line.

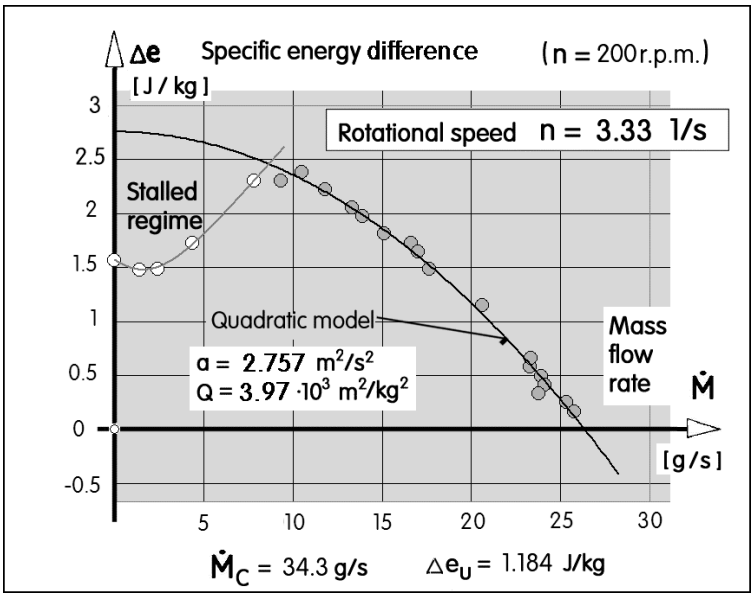

Figure 3 **An example of blower loading characteristic, evaluated experimentally at a very low rotational speed.**

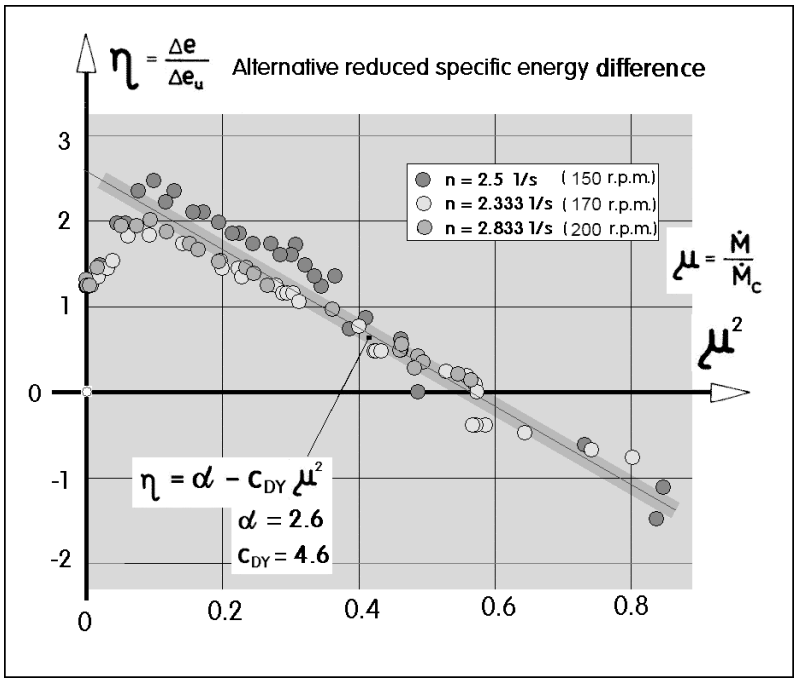

Figure 4 **The universal non-dimensional diagram describing the loading properties of the investigated blower at any driving speed.**

Acknowledgement ***The authors gratefully acknowledge the support of the Grant Agency of the Academy of Sciences of the Czech Republic by grant No. 207 60705.***

Reference:

[1] Tesař V. : „*Mechanika tekutin pro 4-leté studijní obory*“, in Czech, textbook ČVUT in Prague, various editions 1983 - 1990

DESIGN AND TESTS OF THE CRYOSTAT WITH AN EXPERIMENTAL CELL FOR TURBULENT THERMAL CONVECTION

Urban P., Hanzelka P., Musilova V., Srnka A., Skrbek L.[+]

Institute of Scientific Instruments of the ASCR, v.v.i., Kralovopolska 147, Brno
[+]Faculty of Mathematics and Physics, Charles University, Ke Karlovu 3, Prague

Cryogenic helium gas is a useful working fluid for experimental studies of thermal convection. Helium properties have strong dependence on pressure and temperature in comparison with commonly used fluids such as air, water, or Hg. In the vicinity of the critical point of helium (5.20 K, 2.26 bar) the Rayleigh number, *Ra,* can be easily varied over a wide range up to very high values in a relatively small cell. Niemela *et al.* [1] have reached *Ra* about 1e17 - value of the order characteristic for the turbulence in the atmosphere.

We have designed the cryostat equipped with the experimental cell for experimental investigation of cryogenic turbulent convection at very high Rayleigh numbers (10e6 < *Ra* < 2e15) with cryogenic 4He gas as a working fluid [1]. The cell is realized as a stainless steel cylindrical vessel, closed on top and bottom by high conductivity copper plates. The geometry of the cylindrical cell is characterized by the aspect ratio $G = D/L$, where D is its inner diameter and L denotes the distance between plates. We plan to use the cell primarily to investigate the functional dependence of the Nusselt number, *Nu*, on Rayleigh number, Prandtl number, *Pr*, and geometry of the cell, *G,* under Boussinesq conditions.

The main goal of our study is to resolve the very important question whether transition to the so-called ultimate Kraichnan regime within a range of available *Ra* exists. Kraichnan predicted that for high *Ra* numbers the Nusselt number (*Nu*) should scale according to asymptotic relation $Nu \sim Ra^{b} Pr^{c}$ with $b = 1/2$ and $c = -1/4$ with a $(\log Ra)^{(-3/2)}$ correction [2]. In the region of lower *Ra*, where Kraichnan regime (*Ra* scaling 1/2) is not expected, various theories predicted $Nu \sim Ra^{b}$ with two different values of the power exponent ($b = 1/3$ or $b = 2/7$), or more complicated relation for *Nu* was derived. Nowadays, theoretically acquired dependences $Nu \sim Ra^{2/7}$ and $Nu \sim Ra^{1/3}$ as well as the theoretical model by Grossmann and Lohse, who suggested that *Nu*(*Ra*) dependence does not follow any strict power-law, are widely discussed on the basis of the available experimental data.

Chavanne *et al.* measured the *Nu*(*Ra*) dependence in a cell with $G = 1/2$ and at *Ra* ranging from 1e7 up to 6e12 under Boussinesq conditions with constant $Pr \sim 0.7$ [3]. Under these conditions they obtained exponent *b* near to 2/7. They achieved the highest *Ra* up to 1e14 under non-Boussinesq conditions with *Pr* from 0.65 up to 35. Above about *Ra* = 3e11 they observed a new regime characterized by $Nu \sim Ra^{0.38}$ and different character of temperature fluctuations. They interpreted this finding as a transition to the Kraichnan regime.

Niemela *et al*. published another result for the same aspect ratio, but with the convection cell 5 times higher [1]. They obtained the dependence $Nu \sim Ra^{0.309}$ for *Ra* ranging from 1e6 up to 1e17. After application of corrections for parasitic heat conductivity effects of a sidewall and copper plates the exponent *b* is closer to 1/3. Later Niemela and Sreenivasan performed additional experiments to check the dependence *Nu*(*Ra*) with the aspect ratios $G = 1$ and 4. From these measurements, they also obtained a single power law with exponent *b* close to 1/3.

Experimental data are influenced by various construction details of the cell such as sidewall thermal conduction, heat capacity and thermal conductivity of the plates and their surface roughness. In comparison with apparatuses built in other laboratories our cell requires much lower correction for the sidewall thermal conduction. Schematic representation of the ConEV

(Convection Experimental Vessel) cryostat and of the cylindrical convection cell is shown in Fig. 1.

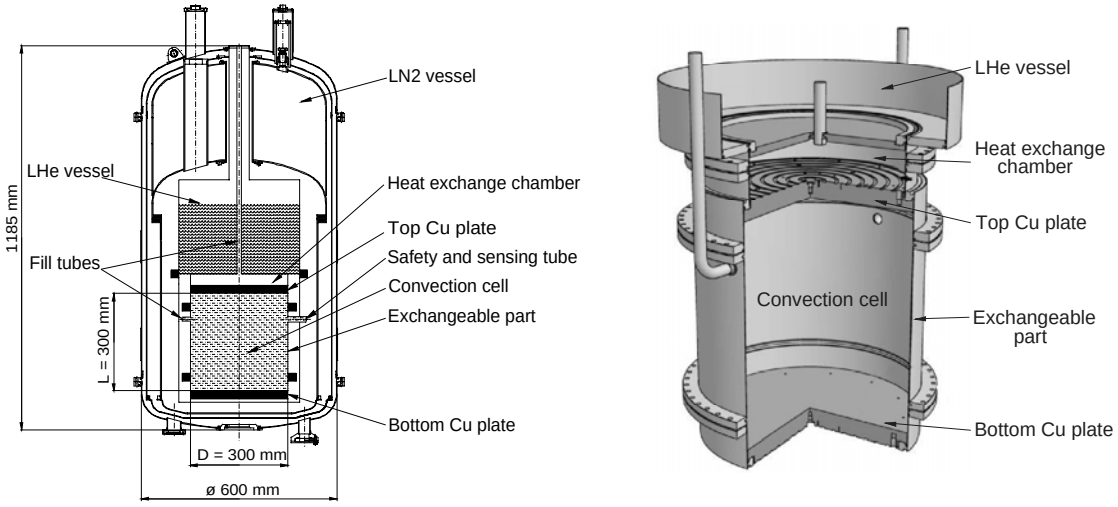

Fig. 1: Schematic representation of the ConEV Cryostat and detailed view of the convection cell

The cryostat configuration is typical for NMR magnet cryostats. The liquid nitrogen (LN2) vessel (60 litres) is situated above the liquid helium (LHe) vessel (28 litres) and the convection cell (21 litres of cold helium gas). Convection cell is thermally connected with LHe vessel by a heat exchange chamber filled by gaseous He. Radiation heat flux from outer wall to LN2 vessel is reduced by the thermal shield that is cooled by cold gaseous nitrogen. The convection cell is shielded by an aluminium shield cooled by liquid He. Evaporation rates of LN2 and LHe are 5 l and 1.2 litres per day, respectively.

Parameters of the convection cell:

- cylindrical experimental cell 300 mm in diameter and up to 300 mm in height
- *Ra* up to about 1e15 under Boussinesq condition
- cylindrical cell with the top and bottom made of 28 mm thick high conductivity copper (residual resistance ratio RRR = 290, i.e. thermal conductivity of about 2kW/mK)
- the cell design allows to change the aspect ratio $G = D/L$ from 1 to 2.5, via exchange of its middle part
- very thin cylindrical sidewall is not in direct contact with copper plates, this substantially reduces parasitic sidewall heating effect
- the cell was designed for measurements at pressures from 100 Pa to 250 kPa at temperatures up to about 8 K

Our newly developed cylindrical convection cell with variable aspect ratio *G* and very thin stainless steel wall is well suited to elucidate the transition to Kraichnan regime as well as the controversy about the $Nu(Ra,Pr,G)$ dependence. We have assembled the cell and leak-tested it both at room and helium temperature. Assembly of the entire cryostat is under progress and we plan to obtain first scientific data till the end of this year.

This research is supported by GACR under grant 2002/05/0218.

References

[1] Niemela J J, Skrbek L, Sreenivasan K R, Donnelly R J, Nature **404,** 837 (2000).
[2] Kraichnan, R.H.: Phys. Fluids **5,** 1374 (1962).
[3] Chavanne X, Chilla F, Chabaud B, Castaing B, Chaussy J, Hebral B: J Low Temp Phys **104**, 109 (1996).
[4] A. Srnka , P. Hanzelka , V. Musilova., P. Urban, L. Skrbek: Proc. of the ICEC21 Multiconf. CryoPrague 2006, , Prague, Vol.1, 661 (2006).

DYNAMICS OF CONTROLLED BOUNDARY LAYER SEPARATION

Václav Uruba, Martin Knob
Institute of Thermomechanics, AS CR, v. v. i., Praha

Abstract:

The results of experimental study on a boundary layer separation control are given in the paper. The boundary layer on a flat wall is subjected to adverse pressure gradient. Three control strategies have been chosen for the study, both passive (rough wall, vortex generator) and active (synthetic jet). The separation process is investigated using TR-PIV method. Dynamical aspects of the phenomenon are analyzed in details.

Experimental setup

In Fig. 1 the schema of experimental setup is shown. Downstream the starting section **A**, the upper wall is inclined with angle $\alpha = 16°$, while the bottom plane wall is used to study the boundary layer separation. To prevent separation from the upper wall is permeable and aspirated. The section **B** represents the "mean" position of a boundary layer separation.

The mean flow velocity outside the boundary layer in section **A** was 12.4 m/s, the boundary layer was of turbulent nature, about 5 mm thick.

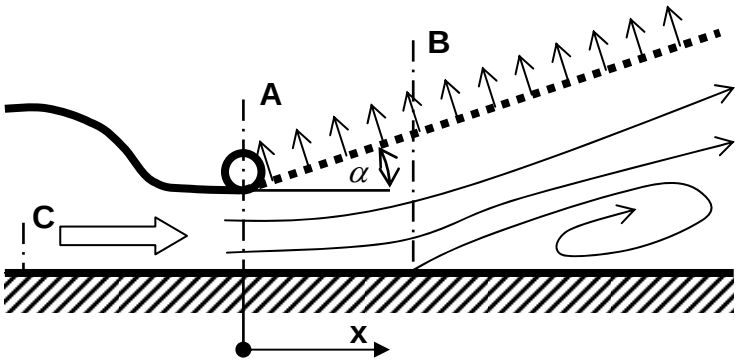

Fig. 1 – Schema of the experimental setup

The TR-PIV measuring system DANTEC was used for experiments. Detailed description of the experimental setup is given in URUBA, KNOB, POPELKA, 2007.

Three types of flow-control devices were used – wall roughness, vortex generator and synthetic jet (the first two passive, the last active). All control devices were placed near the **A** section. The wall roughness was simulated by the strip of sand paper, the synthetic jet was fabricated after the NASA design (see CHEN, 2002) and the vortex generator was of the usual type with inclined fences.

Results

The local properties of the boundary layer related to its separation was indicated using the Forward-Flow-Fraction coefficient *FFF* defined in URUBA, JONÁŠ, MAZUR, 2007 as a fraction of the time of observation of forward flow direction in a given point. The mean position of the point of separation could be evaluated in two

ways as a position in which 1) mean streamwise velocity U near the wall is 0; 2) FFF near the wall is 0.5.

In Fig. 2 the courses of FFF are shown with dashed limit $FFF = 0.5$. The mean positions of the point of separation were evaluated using both above given definitions for all cases.

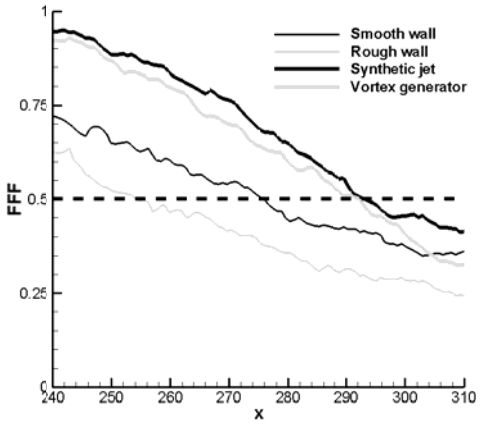

Fig. 2 – Forward-Flow-Fraction coefficient near the wall

Obviously, application of the synthetic jet shifted the separation point significantly in the streamwise direction (compare with the smooth wall case), however the vortex generator exhibits almost the same effect. Surprising is the rough wall case, which shows separation even earlier then the smooth wall case. The reason for this behaviour is the fact, that the boundary layer is in turbulent state even for the smooth wall and abrupt perturbations excited by the rough wall promote separation. Extended region of forward-flow-fraction coefficient values far from both 0 and 1 in Fig. 2 indicates highly dynamical behaviour in the near-wall region. Much more intensive fluctuation activity in the separation region has been detected in the cases of smooth and rough wall, than for control by synthetic jet and vortex generator. These results have been verified using other methods, namely spectral analysis, histograms and spacio-temporal analysis.

Acknowledgement

The authors gratefully acknowledge financial support of the Grand Agency of the Academy of Sciences of the Czech Republic by the research project No. IAA2076403 and Grand Agency of the Czech Republic No. 101/05/0675.

References

CHEN, F.-J. 2002. *Optimized Synthetic Jet Actuators*. LAR 16234, NASA Tech Briefs, July 2002.

URUBA, V., JONÁŠ, P., MAZUR, O. 2007. *Control of a Channel-Flow Behind a Backward-Facing Step by Suction/Blowing*. International Journal of Heat and Fluid Flow. Volume 28, Issue 4, pp. 665-672.

URUBA, V., KNOB, M., POPELKA, L. 2007. *A Boundary Layer Separation Dynamics*. Engineering Mechanics 2007, book of extended abstracts. Ed.: Zolotarev, Praha, Institute of Thermomechanics AS CR, v.v.i., pp. 297-298.

CRITICAL PROBLEMS OF BOUSSINESQ-TYPE TURBULENCE MODEL APPLICATION IN INTERNAL COMBUSTION ENGINES

O. Vítek and M. Polášek and K. Kozel and J. Macek
Czech Technical University in Prague, Josef Božek Research Center, Prague

Introduction

Nowadays it is a usual routine to apply two-equation turbulence models for modelling of compressible transient turbulent flow in internal combustion engine (ICE). No special turbulence models for ICE are developed. Instead, classical models (developed for the needs of external aerodynamics) are applied (the model constants might be slightly different). What is missing (or it is unknown to the authors) is that no comprehensive comparison of measured Reynolds stresses with predicted/calculated ones is carried out. It is a critical question as correlations of fluctuating terms of Favre averaged mathematical model are the dominant ones in ICE. The presented paper main target is to stress some problems of turbulence modelling based on Boussinesq hypothesis for the case of ICE.

Theoretical Background

The mathematical model is based on a Favre-averaged integral Navier-Stokes equation set written for arbitrary movable control volume (Advanced Multizone Eulerian Model). From numerical point of view, the finite volume cell-centered method is implemented. The numerical solution is performed by means of explicit multi-stage Runge-Kutta method. As far as modelling of combustion is concerned, the *Level Set* approach [3] is applied. Mass balance of each component (air, fuel and burnt gas) is considered, diffusion across the flame front is neglected. Source term in energy equation due to combustion process corresponds with the amount of burnt fuel. The mathematical model was applied to create a Fortran code AMEM3D which deals with modelling of in-cylinder phenomena during compression stroke and expansion stroke of spark ignited (SI) 4-stroke ICE.

Result Discussion

One of the encountered problems was that Reynolds stresses were too small when compared with measurement [1] regardless of applied turbulence model, initial conditions or other parameters (numerical solution preciseness, mesh coarseness, etc.). Considering the fact that the engine geometry is very simple, and hence the flow structures are relatively simple as well, it was a negative surprise. On the other hand, it was proven (e.g. [4, 6]) that Boussinesq-type turbulence models applied for the case of ICE have many of the qualitative properties that are known from experience. When comparing predicted and measured integral length scale, the measurement [2] confirms the assumption that turbulent properties are more or less homogeneous, especially near TDC. The theoretical results basically predicts the same. However, the experimental data suggest that the value of integral length scale is almost symmetrical with respect to TDC. This was not proven by calculations. If the measured integral length scale is applied for the case of one-equation turbulence model, there is no improvement of predicted Reynolds stress tensor components. The AMEM3D code was verified against the commercial CFD code to make sure that there is no fundamental problem within the developed algorithm. The main result of this comparison was that the results of both CFD codes are comparable.

It is well know that turbulence properties decrease during compression stroke (unless they are increased by means of combustion chamber shape) and that turbulence generated during intake stroke is dumped at early compression stroke. Moreover, if there are significant differences of properties at the end of intake stroke, there will be much smaller at the end of compression stroke. Generally speaking, this empirical knowledge can be confirmed by computations. Even if different turbulence models are applied, the results satisfy that under the assumption that there is significant swirling motion at the beginning of compression stroke. On the other hand, if there is no initial swirl and different turbulence models are applied, the results are significantly different. The differences among considered turbulence models become more and more significant. The biggest differences occur at the TDC. More detailed analysis in [4] suggests that the discussed phenomenon is mainly due to non-linearity of dissipation equation, especially its sink term. It was confirmed that if the considered process is dominated by production of turbulence specific energy k (k increases in time), the dissipation is not adjusted quickly enough – the differences are even more significant during the computation. However, if the process is dominated by dissipation of k (k is

decreased in time), all models predict almost the same results.

Regarding application of simple combustion model based on the *Level Set* approach, there are two issues. Firstly, the model should be suitable for SI engine combustion modelling as the mixture is already well mixed and turbulent transport is the dominant phenomenon – this statement is valid if temperatures are high enough which is the case when engine load is high. Taking into account this fact, it is a bit surprising that the shape of ROHR is relatively different when compared with experimentally measured one. Moreover, the ROHR shape cannot be changed by means of tuning the model constants. The only fact which may change the shape of calculated ROHR is the chemical dissociation (not taken into account in presented results) – it can work as a capacitor which stores the energy at very high temperatures and once the temperature decreases, the energy is released back. There seems to be no other reason that combustion speed should be decreased at the end of combustion process if turbulent transport is the dominant factor. Secondly, it was proven that combustion model constants should be tuned in such a way that they compensate for the influence of both applied turbulence model and mesh coarseness. Especially the latter phenomenon is very significant.

Conclusion

The presented contribution deals with significant problems of Boussinesq-type turbulence model application in ICE. The paper main target was to stress the important problems of turbulence modelling in ICE.

It seems that Reynolds stress quantitative prediction is important weak point of the considered approach. If turbulent momentum transport cannot be trusted, temperature turbulent transport is most likely wrong as well. This conclusion might cast doubts over chemical-kinetics-based simulations for which the proper temperature prediction is very important. Moreover, it seems that different turbulence models vary significantly in modeling of dissipation. This causes that the results might be very different. On the other hand, it should be mentioned that two-equation turbulence models have such properties that qualitative influence of many phenomena is in a good correspondence with experimental knowledge (detailed description is presented in [4, 6]).

Simple combustion model based on assumption that turbulent transport is the dominant term (which should be valid for SI engine under high engine load) has many positive properties (more details can be found in [4]). However, the shape of ROHR and significant influence of applied mesh are the most important weak points.

Acknowledgement

This work has been supported within the MŠM project Z20760514 ”Komplexní dynamické systémy v termodynamice, mechanice tekutin a těles”. This help is gratefully appreciated.

Reference

[1] Dimopoulos, P. and Boulouchos, K. *Reynolds Stress Components in the Flow Field of a Motored Reciprocating Engine*. *SAE Technical Paper Series*, March 1995. Paper 950725.

[2] Michard, M., Lengyel, I., and Grosjean, N. *Measurements of Turbulence Length Scales in a Motored Reciprocating Engine*. *In: 2nd International Symposium on Experimental and Computational Aerothermodynamics of Internal Flows – Proceedings*, Vol. 2:381–386, July 1993.

[3] Peters, N. *Turbulent Combustion*. The Press Syndicate of the University of Cambridge, The Pitt Building, Trumpington Street, Cambridge, 2000. ISBN 0-521-66082-3.

[4] Vítek, O. *Simulace dějů v pístovém motoru s vlivem turbulence*. Ph.D. Thesis, CTU in Prague, Department of Automotive Engineering, 2006. (In Czech).

[5] Vítek, O., Polášek, M., Kozel, K., and Macek, J. *Premixed Turbulent Combustion Modeling Using Level Set Approach*. *GAMM 2005 Abstracts*, Vol. 1:182, March 2005.

[6] Vítek, O., Polášek, M., Kozel, K., and Macek, J. *Linear Turbulence Model Validation for the Case of 3-D In-cylinder Phenomena Modeling*. *Journal of Middle European Construction and Design of Cars (MECCA)*, Voloume V. (04/2006 + 01/2007):24, 2007. ISSN 1214-0821.

[7] Wilcox, D. C. *Turbulence Modeling for CFD*. DCW Industries, Inc., 5354 Palm Drive, La Canada, California 91011, 2. edition, March 2000. ISBN 0-9636051-5-1.

INVESTIGATION OF HYSTERESIS OF THE COANDA EFFECT AT THE FLAT PLATE

Zygmunt Wierciński*, Aldona Skotnicka
University of Warmia and Mazury, Olsztyn, *also Institute of Fluid-Flow Machinery, Gdansk

Summary: The hysteresis of the Coanda effect was investigated with the 2D stream coming from the slot in the neighbourhood of the plate at the experimental rig at the UWM, Olsztyn. The measurements were made for different Reynolds numbers based on the slot dimension and stream velocity. The measurement of the free stream, the wall jet velocity profiles and the pressure distribution on the plate were accomplished. The angles of the plate arrangement (hysteresis angle) according to the stream axis were measured where the stream separate and attached the plate when the plate was approaching or walking away the stream axis. The hysteresis angle is equal to the 15 to 20 degrees depending on the Reynolds number. The visualization of hysteresis of the Coanda effect was also made by means of the smoke.

1. **Introduction** The Coanda effect is observed as a tendency of the stream coming from the slot to stay attached to the plate or convex surface. The Coanda effect is well known in the ventilation as an undesirable phenomenon changing the designed air distribution in the ventilated room. It also sometimes used to change the air direction at the outlet of the vent in a well-thought- up way.
It is known that there is the hysteresis of Coanda effect which is rather not well investigated [1]. The aim of this paper is - to some extent – to fill out this gap. In [1] the hysteresis is shown as a function of l/b, where l=length of the plate and the width of the air outlet orifice and for the so called high Reynolds number i.e. Re=50000. In the ventilation problems the Reynolds number is often much smaller and in our investigations it is in the range of Re= 7000 till almost 40000. A little more distant target of our investigation is the application of the hysteresis phenomenon to enhance the mixing ventilation in a room.

2. **Experimental rig** The investigation was carried out in the experimental rig in the lab of the Chair of Environmental Engineering at the UWM in Olsztyn. The stream air was coming from the twodimensional Witoszynski nozzle of dimensions h*b, where h=0.6 m = const and b = 5, 10 and 20 mm was changing. The length of the plate of length l = 1.0 m was placed at the edge of slot and the plate can be turned of the angle 0 to 90 degrees was, thus investigations were made for three different values of l/b = 50, 100 and 200.
The velocity range used during the investigation was 5 m/s to 32 m/s so the Reynolds numbers determined as by Newman was Re= 7000 till almost 40000.
Firstly, the histeresis of the Coanda affect at the plate was investigated by measuring the limiting angle when the stream is attached and detached [3]. The visualisation of the hysteresis of the Coamda effect were also made. Than the measurements of the free stream from the twodimensional slot was made, and next the wall jet for the angle α=0 and the critical maximum angle of attachment and separation [2]. Furthermore the measurements of static pressure in 50 points at the plate surface were made. Additionally, the pressure force acting on the plate was calculated by means of the integration of static pressure. For the critical angle of plate deflection also the separation

bubble length at the beginning of plate was measured by means of visualisation (threads).

3. Results of investigation

The limited angles of hysteresis for different Reynolds numbers and l/b are presented, Fig.1 and 2.

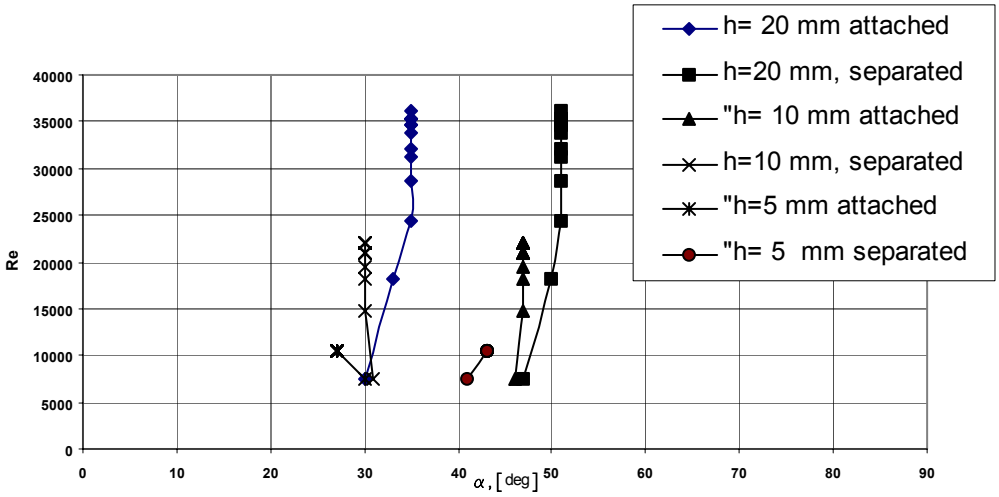

Fig.1 Hysteresis limits of the Coanda effect versus Reynolds number

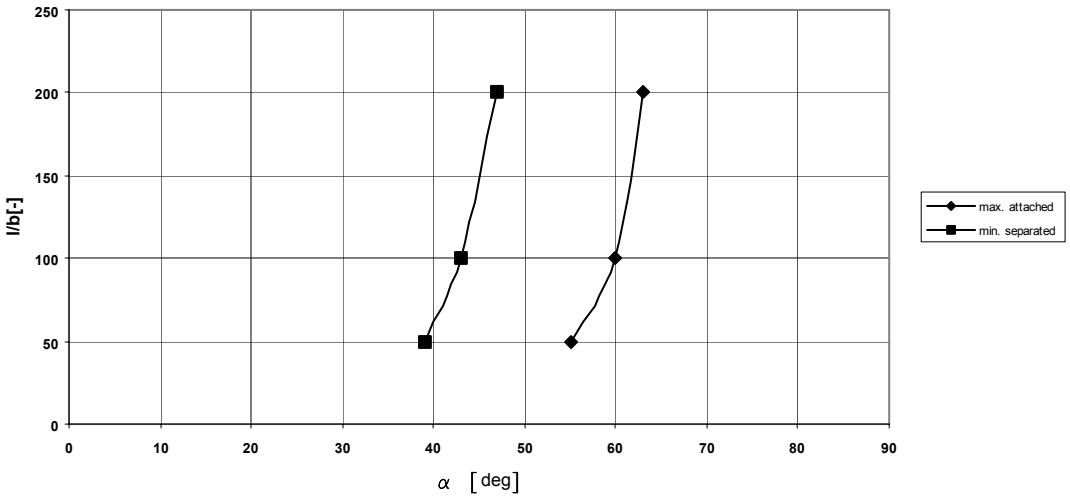

Fig. 2. Hysteresis limits of the Coanda effect versus nondimensional length of plate l/b

4. Conclusions Results in Fig.1 show that the hysteresis phenomenon is Reynolds number dependant, while results in the Fig. 2, given as the limited angle for the highest Reynolds number used in experiment (for each width orifice applied), are very similar to results given by Newman [1] for the Reynolds number Re>50000.

References:

[1] Newman, Newman, B.G.,The deflexion of plane jet by adjacent boundaries. Coanda effect in Boundary layer and flow control, Ed. G. V. Lachman, Pergamon Press, Oxford, 1961

[2] Pietrzak, P.,Gajewski, M., Badanie zjawiska histerezy efektu Coanda, 2007, Praca dyplomowa, UWM

[3] Wiercinski, Z., Siepsiak-Skotnicka, A., Wesołowski, M, 2007, Badania swobodnego i przysciennego strumienia w efekcie Coanda, Raport KIS nr1/2007, WNT, UWM, Olsztyn

LOCAL FRICTION COEFFICIENT VARYING IN TIME IN THE BOUNDARY LAYER INDUCED BY WAKES

Zygmunt Wierciński*, Jacek Żabski
Institute of Fluid-Flow Machinery, Gdańsk, *also UWM, Olsztyn

Summary: The measurements of the boundary layer on the flat plate induced by wakes were made at the subsonic wind tunnel. The phase averaging of the velocity signal was accomplished in one period of time T of the oncoming disturbing wake generated by the single rode in the up and down motion situated upstream to the plate. The local friction coefficient C_f in the period time T was determined using the phase averaged velocity profile across the boundary layer. The measurements were made for different angle of incidence of the plate.

1. **Introduction** The interaction of wakes and boundary layer is the rather complex phenomenon often encountered in the different energy equipment and especially in turbomachinery [1]. The aim of the investigation presented in this paper is to determine the phase averaged characteristics of the boundary like δ, δ^* , δ^{**}, H and C_f on a plate as a function of one period of the disturbance τ i.e. oncoming wake generated by a rode moved up and down. The measurements of time averaged characteristics of boundary layer induced by wakes were presented in [2].
Also the velocity distribution in different time of the period was measured. The results of the measurement can be used for validation of numerical codes simulating the flow around the blades in turbomachinery.

2. **Experimental rig** The investigation was carried out in the subsonic wind-tunnel of small turbulence level at the Institute of Fluid-Flow Machinery in Gdańsk. The flow with wakes is generated by means of single rod in up and down motion of 4 Hz. The flat plate of dimensions: 0.7 m long, 0.6 m wide and 0.012 m thick was used for the cold boundary layer investigations. The measurements were carried out for the oncoming velocity U_o=15 m/s and for different angle of inclination of the plate α = 0 to 2.5°. The velocity fluctuations across boundary layer are measured by means of the single hot-wire probe. The special electronic device was used to accomplish the phase (group) averaging of the velocity signal in the boundary layer.
First the measurement of the boundary layer without outside flow disturbances were carried out. Next the measurement of boundary with oncoming wakes were made.

3. **Results of measurements** The local shear coefficient C_f was find out by means of the velocity gradient in the boundary layer after the phase averaged velocity was determined. Fig.1 shows the C_f coefficient for the U_o=15 m/s at x=165 mm and for three different Re= (1.68, 368 and 6.57)$\cdot 10^5$. In Fig. 2 the C_f as the function of Re and the disturbances period τ is shown. As expected, the decreasing tendency of the C_f coefficent versus Re is clearly shown. In the region of wakes the increase of the C_f of about 75% is also shown. Furthermore the time shift of the wake can be observed in the Fig.1. In Fig. 2 the time variation of the C_f is seen as the double loop, each connected with the first and second wake, appropriately.

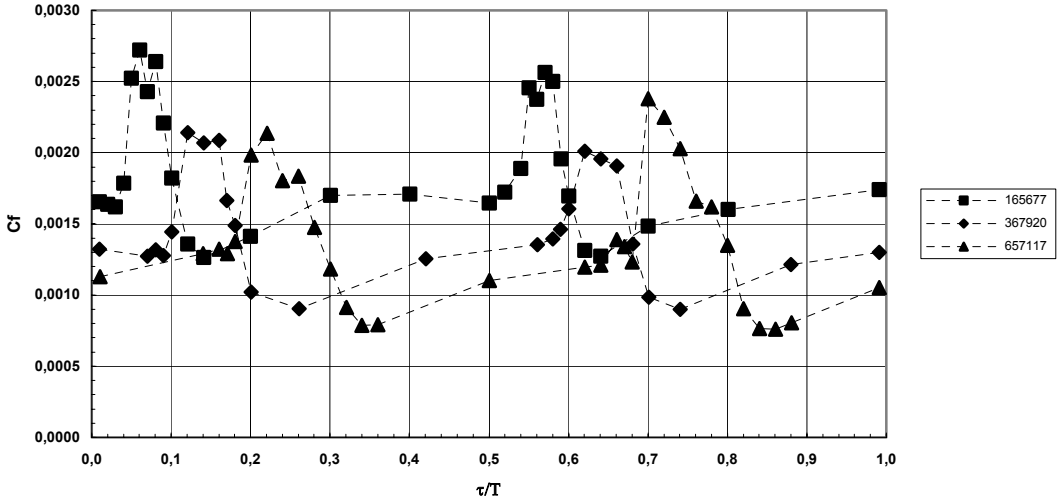

Fig. 1 Variation of C_f in period time τ for three different Reynolds numbers for the incidence angle $\alpha = 0.44$ °

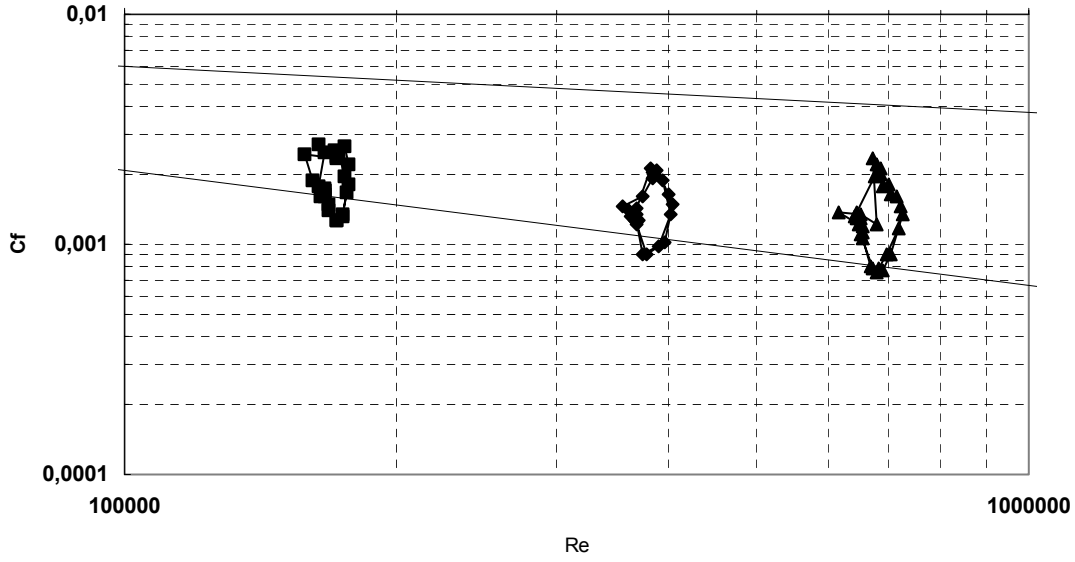

Fig. 2 Variation of C_f=f(Re) in period time τ for three different Reynolds numbers

4. Conclusions

The results of the measurements of the C_f coefficient as a function of the time period of disturbance generated by the rode show great changes which lie between the laminar and turbulent lines. The same great changes are also shown for other characteristics of boundary layer induced by wakes. This measurements can be used for validation of the time-averaged calculation of the code based on the Reynolds assumption.

References:

[1] Mayle, R.E., 1991, The role of laminar-turbulent transition in gas turbine engines.J. Turbomachinery, Vol. 113, pp.509-537

[2] Wiercinski, Z., 1999, Laminar-turbulent transition in the boundary layer induce by wakes, Bull. IFFM, No.499/1450/99

LIST OF PARTICIPANTS

1. **ANTOŠ** Pavel, Ing., ÚT AV ČR, v. v. i., Dolejškova 5, 182 00 Praha 8, (antos@it.cas.cz)
2. **BEDNÁŘ** Lukáš, Ing. ŠKODA POWER, a.s., Tylova 57, 316 00 Plzeň (lukas.bednar@skoda.cz)
3. **BENETKA** Jiří Ing. CSc., VZLÚ, V Mezihoří 20a, 180 00 Praha 8-Libeň (benetka@vzlu.cz)
4. **BERTOLA** Volfango, Dr., University of Edinburgh, School of Engineering and Electronics, The King´s Buildings, Mayfield Road, Edinburgh EH9 3JL, United Kingdom (v.bertola@ed.ac.uk)
5. **BODNÁR** Tomáš, Department of Technical Mathematics, Faculty of Mechanical Engineering, Czech Technical University of Prague, Karlovo nám. 13, 121 35 Prague 2, Czech Republic (bodnar@marian.fsik.cvut.cz)
6. **BRECHLER** Josef, RNDr., Doc., UK, Matematicko-fyzikální fakulta, Katedra meteorologie a ochrany prostředí (josef.brechler@mff.cuni.cz)
7. **DVOŘÁK** Václav, Ing., Ph.D., Technická univerzita v Liberci, Hálkova 6, 461 17 Liberec (vaclav.dvorak@tul.cz)
8. **FIŠER** Jan Ing., Vysoké učení technické v Brně, Technická 2, 616 69 Brno (fiser@fme.vutbr.cz)
9. **FOŘT** Jaroslav, Doc., Ing., CSc., Centre of Power Engineering, Institute of Thermomechanics AS ČR, Technická 4, 166 07 Praha 6, Czech Republic (fort@marian.fsik.cvut.cz)
10. **FUKA** Vladimír, Mgr., Katedra meteorologie a ochrany prostředí, Matematicko-fyzikální fakulta, Univerzity Karlovy v Praze (vladimír.fuka@gmail.com)
11. **FURMÁNEK** Petr, Ing., České vysoké učení technické, Fakulta strojni, Karlovo nám. 13, Praha 2, 121 35 (petr.furmanek@fs.cvut.cz
12. **FÜRST** Jiří, Doc. Ing. PhD., České vysoké učení technické, Karlovo nám. 13, Praha 2 121 35 (jiri.furst@fs.cvut.cz)
13. **HADRAVA** Martin, Univerzita Karlova, Matematicko-fyzikální fakulta, Ke Karlovu 3, 121 16 Praha 2 (martin.hadrava@seznam.cz)
14. **HÁJEK** Jaroslav, Mgr. Výzkumný a zkušební letecký ústav, Beranových 130, 199 00 Praha 9 (hajek@vzlu.cz)
15. **HOLMAN** Jiří Ing,, České vysoké učení technické, Karlovo nám. 13, 121 35 Praha 2 (jirka.holman@seznam.cz)
16. **HOZNEDL** Michal, Ing., ŠKODA POWER, a.s., Tylova 57, 316 00 Plzeň (michal.hoznedl@skoda.cz)
17. **HYHLÍK** Tomáš, Ing., ČVUT v Praze, Fakulta strojní, Ústav mechaniky tekutin a energetiky, (tomas.hyhlik@fs.cvut.cz)
18. **CHÁRA** Zdeněk Ing. CSc., Ústav pro hydrodynamiku AV ČR v. v. i., Pod Paťankou 5, 166 12 Praha 6 (chara@ih.cas.cz)

19. **JELÍNEK** Tomáš, Ing., Výzkumný a zkušební letecký ústav, V Mezihoří 20a, 1801 00 Praha 8-Libeň (jelinek@vzlu.cz)
20. **JONÁŠ** Pavel, RNDr., DrSc., Ústav termomechaniky AV ČR, v. v. i., Dolejškova 5, 182 00 Praha 8 (jonas@it.cas.cz)
21. **KHARLAMOV** Alexander, Mgr., Ústav pro hydrodynamiku AV ČR, v. v. i., Pod Paťankou 30/5, 166 12 Praha 6 (charlamov@ih.cas.cz)
22. **KELLNEROVÁ** Radka, Mgr., Ústav termomechaniky AV ČR, v. v. i., Dolejškova 5, 182 00 Praha 8 (radka.kellnerova@email.cz)
23. **KLADRUBSKÝ** Milan, Ing., Výzkumný a zkušební letecký ústav a.s., Beranových 130, 199 00, Praha 9 (kladrubsky@vzlu.cz)
24. **KNOB** Martin, Ing., Ústav termomechaniky AV ČR, v. v. i., Dolejškova 5, 182 00 Praha 8 (knob@it.cas.cz)
25. **KOLÁŘ** Jan, Ing., Technická univerzita Liberec, Katedra energetických zařízení, Hálková 6, Liberec, 461 17 (banan1@seznam.cz)
26. **KOPÁČEK** Tomáš Ing., CTU in Prague (kopacek@vzlu.cz)
27. **KOZEL** Karel, Prof., Department of Technical Mathematics, Faculty of Mechanical Engineering, Czech Technical University of Prague, Karlovo nám. 13, 121 35 Prague 2, Czech Republic (kozelk@fsik.cvut.cz)
28. **KUČERA** Václav RNDr., Univerzita Karlova v Praze, Katedra numerické matematiky, Sokolovská 83, Praha 8 (vaclav.kucera@email.cz)
29. **MAZUR** Oton, prom. fyz., Ústav termomechaniky AV ČR, v. v. i., Dolejškova 5, 182 00 Praha 8 (mazur@it.cas.cz)
30. **MATĚCHA** Jan, Ing., Department of Fluid Dynamics and Power Engineering, FME, CTU, Technická 4, 166 07, Praha 6 (jan.matecha@fs.cvut.cz)
31. **MATĚJKA** Milan, Ing., ČVUT v Praze, Fakulta strojni, Ústav mechaniky tekutin a energetiky, Technická 4, 166 07 Praha 6 (milan.matejka@fs.cvut.cz)
32. **MATĚJÍČEK** Luboš, Dr., Univerzita Karlova v Praze, Přírodovědecká fakulta, Albertov 6, 128 43 Praha 2 (lmatejicek@natur.cuni.cz)
33. **MICZÁN** Martin, České vysoké učení technické v Praze, Fakulta strojní, Ústav mechaniky tekutin a energetiky, Technická 4, 166 07 Praha 6 (martin.miczan@seznam.cz)
34. **MUŽÍK** Tomáš, Ing., České vysoké učení technické v Praze, Ústav mechaniky tekutin a energetiky, Technická 4, 166 07 Praha 6 (muzik.tomas@centrum.cz)
35. **MÜLLER** Miloš, Ing., Technical University of Liberec, Department of Power Engineering Equipment, Hálkova 6, 461 17 Liberec (milos.muller@tul.cz)
36. **NĚMEC** Martin, Ing., VZLÚ, Beranových 130, 195 05 Praha 9 – Letňany (nemec@vzlu.cz)
37. **NĚNIČKA** Václav, RNDr., CSc., Institute of Thermomechanics AS CR, v. v. i., Dolejškova 5, 182 22 Praha 8 (nenicka@it.cas.cz)
38. **NOVOTNÝ** Jan, Ing., Department of Fluid Dynamics and Power Engineering, FME, CTU, Technická 4, 166 07 Praha 6 (jan.novotny@fs.cvut.cz)

39. **PACÁK** Aleš, Ing. Západočeská univerzita v Plzni, Fakulta strojni, Katedra energetických strojů a zařízení, Univerzitní 8, 306 14 Plzeň (alpa@kke.zcu.cz)
40. **PELANT** Jaroslav, RNDr., CSc., Výzkumný a zkušební letecký ústav, Beranových 130, 199 05 Praha 9 (pelant@vzlu.cz)
41. **PIRKL** Luboš, Czech Technical University of Prague, Department of Technical Mathematics, Faculty of Mechanical Engineering, Karlovo nám. 13, 121 35 Prague 2, (lubos.pirkl@seznam.cz)
42. **POPELKA** Lukáš, Ing. PhD., Ústav termomechaniky AV ČR, v. v. i., Dolejškova 5, 182 00 Praha 8 (popelka@it.cas.cz)
43. **PRACHAŘ** Aleš, RNDr., PhD., Výzkumný a zkušební letecký ústav, a.s., Beranových 130, 199 05 Praha 9 (prachar@vzlu.cz)
44. **PŘÍHODA** Jaromír, Prof., Ing., CSc., Institute of Thermomechanics AS CR v. v. ï., Dolejškova 5, 182 00 Praha 8 (prihoda@it.cas.cz)
45. **REDONDO** José Manuel, prof., Department de Fisica Aplicada, Universitat Politecnica de Catalunya, Campus Nord – Edifici B4/B5,C/ Jordi Girona Salgado, 1-3. 08034 Barcelona, Spain (redondo@fa.upc.es)
46. **RŮŽIČKA** Martin, RNDr., Department of Numerical Mathematics, Charles University in Prague, Faculty od Mathematics and Physics, Sokolovská 83, 186 75 Praha 8 (mart.in.ruza@seznam.cz)
47. **SCHMORANZER** David, prom.fyz., Faculty of Mathematics and Physics, Charles University, V Holešovičkách 2, 180 00 Praha 8 (david.sch@seznam.cz)
48. **SEKULA** Emil, PhD. Student, Universitat politecnica de Catalunya, Barcelona, Passeig de la zona Franca 162 D24, 08038 Barcelona, Spain (sekula@gmail.com)
49. **SIEPSIAK-SKOTNICKA** Aldona, Mgr., Eng., University of Warmia and Mazury, Olztyn, 10-724 Olsztyn Heweliusza 4, Polsko
50. **SLÁDEK** Ivo, Ing. PhD., Ústav termomechaniky AV ČR, v.v.i., Dolejškova 5, 182 00 Praha 8 (isladek@visteon.com)
51. **SLANEC** Jan, Ing., ČVUT v Praze, Fakulta strojni, Technická 4, 166 07 Praha 6 (jan.slanec@fs.cvut.cz)
52. **SKRBEK** Ladislav, Doc., RNDr., DrSc., Joint Low Temperature Laboratory, Institute of Physics ASCR, V Holešovičkách 2, 180 00 Prague 8, Czech Republic (skrbek@fzu.cz)
53. **STANISLAV** Jiří, Ing., Ústav termomechaniky AV ČR, v. v. i., Dolejškova 5, 182 00 Praha 8 (jiri.stanislav@fs.cvut.cz)
54. **STRAKA** Petr, Ing., VZLÚ, a.s. Beranových 130, 199 05 Praha 9-Letňany (pe25tr@seznam.cz)
55. **SVÁČEK** Petr, RNDr., PhD., ČVUT v Praze, Fakulta strojni, Ústav technické matematiky, Karlovo nám. 13, 121 35 Praha 2 (petr.svacek@fs.cvut.cz)
56. **ŠAFAŘÍK** Pavel, Doc., Ing., CSc., ČVUT, FS, Ústav mechaniky tekutin a energetiky, odbor Mechaniky tekutin a termodynamiky, Technická 4, 166 07 Praha 6 (safarik@fsid.cvut.cz)
57. **ŠIMÁK** Jan Mgr., Výzkumný a zkušební letecký ústav, a.s., Beranových 130, 199 05 Praha 9 (simak@vzlu.cz)

58. **ŠTEMBERA** Vítězslav Mgr., Ústav termomechaniky AV ČR, v. v. i., Dolejškova 5, 182 00 Praha 8 (vitastembera@hotmail.com)

59. **TESAŘ** Václav, Prof., Ing., CSc., Institute of Thermomechanics AS CR, v. v. i., Dolejškova 5, 182 00 Praha 8 (tesar@it.cas.cz)

60. **ULMAN** Pavel, Ing., Ústav přístrojové techniky AV ČR, v. v. i., Královopolská 147, 612 64 Brno (urban@isibrno.cz)

61. **URUBA** Václav, Ing. CSc., Ústav termomechaniky AV ČR, v. v. i., Dolejškova 5, 182 00 Praha 8 (uruba@it.cas.cz)

62. **VÍTEK** Oldřich, Ing., PhD., Josef Božek Research Centre, CTU Prague, Technická 4, Prague 6 (oldrich.vitek@fs.cvut.cz)

63. **WIERCINSKI** Zygmunt, DSc., Institute of Fluid-Flow Machinery, Polish Academy of Sciences, 14 Fiszera Street, 80-952 Gdansk, Poland (zw@imp.gda.pl)

64. **ZABSKI** Jacek, Mgr., Eng., Institute of Fluid-Flow Machinery, Polish Academy of Sciences, 14 Fiszera Street, 80-952 Gdansk, Poland (zw@imp.gda.pl)

CONTENTS


NOTES

ISBN 978-80-87012-07-09